2012

Catalytic mechanisms of thymidylate synthases: bringing experiments and computations together

Zhen Wang
University of Iowa

CATALYTIC MECHANISMS OF THYMIDYLATE SYNTHASES: BRINGING EXPERIMENTS AND COMPUTATIONS TOGETHER

by

Zhen Wang

An Abstract

Of a thesis submitted in partial fulfillment
of the requirements for the Doctor of
Philosophy degree in Chemistry
in the Graduate College of
The University of Iowa

December 2012

Thesis Supervisor: Professor Amnon Kohen

ABSTRACT

The relationship between protein structure, motions, and catalytic activity is an evolving perspective in enzymology. An interactive approach, where experimental and theoretical studies examine the same catalytic mechanism, is instrumental in addressing this issue. We combine various techniques, including steady state and pre-steady state kinetics, temperature dependence of kinetic isotope effects (KIEs), site-directed mutagenesis, X-ray crystallography, and quantum mechanics/molecular mechanics (QM/MM) calculations, to study the catalytic mechanisms of thymidylate synthase (TSase). Since TSase catalyzes the last step of the sole intracellular *de novo* synthesis of thymidylate (*i.e*. the DNA base T), it is a common target for antibiotic and anticancer drugs. The proposed catalytic mechanism for TSase comprises a series of bond cleavages and formations including activation of two C-H bonds: a rate-limiting C-H→C hydride transfer and a faster C-H→O proton transfer. This provides an excellent model system to examine the structural and dynamic effects of the enzyme on different C-H cleavage steps in the same catalyzed reaction. Our experiments found that the KIE on the hydride transfer is temperature independent while the KIE on the proton transfer is temperature dependent, implying the protein environment is better organized for H-tunneling in the former. Our QM/MM calculations revealed that the hydride transfer has a transition state (TS) that is invariable with temperature while the proton transfer has multiple subsets of TS structures, which corroborates with our experimental results. The calculations also suggest that collective protein motions rearrange the network of H-bonds to accompany structural changes in the ligands during and between chemical transformations. These computational results not only illustrate functionalities of specific protein residues that reconcile many previous experimental observations, but also provide guidance for future experiments to verify the proposed mechanisms. In addition, we conducted experiments to examine the importance of long-range interactions in TSase-catalyzed reaction, using

both kinetic and structural analysis. Those experiments found that a remote mutation affects the hydride transfer by disrupting concerted protein motions, and Mg^{2+} binds to the surface of TSase and affects the hydride transfer at the interior active site. Both our experiments and computations have exposed interesting features of ecTSase that can potentially provide new targets for antibiotic drugs targeting DNA biosynthesis. The relationship between protein structure, motions, and catalytic activity learned from this project may have general implications to the question of how enzymes work.

Abstract Approved: _____

Thesis Supervisor

_____

Title and Department

_____

Date

CATALYTIC MECHANISMS OF THYMIDYLATE SYNTHASES: BRINGING EXPERIMENTS AND COMPUTATIONS TOGETHER

by

Zhen Wang

A thesis submitted in partial fulfillment
of the requirements for the Doctor of
Philosophy degree in Chemistry
in the Graduate College of
The University of Iowa

December 2012

Thesis Supervisor: Professor Amnon Kohen

Graduate College
The University of Iowa
Iowa City, Iowa

CERTIFICATE OF APPROVAL

PH.D. THESIS

This is to certify that the Ph.D. thesis of

Zhen Wang

has been approved by the Examining Committee
for the thesis requirement for the Doctor of Philosophy
degree in Chemistry at the December 2012 graduation.

Thesis Committee: _____
Amnon Kohen, Thesis Supervisor

_____
Vicente Moliner Ibáňez

_____
Daniel M. Quinn

_____
M. Lei Geng

_____
Alexei V. Tivanski

To My Parents Baocheng Wang and Jun Zeng

献给我的父亲王宝成和母亲曾军

生于忧患，死于安乐
(He who can thrive in calamity may perish in comfort.)
.
《孟子•告天下》
(Mencius, *Gaozi II*)

ACKNOWLEDGMENTS

Here I am! At the end of my PhD studies? Yes, but more importantly, at the entrance to a whole new adventure, with the highest degree one can ever get in Chemistry. I cannot stop smiling just imagining all the new projects that I will be working on in the next few years, and the projects that I cannot imagine yet in the far future! It is always good to remember what has been left behind while looking forward. At this moment, my heart is filled with gratitude to so many people who have helped me to reach this milestone of my life.

I first want to thank my parents for being my rock. Their kind hearts and positive attitude towards life were the very first lessons in my early childhood, which have shaped the majority of my philosophy in life. I know that my parents can never understand my work or even my enthusiasm for science, but it never stopped them from encouraging me to reach for my dreams. I can only imagine how difficult it was for them to watch their only child leave for a destination that is half the globe away. Indebted to my parents' love and support, I am always motivated be healthier, happier, and more accomplished in every single task.

It is probably fair to say that Zhen Wang would be a different person at this moment if I did not receive my PhD training from such a wonderful advisor, Prof. Amnon Kohen. During my PhD studies, I shifted my research interests multiple times--from basic enzyme kinetics to protein dynamics, from experiments to computations, *etc*.--and Amnon has always been patient and encouraging. It is amazing to sit and think how much I have learned from Amnon in the past few years, besides the scientific knowledge and skills. To name a few important lessons from Amnon: (1) Ask the right questions; (2) Be observing, but stay focused; (3) Be honest about a mistake; (4) Find a balance between career and family. I know I still need to keep working on the last one in the years to come.

I also want to thank my husband and soulmate, Dr. Jigar Bandaria, for being my best friend and greatest support. I still vividly remember Dr. Mike Nydegger's comment a few years ago, "Zhen is a Chinese female version of Jigar!" Later on both of us realized that was not a joke... I never imagined I could ever meet someone who is so similar to me, but better!! Jigar has offered many good suggestions and inspirations for my research, and I am lucky to be spending my future life learning from his many good qualities.

I also owe massive thanks to Prof. Vicente Moliner and Dr. Silvia Ferrer at Universitat Jaume I, Castellón, Spain, who have provided professional guidance for the theoretical part of my PhD research. When I visited their lab for five months last year, they were very patient with my numerous questions every day, which greatly accelerated the development of my computation skills. Those five months were not only a turning point in my career, but also one of the greatest periods of time in my life. I have learned a lot from my colleagues in Vicente's lab on computations as well as on how to live a happier life.

During my PhD studies, I was very lucky to have met many kind people and to receive a lot of help. Thanks to Prof. Christopher Cheatum for reshaping my understanding of many concepts in physical chemistry, including the "Marcus-like model". Thanks to Prof. Anatoly Chernyshev (Sultanate of Oman) for the mentorship during my early PhD studies. Thanks to Prof. Mark Arnold for providing lab space, and to Prof. Adrian Elcock for providing computation resources. Thanks to Dr. Mike Nydegger and Dr. Irma Nydegger for being my family in Iowa before they moved away. Thanks to all the group members in Amnon's lab for the support and company over the past years. Especially, thanks to Dr. Arundhuti Sen for teaching me all the fancy English words; to Dr. Vanja Stojković for being there for me during my most difficult times in Iowa; to my baby sister, Tatiana Mishanina, for all her support during the good and bad times; to Daniel Roston for all the funny memories of our sensible and (mostly) futile discussions; to Eric Koehn for helping me understand organic chemistry and agreeing to

collaborate in the future; and to Thelma Abeysinghe for being a great friend and coworker in the thymidylate synthase project. Also thanks to all the group members in Prof. Cheatum's lab for treating me like a member. Thanks to Casey Westlake for answering my English questions, and bearing with me in my "thesis-writing mood" during this last year. I'd also like to take this opportunity to thank all the faculty and staff members in the Chemistry Department. Especially, I have learned a lot from Prof. Daniel Quinn, Prof. Claudio Margulis, Prof. Sara Mason, Prof. Lei Geng, and Prof. Alexei Tivanski. I have also received enormous help from the front office (Sharon Robertson), the Chem Store (Tim Koon and Andy Lynch), the mechanic shop (Frank Turner), the electronic shop (Mike Estenson), the IT center (David Sansbury, Jeff Miller, Jon Yates, Chris McGee, and Brenna Faler), the Chem Center (Janet Kugley and Jessica R. Alberhasky), and the Teaching labs (Earlene Erbe) et al. It would be impossible for me to accomplish anything in the past six years if you were not there to help, so thanks a lot to all of you. It is a wonderful department and I will miss you all.

ABSTRACT

The relationship between protein structure, motions, and catalytic activity is an evolving perspective in enzymology. An interactive approach, where experimental and theoretical studies examine the same catalytic mechanism, is instrumental in addressing this issue. We combine various techniques, including steady state and pre-steady state kinetics, temperature dependence of kinetic isotope effects (KIEs), site-directed mutagenesis, X-ray crystallography, and quantum mechanics/molecular mechanics (QM/MM) calculations, to study the catalytic mechanisms of thymidylate synthase (TSase). Since TSase catalyzes the last step of the sole intracellular *de novo* synthesis of thymidylate (*i.e*. the DNA base T), it is a common target for antibiotic and anticancer drugs. The proposed catalytic mechanism for TSase comprises a series of bond cleavages and formations including activation of two C-H bonds: a rate-limiting C-H→C hydride transfer and a faster C-H→O proton transfer. This provides an excellent model system to examine the structural and dynamic effects of the enzyme on different C-H cleavage steps in the same catalyzed reaction. Our experiments found that the KIE on the hydride transfer is temperature independent while the KIE on the proton transfer is temperature dependent, implying the protein environment is better organized for H-tunneling in the former. Our QM/MM calculations revealed that the hydride transfer has a transition state (TS) that is invariable with temperature while the proton transfer has multiple subsets of TS structures, which corroborates with our experimental results. The calculations also suggest that collective protein motions rearrange the network of H-bonds to accompany structural changes in the ligands during and between chemical transformations. These computational results not only illustrate functionalities of specific protein residues that reconcile many previous experimental observations, but also provide guidance for future experiments to verify the proposed mechanisms. In addition, we conducted experiments to examine the importance of long-range interactions in TSase-catalyzed reaction, using

both kinetic and structural analysis. Those experiments found that a remote mutation affects the hydride transfer by disrupting concerted protein motions, and Mg^{2+} binds to the surface of TSase and affects the hydride transfer at the interior active site. Both our experiments and computations have exposed interesting features of ecTSase that can potentially provide new targets for antibiotic drugs targeting DNA biosynthesis. The relationship between protein structure, motions, and catalytic activity learned from this project may have general implications to the question of how enzymes work.

TABLE OF CONTENTS

LIST OF TABLES

LIST OF FIGURES

CHAPTER I

INTRODUCTION

Enzymes have been practicing their skills for more than 3 billion years,[1] and their high proficiency and specificity have intrigued biochemists ever since the first observation of enzymatic activity in test tubes in 1833.[2] Before James Sumner isolated and crystalized urease in 1926,[3] most biochemists believed that enzymes are chemical catalytic agents carried by proteins.[4] Sumner's postulate that "enzymes are proteins" started to be widely accepted after J. Northrop and M. Kunitz crystallized several other enzymes.[5-7] Numerous efforts have followed up those pioneering experiments to elucidate the catalytic mechanisms of enzymes, and the fundamental views in this field have continued to evolve with accumulating knowledge.[8,9] From Fischer's "lock-and-key" model[10] to Koshland's "induced fit"[11] model, the flexibility in protein structures has been recognized as an important factor for specific interactions between enzymes and substrates. A currently emerging view extends the "induced-fit" model and proposes that protein motions also contribute to cleavage/formation of chemical bonds (i.e. chemical steps). Examination of such proposal requires techniques that can specifically probe the chemical step of interest within the complex reaction cascade of an enzyme (Figure 1-1). This research field has benefited from combination of various experimental and theoretical approaches in studying enzymatic reactions.[12-27]

Kinetic Isotope Effect

Kinetic isotope effect (KIE) is one of the most useful experimental techniques to study enzymatic reactions, which can answer a wide range of questions from the basic catalytic mechanism to the structure of transition state of a chemical step.[28-30] KIE is the ratio of reaction rates measured for reactants that differ only in their isotopic composition. KIEs can be classified as primary (1°) or secondary (2°) KIEs, based on whether the isotopic difference is in atoms directly involved in breaking/forming bonds

during the step of interest. Depending on the experimental design, KIEs can be measured on the first-order rate constant (k_{cat} or V, also referred to as "turnover number"), second-order rate constant (k_{cat}/K_m or V/K), single-turnover rate, *etc*. of an enzymatic reaction. Due to isotopic labeling in specific atoms of the substrates, KIE experiments can expose information relevant to the chemical step(s) of interest. However, other mechanistic steps often cause "kinetic complexity" that diminish the observed KIE from the "intrinsic" KIE value on that step, *e.g*. $(k_H/k_i)_{int}$ for a H-transfer step[i] (where i is another isotope of hydrogen) (Figure 1-1).[29,31,32] The observed KIE is then:

$$\mathrm{KIE}_{\mathrm{obs}} = \frac{\left(k_{\mathrm{H}}/k_i\right)_{\mathrm{int}} + C_f + C_r \cdot \mathrm{EIE}}{1 + C_f + C_r} \tag{1}$$

where EIE (equilibrium isotope effect) is the isotope effect on the equilibrium constant of the reaction; C_f and C_r are the forward and reverse "commitments to catalysis", respectively. C_f is the ratio between the forward rate of isotopically sensitive step (the step of interest) and the net reverse rate of non-isotopically sensitive steps that precede that step. Similarly, C_r is the ratio between the reverse rate of isotopically sensitive step to the net forward rate of non-isotopically sensitive steps that follow that step. For an irreversible step, $C_r = 0$ and all the kinetic complexity is caused by C_f from the preceding steps. Analyzing the kinetic commitments can sometimes provide valuable information on the reaction mechanism, as will be illustrated in Chapters II, III, and IV. Chapter II also provides details of how to extract the intrinsic KIE from the values of $\mathrm{KIE}_{\mathrm{obs}}$ measured on V/K, using Northrop's method.[29,31,32] Chapter IV presents KIE measurements on both V and V/K of the same enzyme, providing complementary information of the reaction mechanism.

---

[i] Throughout the thesis, we use "H-transfer" to generally denote the transfer of proton, hydride, or hydrogen atom.

Interpretations of KIE

The semi-classical models mostly ascribe 1° KIE to the quantum effects in the zero-point energy (ZPE) levels in the ground state (GS) and transition state (TS), neglecting quantum mechanical tunneling (Figure 1-1).[33] A number of theoreticians realized the importance of tunneling for H-transfer reactions and developed models that explicitly account for this quantum effect. Most notably, Bell's correction approximated the tunnel effect by truncating the activation energy barrier on the one-dimensional reaction coordinate (RC) (Figure 1-1).[34] However, the models with "tunneling corrections" cannot explain the discoveries in the past decade that many wild-type (WT) enzymes present temperature-independent 1° KIEs on the catalyzed H-transfer steps with their natural substrates under physiological conditions.[19,35-40] This discrepancy between theories and experiments stimulated a reevaluation of the involvement of quantum mechanical tunneling and protein motions in H-transfer reactions in enzymology. An inspiration came from the Marcus theory of electron transfer,[41] which uses the relatively slow solvent reorganization as the RC to construct an energy-degenerate state for the fast electron tunneling (based on the Franck-Condon principle[42-44]). By analogy, some physical chemists decided to use the "heavy atom reorganization" as the RC to generate the "tunneling ready state" (TRS) for H-transfer, which has developed into the "Marcus-like model" (Figure 1-2).[19,23,25,27,45-48] This model suggests that protein motions can facilitate an enzymatic H-transfer in three aspects. First, conformational fluctuations of the protein "pre-organize" an electrostatic environment that is favorable for formation of the "reactive complexes".[19,49-52] Secondly, "fine-tuning" of the conformations of reactive complexes further "reorganize" the active site to accommodate structural changes in the substrates going from the reactant state to the TRS of H-transfer. Thirdly, the fluctuation of donor-acceptor distance (DAD) at the TRS affects the H-tunneling probability. While the DAD fluctuation at TRS determines the magnitude and temperature dependence of the intrinsic KIE, pre- and re-organization affects the rate (and activation energy

parameters) of the H-transfer and thus the commitments to catalysis in experimental KIE measurements (C_f and C_r in Eq 1).[29,32] Marcus-like model and its interpretation of experimental KIE results will be discussed in more detail in Chapters II, III and IV. This is an actively evolving research field, and Figure 1-2 provides a graphical illustration of my *current* understanding of the Marcus-like model.

Computer Simulations

While the Marcus-like model appears to explain the KIE results, it does not provide the molecular mechanisms behind the experimental observations. The fast development of computer technology in recent decades has provided very powerful tools to investigate chemical reactions *in silico* at atomic level. Computational chemistry incorporates theoretical formulae into efficient computer programs to calculate structures and properties of substances. The computational methods range from the accurate quantum mechanical (QM) calculations, which solve Schrödinger equation for the molecular Hamiltonian, to the approximate molecular mechanical (MM) calculations, which are based on classical mechanics using force fields parameterized for a specific class of molecules. Among the most notable developments, Warshel *et al*. introduced the hybrid QM/MM method[53] that treats the reaction center (e.g. active site of an enzyme) with QM functions and the rest of the system with MM force fields. The QM/MM method combines the reliability of QM calculations and the efficiency of MM simulations, making it possible to simulate a complex enzymatic system (Figure 1-3). Chapter V provides technical details of how to use QM/MM calculations to study enzymatic reactions, and illustrates the power of theoretical computation as a tool to complement and predict experimental results.

"Case Study": Thymidylate Synthase

My PhD research included a series of studies on the catalytic mechanisms of thymidylate synthase (TSase, or "classical" TSase) with an interactive approach that

takes advantage of both experimental and computational techniques. TSase is an obligate homodimer with "half-of-the-sites" activity, i.e. one competent active site at a time.[54-56] TSase is one of the most conserved enzymes in evolution,[57] which catalyzes the sole intracellular synthesis of thymidine in nearly all organisms, and it is over-expressed in proliferating bacteria and tumor cells.[58,59] Consequently, TSase has been a common target for antibiotic and anticancer drugs. Early mechanistic studies of TSase exploited steady state and pre-steady state kinetics, crystallography, 2° α-hydrogen isotope effects, *etc*., which have been summarized in a few excellent reviews.[60-63] The large collection of experimental data of TSase revealed that protein segments move concertedly throughout the many-step reaction,[62,63] which has invoked the question whether motions of TSase contribute to the activation of chemical bonds. Compared with other "model proteins" such as dihydrofolate reductase, the overall structure of TSase is more rigid and sophisticated, and its catalytic mechanism is more complex (Figure 1-4A). Therefore, lessons from investigating the roles of protein motions in TSase-catalyzed chemical steps are likely to be more applicable to enzymatic reaction mechanisms in general.

The catalytic mechanism of TSase comprises many bond cleavages and formations including activation of two C-H bonds: a reversible C-H→B (B: general base) proton transfer and an irreversible rate-limiting C-H→C hydride transfer (Figure 1-4A). My studies have focused on investigating those two H-transfer steps, which highlighted the integration of different methodologies in addressing specific questions. In the following chapters, all KIEs refer to 1° KIEs unless otherwise specified. Chapter II describes the difference between the temperature dependences of intrinsic KIEs on both H-transfer steps in *Escherichia coli* TSase, and interprets the results with the Marcus-like model.[64] Chapter III presents structural and kinetic analysis of a remote mutant, which suggests that protein motions at various time scales can affect different parameters of the hydride transfer step.[65] Chapter IV extends this methodology to investigate the effects of Mg^{2+} on the catalytic mechanism of TSase, which complements the studies in Chapter III

and highlights the importance of long-range interactions in TSase-catalyzed reaction.[66] Chapter V presents our QM/MM calculations on the proton transfer step and compares the results with the previously calculated hydride transfer step, providing molecular details underlying the experimental KIE results.[67] It is noteworthy that our computational results not only illustrate functionalities of specific protein residues that reconcile many previous experimental observations, but also provide new insights into the catalytic mechanism that can be examined by future experiments.[67,68]

In addition, a new gene that encodes for flavin-dependent thymidylate synthases (FDTSs) has been identified in a number of microorganisms, including several lethal human pathogens.[69-72] The structure and mechanism of FDTS (Figure 1-4B) are very different from human and other classical TSase enzymes, making it an attractive target for novel antibiotics. Like many other flavo-enzymes, FDTS can function as an oxidase, turning oxygen (O_2) into hydrogen peroxide (H_2O_2) with nicotinamide-adenine dinucleotide 2'-phosphate (reduced form, NADPH) or other reducing agents. In Chapter VI, we exploited the oxidase activity of FDTS from *Thermatoga maritima* to probe the binding/release features of the substrates/products for its *in vivo* synthase activity. The experimental results provided insights into previous FDTS studies conducted under aerobic conditions and into the pursuit of unique FDTS inhibitors.[73]

Summary

The synergistic enhancement of the experimental and theoretical efforts in this project demonstrates the necessity and efficiency of combining multiple approaches to study enzyme mechanisms. Our findings not only provide a deeper understanding of catalytic mechanisms of TSase, but also demonstrate indispensable roles of protein motions in enzyme-catalyzed activation of chemical bonds.

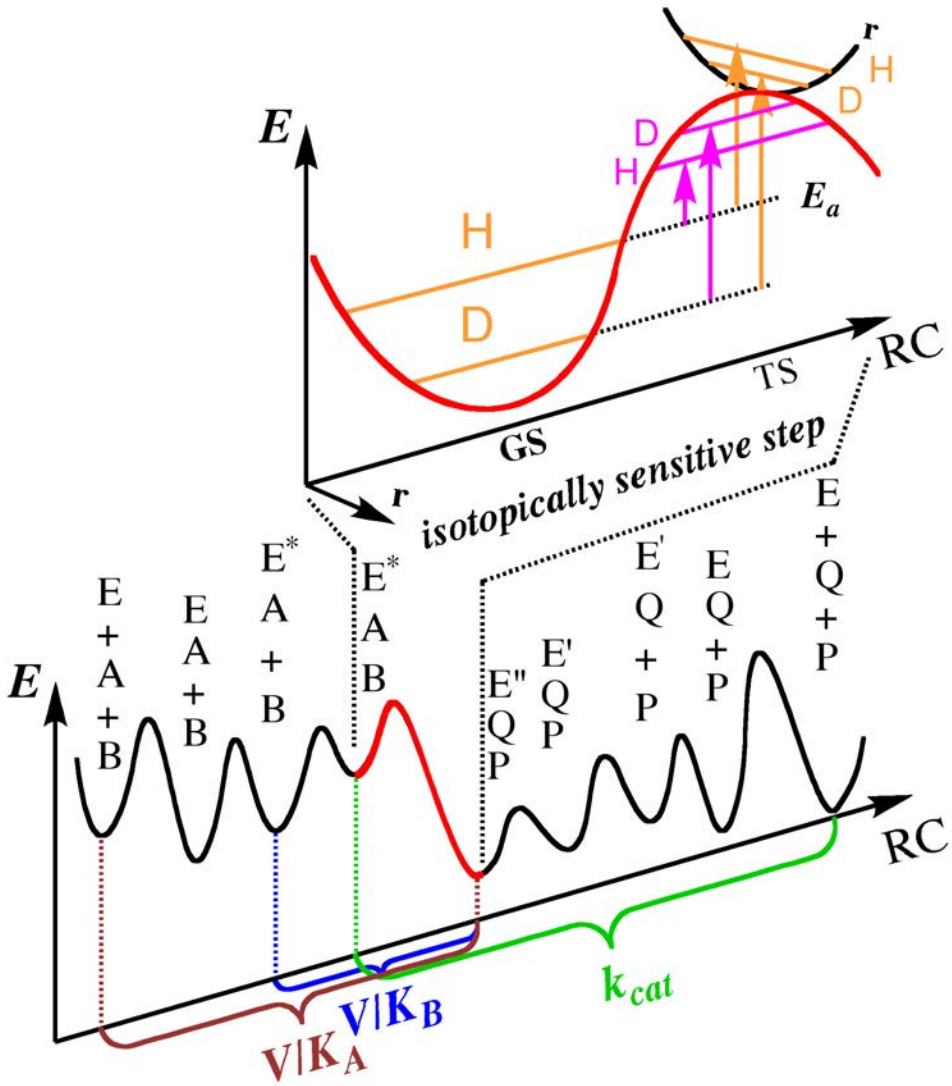

Figure 1-1. An example of enzymatic reaction mechanism with two substrates.

An enzyme catalyzed reaction involves many mechanistic steps along the reaction coordinate (RC), such as binding of the first substrate (A), binding of the second substrate (B), conformational changes of the enzyme (E → E*), chemical step (red, irreversible in this case), and release of products (P and Q), etc. KIEs can be measured either on the first-order rate constant (k_{cat}, or V, green), or on the second-order rate constant for A (V/K_A, brown) or B (V/K_B, blue). In most cases, the chemical step is not rate limiting for either V or V/K, and the kinetic complexity caused by slower steps diminish the observed KIE from its intrinsic value. The semi-classical models mostly ascribe intrinsic KIE to the change in activation energy (Ea) caused by different zero-point energy levels (orange) of isotopes in the ground state (GS) and transition state (TS).[33] Bell's correction approximates the tunnel effect by truncating the parabola of the reaction barrier (magenta).[34]

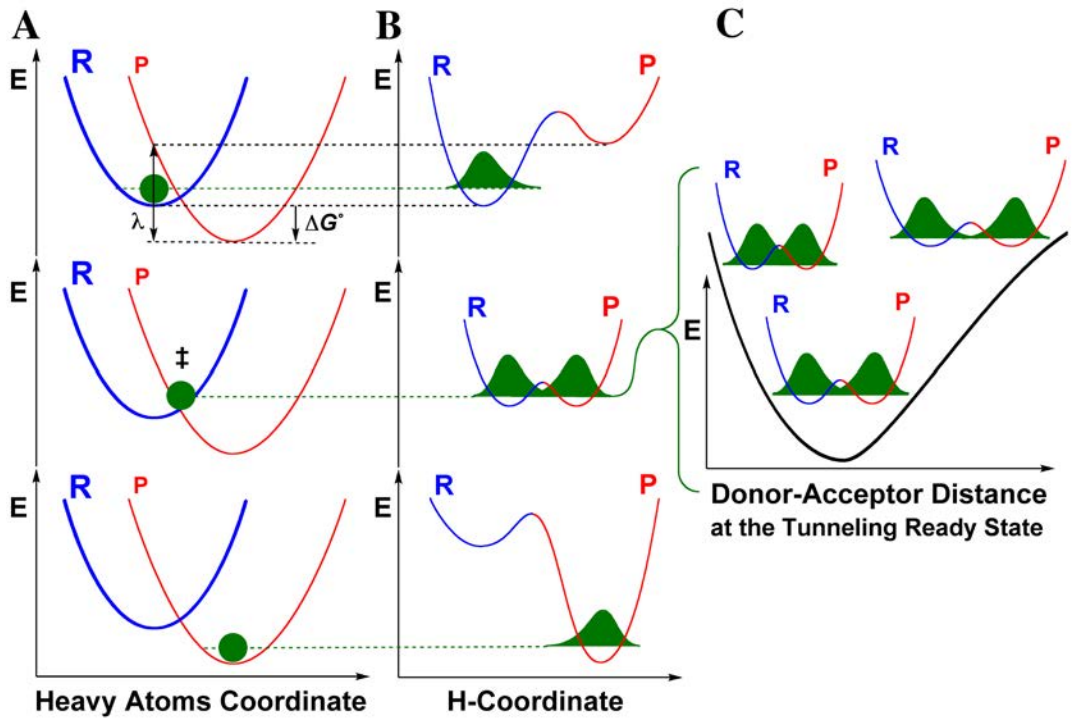

Figure 1-2. Marcus-like model for H-transfer reactions.

As an extension of the Marcus theory of electron transfer,[41] this model makes a Born-Oppenheimer-like separation between the fast hydrogen tunneling (on H-Coordinate, B) and the slower motions of the rest of the system (on Heavy Atoms Coordinate, A).[46,74] Enzyme motions could contribute to an H-transfer reaction by affecting pre- and re-organization of the protein environment, as well as the donor-acceptor distances (DADs) at the tunneling ready state (TRS, where the vibronic energies of the transferring hydrogen in the R and P states are degenerate[25,45,46]).

(A) The "preorganization" generates the diabatic states of the reactants (R, blue) and products (P, red) on the heavy atoms coordinate. The heavy atom "reorganization" brings the system (green) from the reactant state (top) to the TRS (middle, denoted by "‡"), and finally to the product state (bottom). The rate of reaching the TRS depends on the reorganization energy (λ) and the reaction's driving force (ΔG°).

(B) The double-well potential for H-tunneling is modulated by the heavy atom motions throughout the reaction. At a given DAD, the tunneling probability of H-nucleus is proportional to the overlap between the hydrogen wavefunctions (green) at the TRS.

(C) The heavy atom motions also generate a distribution of possible DADs at the TRS, which is assumed to follow Boltzmann distribution in most presentations of the Marcus-like model.[19,25,75] The assumption that all the functional motions of protein are in equilibrium agrees with most established theories. However, "protein promoting vibrations", which are not necessarily equilibrium dynamics, have also been proposed to contribute to the chemical steps.[17] The thermal fluctuation of DADs is the source for temperature dependence of KIE on the H-transfer.

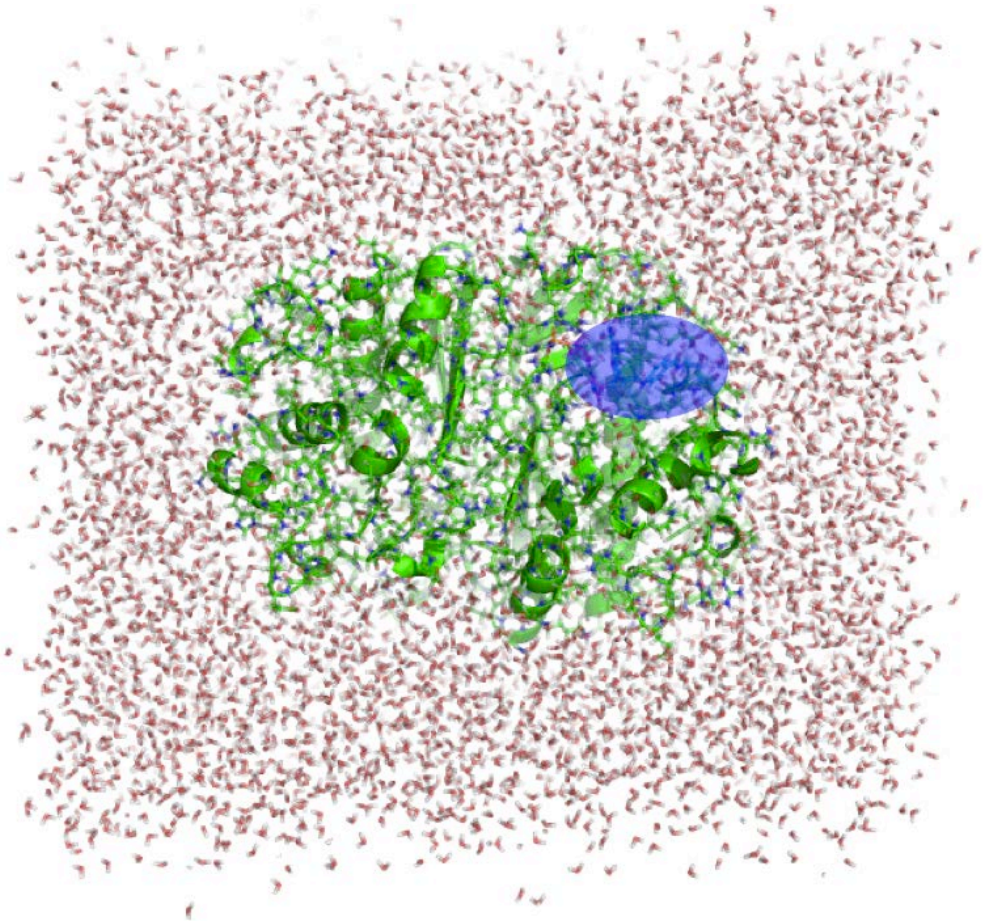

Figure 1-3. The model for QM/MM calculations of thymidylate synthase.

Escherichia coli TSase (green, PDB ID 1TLS) is solvated in a big water box for the hybrid quantum mechanical/molecular mechanical (QM/MM) calculations. Only the active site (blue) is treated with QM functions, and the rest of the system is simulated with MM method. More details are discussed in Chapter V.

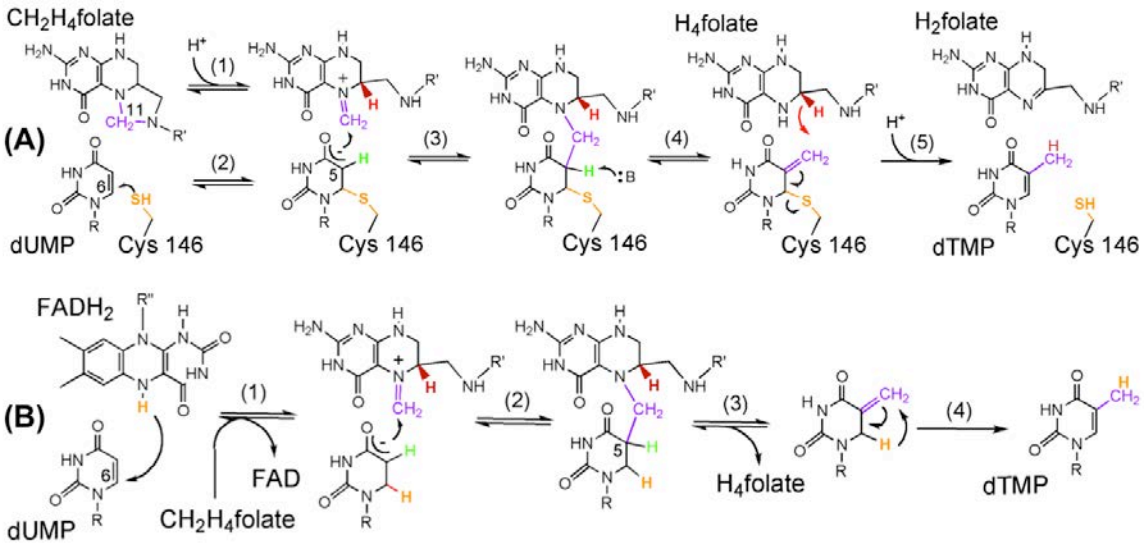

Figure 1-4. The proposed reaction mechanisms for classical TSase and FDTS.

Both TSase and FDTS catalyze the reductive methylation of 2'-deoxyuridine-5'-monophosphate (dUMP) to form 2'-deoxythymidine-5'-monophosphate (dTMP) using N^5,N^{10}-methylene-5,6,7,8-tetrahydrofolate (CH_2H_4folate) as a cofactor. However, their mechanisms are dramatically different. (R = 2′-deoxyribose-5′-phosphate; R′ = (p-aminobenzoyl)-glutamate; R″ = adenosine-5′-pyroposphate-ribityl.)

(A) In the proposed mechanism for TSase, Cys146 is the nucleophile that attacks C6 of dUMP to initiate the reaction. The reaction involves two C-H bond activation steps: a C-H→B proton abstraction from C5 of the nucleotide (step 4), and a C-H→C hydride transfer from C6 of the folate cofactor to the *in situ* formed methylene group of the intermediate (step 5).[61] This scheme describes the traditionally proposed mechanism for TSase, and our QM/MM calculations have provided new insights into this reaction (see Chapter V).[67,68]

(B) The FDTS-catalyze reaction does not require any protein residue as the nucleophile.[76] Compared with the reaction mechanism of TSase, the methylene group also comes from CH_2H_4folate, but the hydride comes from the flavin adenine dinucleotide cofactor (reduced form, $FADH_2$). The proposed mechanism involves a 1,3-hydrogen shift that is unique for FDTS in the pathway of intracellular thymidine synthesis.

CHAPTER II

THYMIDYLATE SYNTHASE CATALYZED H-TRANSFERS: TWO CHAPTERS IN ONE TALE

Introduction

While the last century brought us to a closer understanding of enzyme catalysis, the traditional "lock-and-key" model has been gradually replaced by the views of a more flexible active site. The dynamic nature of enzyme function can be viewed as extended "induced fit", which includes not only the conformational changes upon substrates binding, but also those along the reaction coordinate. This is addressed today as shifts between different populations of protein conformations that are induced by the change in characteristics of the ligands from the reactant to the product states.[14,15,77-79] It is now widely accepted that protein dynamics not only plays an essential role in substrate binding and product release, but is also substantial in promoting the chemical transformations catalyzed by the enzyme.[12,14-16,52,77-85] Although immense experimental and theoretical effort has been devoted to this field, the relationship between enzyme dynamics and catalysis still remains to be an unsolved question. Important insights to this question come from the recent studies on H-transfers in various enzymatic systems, using temperature dependence of the kinetic isotope effect (KIE).[82,83,85-90]

The Marcus-like Model (also addressed as environmentally-coupled tunneling, rate-promoting vibrations, vibrationally-enhanced tunneling, *etc.*)[47,48,82,83,85,87,88] is often used to correlate the KIE data with protein dynamics for enzyme catalyzed H-transfer reactions. In this model, hydrogen is transferred exclusively by quantum mechanical tunneling[13,34,52,82,85,87] and the reaction coordinate comprises two designated coordinates (Figure 2-1). The environmental reorganization coordinate (Q_1) is analogous to the nuclear reorganization coordinate in the Marcus theory (for electron transfer[41]), while the DHA coordinate (Q_2) represents the dimension along which H-tunneling occurs (where D

and A are the donor and the acceptor of H, respectively).[ii] The different forms of Marcus-like model can be summarized by the following equation:

$$k = C(\mathrm{T})e^{-(\Delta G^0+\lambda)^2/(4\lambda \mathrm{RT})}\int_{r_{\min}}^{r_{\max}} e^{F(m,r)}e^{-E_{F(m,r)}/k_B\mathrm{T}}dr \qquad (1)$$

where C(T) is the fraction of the reactive enzymatic complexes for the H-transfer step, sometimes addressed as "pre-orgnization".[iii] The first exponential corresponds to the environmental reorganization on Q_1, which overcomes the barrier that is determined by the reaction driving force (ΔG^0) and the reorganization energy (λ) to approach the tunneling ready state (TRS). The TRS is the ensemble of states along the Q_1 coordinate, where H tunnels between the donor and acceptor (the crossing point in Figure 2-1).[91] When the system is at TRS, H tunnels through the DHA barrier on Q_2, as represented by the integral term in Eq.1. In the integral, represents the hydrogen wave-function overlap between the reactant and the product states of a double-well potential (*i.e.*, a Franck-Condon term, see Figure 2-1), which determines the tunneling efficiency at a specific donor acceptor distance (DAD, denoted as r in Eq. 1). The DAD fluctuations that are commonly assumed to be at thermal equilibrium (*i.e.*, Boltzmann distribution,) determine the probability distribution of TRS ($r_{min}<r<r_{max}$). These DAD fluctuations are also addressed as "gating"[83] or "rate-promoting vibrations"[85,88]. It is noteworthy that, in Eq. 1, the integral is largely dependent on the mass of the transferring particle, and therefore is the dominant factor for KIEs and their temperature dependence. If the enzyme has evolved to optimize the active site for H-transfer, the TRS is believed to be

---

[ii] The DHA coordinate usually includes tens of atoms, as D and A represent all atoms directly involved in the H-transfer, rather than just the donor atom and acceptor atom of hydrogen.

[iii] "Pre-organization" samples various configurations of both the protein and substrates, and thereby determines the average ground-state energies of reactants and products (respectively the minima of the two parabola on Q_1 in Figure 2-1).

well defined (*i.e.* a narrow DAD distribution). In such case, thermal activation of the DAD fluctuations will have minimal effect on the difference in activation energies of the two isotopes, resulting in temperature-independent KIEs. A recent study on formate dehydrogenase with both KIE and time-resolved photon-echo experiments corroborates this suggestion.[36,92]

In this work we study thymidylate synthase (TSase, EC 2.1.1.45), which catalyzes the reductive methylation of 2'-deoxyuridine-5'-monophosphate (dUMP) to form 2'-deoxythymidine-5'-monophosphate (dTMP, one of the four DNA bases) using N^5,N^{10}-methylene-5,6,7,8-tetrahydrofolate (CH_2H_4folate) as both the methylene and hydride donor (Figure 2-5).[61] Since TSase is essential for the *de novo* synthesis of DNA in nearly all organisms including humans, it is a common target for many antibiotic and chemotherapeutic drugs (*e.g.* Tomudex and 5-fluorouracil). In addition to its important biological functions, the emerging large collection of structural and kinetic data of TSase has suggested an intriguing relationship between catalysis and dynamics,[62] which has initiated in-depth examinations of the mechanism from both experimentalists and theoreticians.[35,93-97] The mechanism of TSase comprises a series of bond cleavages and formations including two different C-H bond activations (Figure 2-5): a non-rate-limiting proton transfer (step 4) and a rate-limiting hydride transfer[35,98] (step 5). This provides an excellent model system to examine the physical nature of different C-H bond activations in one enzymatic reaction. Sequential H-transfers have been previously studied with two enzymes using noncompetitive KIE experiments. In the case of morphinone reductase (MR), the flavin cofactor on the enzyme permits convenient spectrophotometric measurements of the reaction rates of both the reductive half reaction (a C-H-N hydride transfer) and the oxidative half reaction (concerted N-H-C hydride and O-H-C proton transfers).[99] These studies of MR indicated that the first hydride transfer has temperature-dependent KIEs and the second hydride transfer has temperature-independent KIEs. In the case of the light-activated enzyme protochlorophyllide oxidoreductase (POR), the

electronically excited-state C-H-C hydride transfer is followed by a ground-state O-H-C proton transfer, and both steps showed temperature-dependent isotope effects at physiological temperatures.[100]

We have performed the competitive KIE experiments on both the proton and hydride transfers catalyzed by *Escherichia coli* Tsase (ecTSase), using specifically labeled C-H bonds of the substrates for that enzymatic reaction. We found that the proton transfer has temperature-dependent KIEs while the hydride transfer has temperature-independent KIEs. The results are discussed below within the framework of Marcus-like Model.

Results and Discussions

The examination on the sequential proton and hydride transfers in the TSase-catalyzed reaction requires different methods to expose the intrinsic KIEs. We have been able to access the temperature dependence of the intrinsic KIEs on both H-transfers, which allows us to compare the nature of these different C-H bond activations.

Intrinsic KIEs on the Non-rate-limiting Proton Transfer

One of the main challenges in enzyme studies is to expose and examine a chemical step that is not rate limiting within the complex catalytic cascade. While the hydride transfer is rate-limiting for both the first and second order rate constants (k_{cat} and k_{cat}/K_M, respectively) for dUMP,[35] the proton transfer is a reversible non-rate-limiting step and is more difficult to study. A previous study monitored the release of [^{3}H]H_2O and production of [^{14}C]dTMP using [2-^{14}C, 5-^{3}H]dUMP as the substrate with a saturating concentration of CH_2H_4folate, which reported a KIE of unity (*i.e.* no isotope effect) on the proton transfer.[101] We have suggested that the observed KIEs for the fast proton transfer are dependent on the concentration of CH_2H_4folate, due to the sequential binding of dUMP and CH_2H_4folate to the enzyme (Figure 2-6).[29,94] Thus, an accurate assessment

of the KIEs on the proton transfer requires optimal reaction conditions in which the concentration of CH_2H_4folate is high enough to ensure sufficient conversion of dUMP to dTMP while low enough to ensure that the observed KIEs will not be masked by the forward commitment to catalysis (see below).[82,102] We improved the competitive KIE methods previously developed in our lab (see Experimental Section), and measured observed H/T and D/T KIEs on the proton transfer. Figure 2-2A shows the observed and intrinsic KIEs on the proton transfer, and 2B the hydride transfer[35]. The intrinsic KIEs were calculated from the observed KIEs using the Northrop method (see Experimental Section). In contrast with the hydride transfer, the observed KIEs on the proton transfer are much smaller than the intrinsic KIEs, suggesting a "kinetic complexity" that masks the intrinsic KIEs on this step.[82,102]

Kinetic Complexity on the Non-rate-limiting Proton Transfer

The observed primary KIEs are usually smaller than the intrinsic ones, due to a kinetic complexity that masks the intrinsic KIEs. For the KIE on the second order rate constant (k_{cat}/K_M or V/K), which is the only KIE measured by the competitive method, this "kinetic complexity" can be described by Eq. 2:[102]

$$KIE_{obs} = \frac{k_L/k_H + C_f + C_r \cdot EIE}{1 + C_f + C_r} \tag{2}$$

where k_L/k_H is the intrinsic KIE as the ratio of the light (k_L) *vs*. heavy (k_H) isotopes for the isotopically sensitive step examined (k_5 in Figure 2-6); *EIE* is the equilibrium isotope effect; and C_f and C_r are the forward and reverse commitments to catalysis, respectively. For the proton transfer catalyzed by TSase, $C_r \approx 0$ since the tritium release is irreversible due to the dilution into ~110 M protons in water. Therefore, Eq. 2 can be simplified as Eq. 3:

$$KIE_{\text{obs}} = \frac{k_{\text{L}}/k_{\text{H}} + C_{\text{f}}}{1 + C_{\text{f}}} \tag{3}$$

and for Figure 2-6:

$$C_{\text{f}} = \frac{k_5\left(k_2 + k_3[\text{B}]\right)}{k_2 k_4} \tag{4}$$

It is apparent form Eqs. 3 and 4 that when the concentration of CH_2H_4folate (B) goes to infinity, C_f will go to infinity and the observed KIE will approach unity (no KIE). At low concentrations of CH_2H_4folate ([B] → 0), on the other hand, C_f will approach the finite value of k_5/k_4, *i.e.*, the ratio between the rate constants of the isotopically sensitive step and the dissociation of CH_2H_4folate from the Michaelis complex (EAB). Empirically, C_f can be calculated from the observed and intrinsic KIEs at each temperature. Figure 2-3 presents the forward commitment plotted *vs*. temperature. The linear Arrhenius plots for both H/T and D/T KIEs data suggest that one single kinetic step is responsible for most of the forward commitment for the proton transfer catalyzed by TSase.

Comparison of the Temperature Dependences of Intrinsic KIEs on the Proton and Hydride Transfers

The intrinsic KIEs on both the proton and hydride transfers were fit to the Arrhenius equation to evaluate their temperature dependences:[iv]

$$\text{KIE} = \frac{k_{\text{L}}}{k_{\text{H}}} = \frac{A_{\text{L}}}{A_{\text{H}}} \exp\left(-\frac{\Delta E_a}{\text{RT}}\right) \tag{5}$$

[iv] For KIE studies, Arrhenius equation and Eyring equation are equivalent, as the temperature factor will cancel out when taking the ratio of two rate constants (A_L/A_H is temperature independent and $\Delta E_a = \Delta\Delta H^{\ddagger}$).

where the subscripts L and H denote a light and a heavy isotope of hydrogen, respectively; k represents the microscopic rate constant of the isotopically sensitive step (step 4 for the proton transfer and step 5 for the hydride transfer in Figure 2-5, respectively), and ΔE_a is the difference in the activation energies of that microscopic step between the light and heavy isotopes; R is the gas constant and T is the absolute temperature. Therefore, the isotope effects on both the pre-exponential factors (A_L/A_H) and the activation energy (ΔE_a) can be accessed by fitting the intrinsic KIEs to Eq. 5 (Figure 2-2). The isotope effects on the Arrhenius parameters of both the proton and hydride transfers are summarized in Table 2-1. The intrinsic KIEs on the hydride transfer are temperature-independent, and the isotope effects on the pre-exponential factors are well above the semi-classical limits.[34,82,103] In contrast, the KIEs on the proton transfer are temperature-dependent and A_L/A_H's are much lower than the semi-classical limit.

Interpretation of the Results within the Framework of the Marcus-like Model

Several theoretical calculations and simulations have examined the temperature dependence of KIEs in various enzymes.[104-107] Although the details of the calculations and simulations are diverse, they agree on the basic notion that the temperature dependence of KIEs reflects how optimal the donor-acceptor geometry is for the H-transfer, or how well the enzyme "fine-tunes" this step. It is important to recognize that the phenomenological models do not replace or conflict with computer simulations at the molecular level. An excellent review explaining the complimentary nature and the relations between these approaches can be found in Ref 20. Here we interpret our results on TSase catalyzed H-transfers within the framework of Marcus-like model.[47,48,82,83,85,87,88]

As mentioned in the introduction section, the temperature dependence of KIEs is mainly determined by the Franck-Condon term and the DAD fluctuations along the Q_2

coordinate (the integral in Eq. 1, also see Figure 2-1). In many cases where the enzyme has evolved to optimize the ensemble of TRS geometries *via* environmental reorganization on Q_1, the integral in Eq. 1 is barely affected by thermal activation of the DAD fluctuations and the KIEs will be mostly temperature-independent. This observation has been reported for various wild-type (WT) enzymes with their natural substrates under physiological conditions.[35-38] If the reorganization is impaired (*e.g.* by mutation,[108] non-physiological conditions[37]), however, the enzyme will need to exploit the DAD fluctuation to sample the TRS-like geometries for efficient tunneling, leading to temperature-dependent KIEs.[v]

For an enzymatic reaction that involves two sequential C-H bond activations, it is not intuitive whether the enzyme would have evolved to optimize both steps or to optimize only a single step. One could expect that the non-rate-limiting step has been optimized and thus is a faster step, or the rate-limiting step has been optimized due to its direct effect on the turnover rate. Our studies with TSase exposed the temperature-dependent KIEs on the proton transfer step and the temperature-independent KIEs on the hydride transfer step, which suggests that the rate-limiting hydride transfer is better optimized than the fast proton transfer. This observation is in accordance with the studies of MR,[99] where the faster hydride transfer (in the reductive half reaction) has temperature-dependent KIEs while the slower hydride transfer (in the oxidative half reaction, which is concerted with a proton transfer) has temperature-independent KIEs. A reasonable interpretation of these findings would be that the same enzyme activates two

---

[v] As a disclaimer to the proposed theme, we wish to point out that the generality of this phenomenon is not yet clear, as only a limited number of enzymes have been studied at this level. Some recent studies have reported temperature-dependent KIEs for the presumed natural substrate under hypothesized physiological conditions,[99, 100] and temperature-independent KIEs with one substrate compared with temperature-dependent KIEs with a 15× faster substrate.[109] Furthermore, it is not always easy to ensure that the natrual substrates and physiological conditions *in vivo* are used for the experiments, and that the intrinsic KIEs have been fully extracted. Finally, one has to bear in mind that enzymes may not evolve to make the chemical reaction as fast as possible, but to best fit the metabolic needs of the organism.

C-H bonds using different physical features, such as different degrees of reorganization. The proton abstraction from C5 of dUMP requires little catalytic enhancement, and can be activated in solution by high pH and free thiolates (analogous to the proton transfer, see Experimental Section), whereas a non-enzymatic equivalent of the hydride transfer has never been observed. This suggests that the hydride transfer requires more enzymatic activation than the proton transfer. As the slowest step of the reaction, the hydride transfer directly limits the overall catalytic-efficiency of Tsase and thus might be under more direct evolutionary pressure to be optimized. A faster proton transfer, on the other hand, will not further enhance the catalytic turnover. Therefore, the enzyme may have evolved to "fine-tune" only the hydride transfer to better optimize the TRS geometries for that step.

Conclusions

We analyzed and compared the nature of two sequential H-transfers catalyzed by Tsase – a non-rate-limiting proton transfer and a rate-limiting hydride transfer. The temperature dependences of intrinsic KIEs on the two H-transfers are dramatically different, which suggests different activation mechanisms. Based on the Marcus-like model and in accordance with the findings of studies using computer simulations,[104-107] our results suggest that Tsase has evolved to optimize the active site better for the hydride transfer than the proton transfer. We hope the current findings will invoke theoretical calculations and high-level simulations that may reveal the molecular details of these two C-H activation steps. Since the detailed molecular mechanisms of both H-transfers are still not clear,[95,96] further investigation on these steps will discern the TRS features and may assist in rational drug design.

Experimental Section

Materials and Instruments

[2-^{14}C] dUMP (specific radioactivity 56 Ci/mol) and [5-^{3}H]-dUMP (specific radioactivity 13.6 Ci/mmol) were from Moravek Biochemicals. Ultima Gold liquid scintillation cocktail were from Packard Bioscience. Liquid scintillation vials were from Fisher Scientific. The WT TSase was expressed and purified following the published procedure.[110] We used an Agilent Technologies model 1100 HPLC system for all the purifications and analytical separations. All other materials were purchased from Sigma.

Experimental Details

Synthesis of [2-^{14}C, 5-^{2}H] dUMP (> 99.5% D)

[2-^{14}C, 5-^{2}H]-dUMP was prepared by adopting the method of Wataya and Hayatsu.[111-113] Briefly, 1 mM [2-^{14}C] dUMP was incubated in a D_2O solution (> 99.96% D) containing 1 M of $_{L}$-cysteine (pD = 8.8) at 37 °C. The complete deuteration (>99.5% D) was achieved after 7 days incubation, verified by ^{1}H NMR measurements. To ensure that no artifacts were induced during the incubation, a portion of the synthesized [2-^{14}C, 5-^{2}H]-dUMP was exchanged with H_2O back to [2-^{14}C] dUMP under the same conditions. The produced [2-^{14}C] dUMP was used for competitive H/T KIE experiments and replicated the observed H/T KIEs with commercial [2-^{14}C] dUMP. It is interesting to note that part of this synthesis is analogous to the TSase-catalyzed proton transfer (step 4 in Figure 2-5).

Competitive KIE Experiments on Proton Transfer (Step 4 in Figure 2-5)

In order to better expose the KIEs of this non-rate-limiting step, we modified the experiment conditions based on the previously developed method.[94] The experiments were performed in 100 mM tris(hydroxymethyl)aminomethane (Tris)/HCl buffer (pH 7.5,

adjusted at the desired temperature), at 5, 15, 25, and 35 ˚C. Each reaction mixture (final volume 1 ml) contained 50 mM $MgCl_2$, 1 mM EDTA, 5 mM formaldehyde, 25 mM DTT , 3 μM CH_2H_4folate, 0.9 Mdpm [5-^{3}H] dUMP, and 0.3 Mdpm [2-^{14}C] dUMP (for H/T KIE measurement) or [2-^{14}C, 5-^{2}H] dUMP (for D/T KIE measurement). At each temperature, the experiments were performed following the previously published procedure.[94] Two independent control experiments (minus enzymes) were performed to deduct the non-enzymatic effects. All the quenched samples were analyzed by RP HPLC separation and liquid scintillation counting (LSC) to obtain the observed KIEs, as described in previous publications.[35] All t_∞ time points were pooled together to provide more accurate average values.

The competitive observed KIEs were determined from three measured values—the fraction conversion (f), the ^{3}H/^{14}C ratio in the products ([^{3}H]H_2O and [^{14}C]dTMP) at each time point (R_t), and the ^{3}H/^{14}C ratio in the products at the infinity time point (R_∞):[82,103]

$$\mathrm{KIE} = \frac{\ln(1-f)}{\ln\left(1 - f \cdot \frac{R_t}{R_\infty}\right)} \tag{6}$$

The fraction conversion f was calculated by:

$$f = \frac{[^{14}\mathrm{C}]\mathrm{dTMP}}{[^{14}\mathrm{C}]\mathrm{dTMP} + [^{14}\mathrm{C}]\mathrm{dUMP}} \tag{7}$$

For quality control, Figure 2-4 presents an example of the observed KIEs (calculated from Eq. 6) as a function of f (calculated form Eq. 7) at 25 ˚C (the data are from 3 independent H/T experiments and 2 independent D/T experiments, with at least 4 KIE measurements per independent experiment). The KIEs do not show any upward or

downward trends as a function of *f* (most artifacts would result in such trends), suggesting that the results are reliable.

Intrinsic KIEs on Proton Transfer (Step 4 in Figure 2-5)

The intrinsic KIEs were calculated using the Northrop method:[82,102]

$$\frac{{}^{\mathrm{T}}(V/K)_{\mathrm{H}obs}^{-1}-1}{{}^{\mathrm{T}}(V/K)_{\mathrm{D}obs}^{-1}-1}=\frac{k_{\mathrm{T}}/k_{\mathrm{H}}-1}{\left(k_{\mathrm{T}}/k_{\mathrm{H}}\right)^{1/3.34}-1} \tag{8}$$

where ${}^{\mathrm{T}}(V/K)_{\mathrm{H}obs}$ and ${}^{\mathrm{T}}(V/K)_{\mathrm{D}obs}$ are the observed H/T and D/T KIEs, respectively; $k_{\mathrm{T}}/k_{\mathrm{H}}$ represents the reciprocal of the intrinsic H/T KIE. The intrinsic H/T KIE was solved numerically. All possible combinations of observed H/T and D/T KIEs were analyzed to get the intrinsic KIEs. All intrinsic KIEs were used to fit to the Arrhenius equation (Eq. 5) to evaluate the isotope effects on Arrhenius parameters and temperature dependence of KIEs. This analysis was carried out with KaleidaGraph (Version 4.03) as the least root-mean-square fit exponential regression. The Northrop method assumes ${}^{\mathrm{T}}K_{\mathrm{eq}}$ close to unity or that $C_{\mathrm{r}} \approx 0$,[102] and the validity of these assumptions for TSase has been discussed above and in Ref 94.

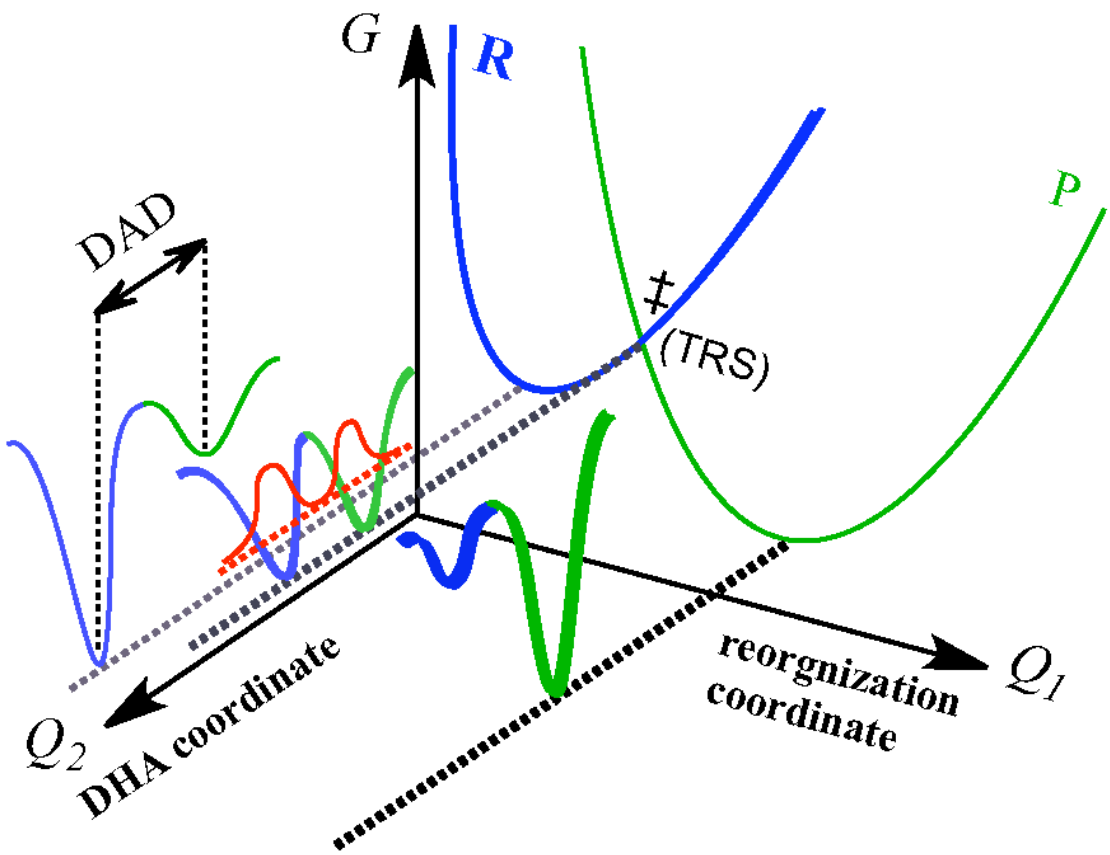

Figure 2-1. An alternative illustration of the Marcus-like model.

The blue and green curves correspond to the reactant and product states, respectively. The red curve represents the hydrogen wave-function overlap at tunneling ready state (TRS).

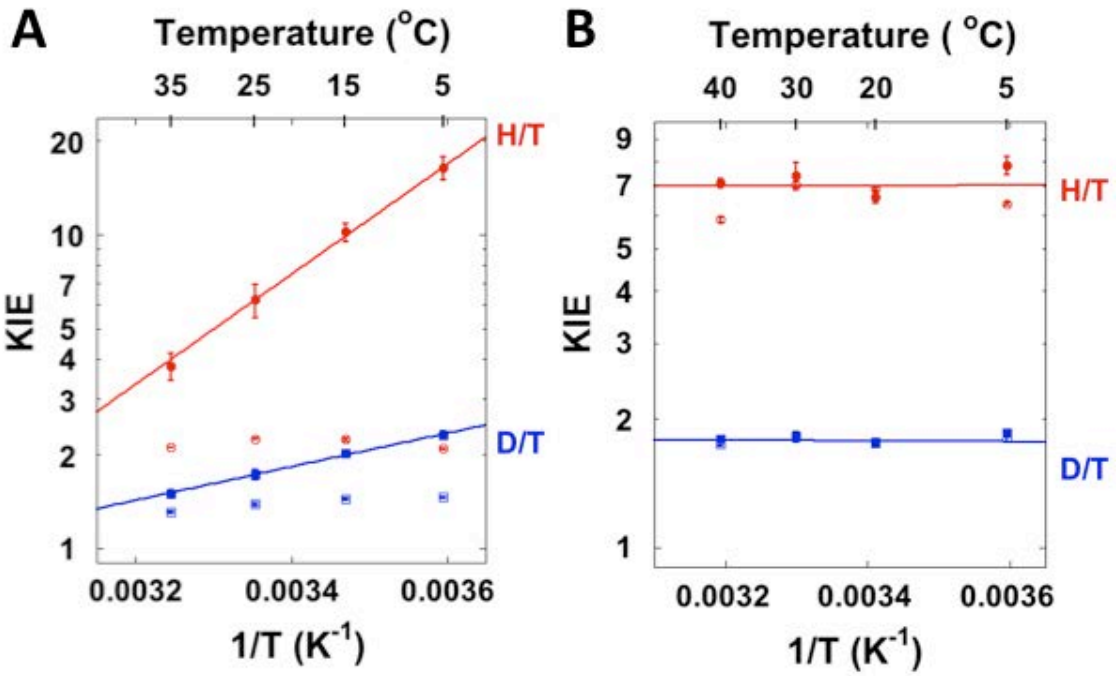

Figure 2-2. KIEs on the proton and hydride transfers catalyzed by WT ecTSase.

The Arrhenius plots of observed (empty structures) and intrinsic (filled structures) primary KIEs on the proton transfer (A) and the hydride transfer[35] (B) catalyzed by ecTSase. The KIEs are shown as average values and standard deviations, while the lines are the non-linear fittings of all calculated intrinsic KIEs to the Arrhenius equation.

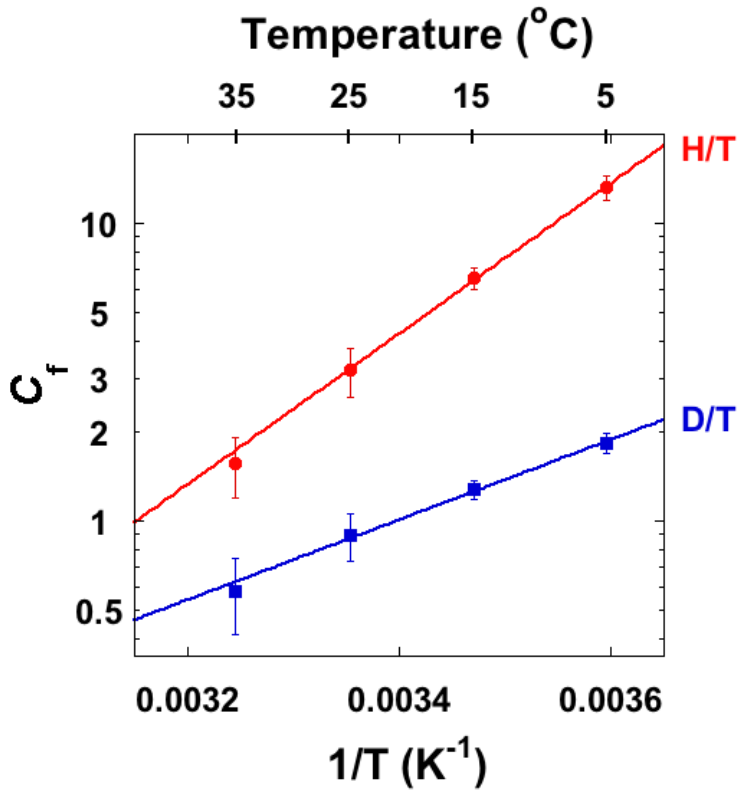

Figure 2-3. Kinetic commitment on the proton transfer in WT ecTSase.

The forward commitment (C_f) on the proton transfer step plotted on the logarithmic scale *vs*. the reciprocal of the absolute temperature. The data are presented as average values and standard deviations (red: H/T; blue: D/T). The lines are the exponential fittings of all calculated C_f values to the Arrhenius equation.

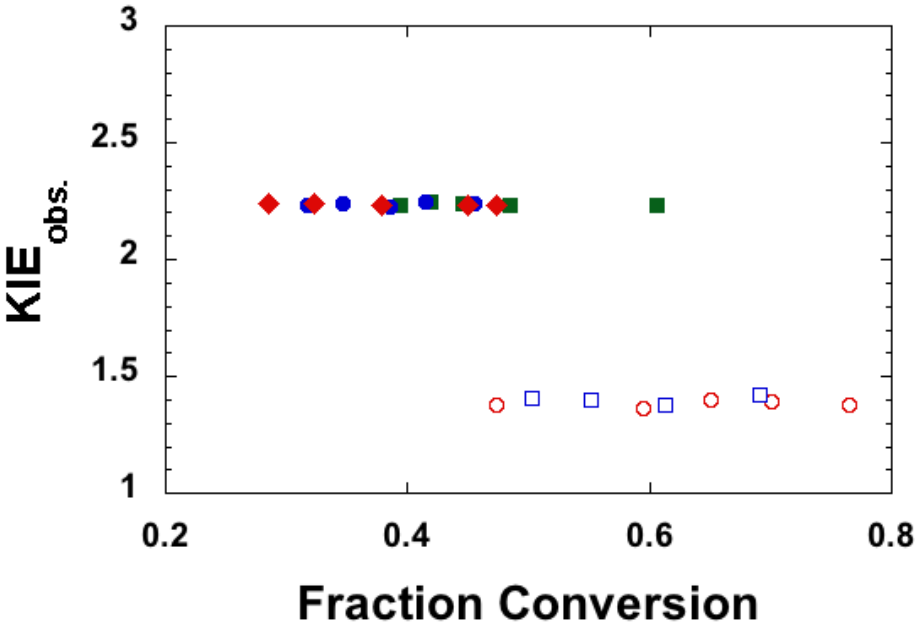

Figure 2-4. The observed KIEs *vs*. fraction conversion for the proton transfer in WT ecTSase.

The observed H/T (filled structures) and D/T (empty structures) KIEs plotted *vs.* fraction conversion as measured at 25 ˚C with 3 μM CH_2H_4folate. The different colors and shapes represent different independent experiments.

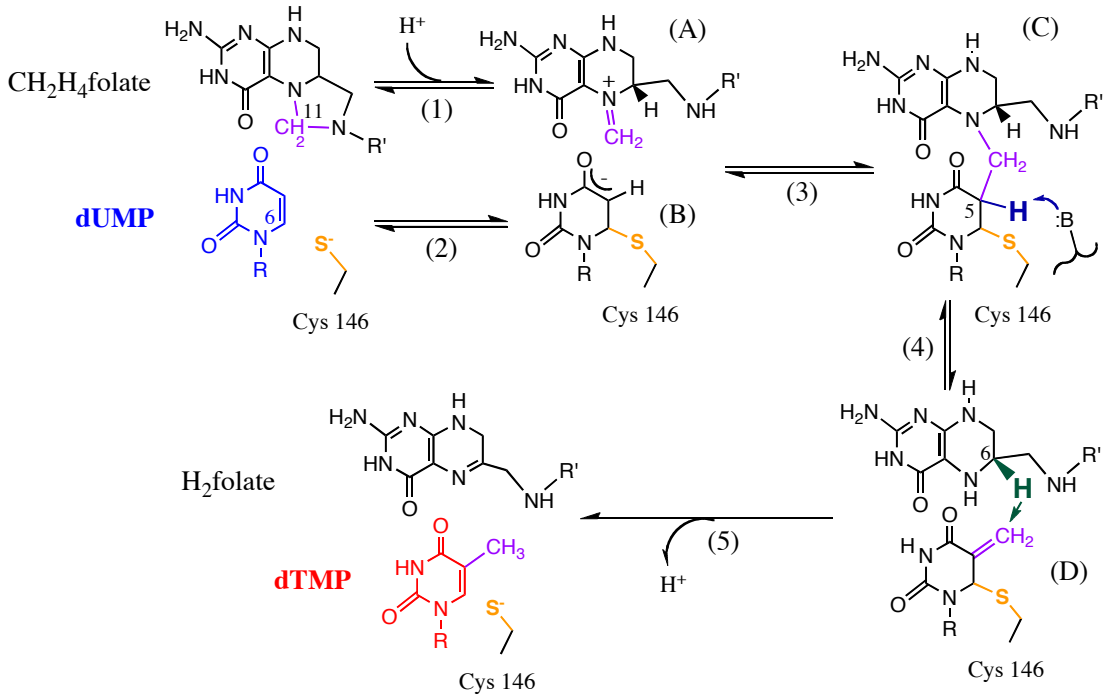

Figure 2-5. Chemical mechanisms of TSase-catalyzed reaction (proton vs. hydride transfers).

Proposed chemical mechanisms of TSase-catalyzed reaction (revised from Ref 61). R=2'-deoxyribose-5'-phosphate; R'=(*p*-aminobenzoyl)glutamate.

$$\mathbf{E} \underset{k_2}{\overset{k_1\mathrm{A}}{\rightleftharpoons}} \mathbf{EA} \underset{k_4}{\overset{k_3\mathrm{B}}{\rightleftharpoons}} \mathbf{EAB} \xrightarrow{k_5} \mathbf{EP} \xrightarrow{k_6} \mathbf{E{+}P}$$

Figure 2-6. A simplified kinetic scheme for WT ecTSase.

A represents dUMP and **B** CH_2H_4folate. The only isotopically sensitive step here is represented by the rate constant k_5.

Table 2-1. Isotope effects on Arrhenius parameters of ecTSase on the proton and hydride transfers.

	Proton Transfer	Hydride Transfer [35]	S.C. A_L/A_T [a]
A_H/A_T	$8.3\times10^{-6} \pm 1.0\times10^{-6}$	6.8 ± 2.8	0.5 – 1.6
A_D/A_T	$2.8\times10^{-2} \pm 0.1\times10^{-2}$	1.9 ± 0.3	0.9 – 1.2
$\Delta E_{a\ \mathrm{H\text{-}T}}$ [b]	-8.0 ±0.1	0.02 ± 0.25	
$\Delta E_{a\ \mathrm{D\text{-}T}}$ [b]	-2.44 ±0.03	-0.04 ± 0.08	

Notes:

[a] Semi-classical limits of isotope effects on the preexponential factor [34,82,103]

[b] The differences in activation energies in the unit of kcal/mol.

CHAPTER III

A REMOTE MUTATION AFFECTS THE HYDRIDE TRANSFER BY DISRUPTING CONCERTED PROTEIN MOTIONS IN THYMIDYLATE SYNTHASE

Introduction

Enzyme catalysis has been a focus of biochemistry research due to its importance in multiple disciplines such as life science, clinical research, and bioengineering. While the views for enzyme-substrate interaction have developed from Fischer's "lock-and-key" model to Koshland's "induced fit" model, Pauling's transition state (TS) stabilization theory remains to be the most recognized principle for the chemical rate enhancement by enzymes. In the past few decades, the advanced experimental and computational techniques unraveled structural and dynamic features of numerous enzymes, allowing researchers to seek for the physical origin of "TS stabilization". This investigation has led to an emerging hypothesis that extends the "induced fit" model and proposes that motions of protein, solvent, and substrates are an important component in a full description of enzyme-catalyzed reactions. Although immense work has examined this hypothesis, it has been most challenging to experimentally illustrate the impacts of protein motions at various timescales on a chemical bond activation step within a complex enzymatic mechanism.

For the examination of enzyme-catalyzed H-transfer reactions, a useful technique is the temperature dependence of kinetic isotope effects (KIEs).[13,19,25-27,52,85,87,105,114-118] The analysis of the temperature dependence (or independence) of KIEs has stimulated the development of various phenomenological models, often summarized as the Marcus-like model (or environmentally-coupled tunneling, protein-promoting vibrations, vibrationally-enhanced tunneling, *etc.*).[17,19,20,25,27,40,45-48,52,118] The readers are referred to Figure 1-1 for more detailed description of this model. Briefly, this model designates

three categories of protein motions that contribute to an enzymatic H-transfer. First, conformational fluctuations of the protein create a favorable environment for formation of the "reactive complexes" for the chemical step. This effect has been previously addressed as "preorganization",[19,50-52,119] and occurs on the second to submillisecond timescales.[vi] At this ensemble of reactive complexes, faster motions of protein, solvent, and ligands (*e.g.* on the nanosecond to picosecond timescales) constitute the "reorganization" of the active site that assists the structural changes in the substrates going from the reactant state to the tunneling ready state (TRS). At the TRS, the fluctuation of donor-acceptor distance (DAD) affects the H-tunneling probability (Figure 1-1). While the DAD fluctuation at TRS determines the magnitude and temperature dependence of the intrinsic KIE, pre- and re-organization affects the rate of the H-transfer and thus the "kinetic commitment" factor in the experimental exposure of KIEs.[29,102] Previous experiments have found temperature-independent KIEs on H-transfer reactions in various wild type (WT) enzymes. These observations suggest the pre- and re-organization of the active site allows the system to reach a well-defined TRS for the H-transfer, which is characterized by a short and narrow DAD distribution.[19,39,40,91,120,121]

In this work we examine the relationship between structure, motions, and reactivity in the enzyme thymidylate synthase (TSase, EC 2.1.1.45) from *E. coli*. This enzyme catalyzes the last step of *de novo* synthesis of 2'-deoxythymidine-5'-mono-phosphate (dTMP) by reductive methylation of 2'-deoxyuridine-5'-monophosphate (dUMP), using (6*R*)-N^5,N^{10}-methylene-5,6,7,8-tetrahydrofolate (CH_2H_4folate) as a cofactor (Figure 3-7).[61] Since dTMP is one of the four DNA nucleotides, TSase is medicinally important as a common target for many antibiotic and chemotherapeutic drugs (*e.g.* Tomudex and 5-fluorouracil). In addition, the large collection of structural and

---

[vi] Preorganization includes all the kinetic steps that lead to formation of the reactive complex. In the current context, it includes the lifetime of the intermediate prior to the H-transfer step, *i.e.* the conformational fluctuations that bring the H-donor to the vicinity of the H-acceptor.

kinetic data of TSase suggested that certain protein residues move synergistically during the catalytic cascade.[62,63] These findings have initiated in-depth examinations of its molecular mechanisms by both experimentalists and theoreticians.[35,64,93-97,122-124] Our previous studies found a temperature-independent KIE on the hydride transfer of WT ecTSase,[35] suggesting the enzyme has evolved to bring the H-donor and acceptor to a well reorganized TRS. This interpretation has been supported by recent quantum mechanics/molecular mechanics (QM/MM) calculations.[96,122-124]

Here we employ both X-ray crystallography and kinetic measurements to study the impacts of protein motions at various timescales on the hydride transfer reaction. A highly conserved tyrosine residue (Y209 in ecTSase) forms one of only two H-bonds with the ribose ring of dUMP, which is remote from the chemical reaction site in ecTSase (Figure 3-7). The crystal structures of the WT and Y209W ternary complexes with dUMP and an analogue of the cofactor, CB3717 (PDB IDs 2G8O and 2G8M, respectively), closely overlapped at a resolution of 1.30 Å.[97] The most conspicuous difference between those two structures was in their anisotropic B factors, which revealed that the atomic vibrations of active site residues are highly correlated in the WT but not in the mutant crystals. This analysis indicated a dynamic effect[vii] that may account for the significantly reduced activity.[97] However, the kinetic experiments preformed in Ref 97 did not identify which specific catalyzed step(s) is/are affected by the mutation. The current study extends the examination of the structural and kinetic properties of this mutant, and compares the temperature dependence of KIEs on the WT- and Y209W-catalyzed hydride transfer reactions. The correlation between the structural and kinetic data allows us to distinguish the mutational effects on protein motions at various timescales that influence the hydride transfer reaction and other catalytic steps.

[vii] Here we do not distinguish "dynamics" as nonequilibrium or nonstatistical dynamics. Thus, the "dynamic effect" simply means the influence of motions of the protein, solvent, and ligands.

Results and Discussions

Trapped Reaction Intermediate (Complex D)
— Impaired "Preorganization"

Previous studies of Y209W employed ß-mercaptoethanol (ß-ME) to preserve a reducing environment in the reaction mixture. Our experiments under the same conditions yielded a new peak in the HPLC analysis of the reaction mixture (Figure 3-5). To investigate the origin of the new peak, we exploited radiolabeled reactants to study this side reaction. When [2-^{14}C]dUMP and [6*R*-^{3}H]CH_2H_4folate were used, the new by-product contained ^{14}C but no ^{3}H radioactivity; and when non-radioactive dUMP and [11-^{14}C]CH_2H_4folate were used, it contained ^{14}C radioactivity. This indicates that the by-product is formed after the methylene transfer (step 4 in Figure 3-7) but before the hydride transfer (step 5). Replacing ß-ME with dithiothreitol (DTT) shifted the elution time of the new peak on the HPLC chromatograph (Table 3-6), indicating the by-product contained the thiol reagent. LC-MS analyses of the samples revealed that the molecular weight of the material was 397 or 473 when ß-ME or DTT was used, respectively, which agree with the structures of 5-(2-hydroxyethyl)thiomethyl-dUMP (HETM-dUMP) and the corresponding DTT-derivative (Figure 3-8). These observations suggest the by-products are formed by nucleophilic attack of the thiols at C7 of the exocyclic intermediate (Complex D in Figure 3-7). This finding indicates that both ß-ME and DTT can diffuse into the active site of Y209W and compete with the hydride donor for the hydride acceptor.

In order to evaluate the integrity of the active site of Y209W, we used a few other thiols of different sizes (Figure 3-8) to compare their ability to access the ternary complex prior to the hydride transfer (Table 3-1). The results suggest that this ability is influenced by the size, hydrophilicity, polarity and flexibility in the structure of the thiol reagent. Particularly, the smallest reagent ß-ME is the most favorable thiol to trap the

intermediate. DTT traps almost equal amount of the intermediate with ß-ME despite its larger molecular size than all other thiols, probably owing to extra hydrophilic groups in its structure that form favorable interactions with the active site environment. L-cysteine does not trap the intermediate at a detectable level, probably due to the strong polarity and rigidity in its structure that hinder its ability to diffuse into the active site.

Prior to the current study, only mutations close to the reaction site, *i.e.*, on residues W82 and V316 (C-terminus) in *L. Casei* TSase (equivalent to residues W80 and I264 in ecTSase) have been reported to produce HETM-dUMP.[125-127] W80 interacts with L143 and orients the latter to seal the active site cavity, and I264 interacts with the cofactor and is crucial for the ternary complex formation.[62,63,93] Being farther from the hydride transfer site, the effect of Y209 on the solvent-accessibility of the exocyclic intermediate is not trivial. However, DTT can trap 70% of the exocyclic intermediate in Y209W but only an insignificant amount in W80M,[93] suggesting that the reactive complex prior to the hydride transfer is less stable in the former. The formation of thiol-trapped intermediates suggest that the Y209W mutation deteriorates the ability of the enzyme to preorganize the active site for the hydride transfer, which significantly reduces the hydride transfer rate and thus the overall activity of the protein.

Steady-State Kinetics and Activation Parameters

Due to the formation of HETM-dUMP, the presence of ß-ME in the previous experiments[97] has distorted the measured kinetic data of Y209W. Thus, we employed a non-thiol reducing agent, tris(2-carboxyethyl)phosphine (TCEP),[128] to ensure accurate measurements of the kinetic parameters of Y209W. Similar to the WT TSase,[35] the activity of Y209W is inhibited by high concentrations of the cofactor CH_2H_4folate (Figure 3-1). The concentration of the substrate dUMP was kept constant close to saturation, and the data at each temperature were fit to the non-linear Michaelis-Menten equation with substrate inhibition (Figure 3-1A):[35,129]

$$\frac{v}{[\mathrm{E}]_\mathrm{t}} = \frac{k_{cat}[\mathrm{S}]}{K_m^{\mathrm{CH_2H_4folate}} + [\mathrm{S}]\left(1 + [\mathrm{S}]^2 / K_I^{\mathrm{CH_2H_4folate}}\right)} \tag{1}$$

where $[\mathrm{E}]_\mathrm{t}$ is the total enzyme concentration; [S] is the concentration of CH_2H_4folate; $K_m^{\mathrm{CH_2H_4folate}}$ and $K_I^{\mathrm{CH_2H_4folate}}$ are the Michaelis constant and the inhibition constant of CH_2H_4folate, respectively. We also measured the Michaelis constant of dUMP (K_m^{dUMP}) at 25 ˚C (Figure 3-6).

Table 3-2 compares the kinetic parameters of the WT and Y209W TSase with ß-ME or with TCEP at 25 ˚C. In contrast to our previous study of Y209W with ß-ME,[97] the data with TCEP indicate a larger effect on $K_m^{\mathrm{CH_2H_4folate}}$ than on K_m^{dUMP} (the last column of Table 3-2). This discrepancy probably arises from the presence of ß-ME in the previous experiment, which complicated the observed kinetics of Y209W as discussed earlier. The new observation agrees with previous findings for other Y209 mutants (F, M, and A),[97] and suggests that although Y209 only forms H-bond with dUMP, mutations on this residue lead to a non-local effect on the interactions with CH_2H_4folate. Based on our new kinetic data, the Y209W mutation causes about 500-fold decrease in k_{cat}, and more than 2000-fold and 7000-fold decrease in k_{cat}/K_m's for dUMP and CH_2H_4folate, respectively. The values of k_{cat}, $K_m^{\mathrm{CH_2H_4folate}}$, and $K_I^{\mathrm{CH_2H_4folate}}$ at different temperatures are summarized in Table 3-7. The activation parameters of the initial velocities are summarized in Table 3-3. Compared with the WT enzyme, the Y209W mutation mainly affects $\Delta H^{\ddagger}$ of k_{cat} in the lower temperature range (5-25 ˚C, see Figure 3-1B and Table 3-3). The temperature dependence of k_{cat} changes above 25 ˚C (i.e., k_{cat} at 35 ˚C is higher than the extrapolation from the lower temperature range), which agrees with the change in the rate-limiting step revealed by the KIE experiment below.

KIE on the Hydride Transfer Step

— Effects on the "Reorganization" and TRS

We used the competitive H/T and D/T method[29,30,102,118] to measure the H/T and D/T KIEs on the second order rate constant, k_{cat}/K_M with Y209W in 5-35 ˚C. The observed KIEs follow the Swain-Schaad relationship at 5 and 25 ˚C (Table S4), indicating that hydride transfer is rate limiting in the 5-25 ˚C temperature range, and the intrinsic KIEs are the same with the observed values at each temperature.[29,30,102,118] Thus, the higher $\Delta H^{\ddagger}$ of k_{cat} (*vs*. WT TSase) in this temperature range suggests the Y209W mutation increases the reorganization energy for the hydride transfer.[19,50-52,119] At 35 ˚C, the observed KIEs do not follow the Swain-Schaad relationship, and we used the Northrop method to extract the intrinsic KIEs from the observed values.[29,102] The observed KIEs being smaller than their intrinsic values indicates that the hydride transfer is not rate limiting at that temperature due to kinetic complexity.[29,30,102,118] These data corroborates the steady state kinetic data in the previous section that suggested a change in the kinetics between 25 ˚C and 35 ˚C. Since hydride transfer is not rate limiting for Y209W at 35 ˚C, the significant increase in both $\Delta H^{\ddagger}$ and $\Delta S^{\ddagger}$ of k_{cat} at this temperature (Table 3-3) suggests that the mutation also affects other kinetic steps during the catalytic turnover.

Figure 3-2 shows the temperature dependence of intrinsic KIEs on the WT- and Y209W-catalyzed hydride transfers, and the observed KIEs for the mutant at 35 ˚C. The intrinsic KIEs were fit to the Arrhenius equation:

$$\mathrm{KIE} = \frac{k_{\mathrm{L}}}{k_{\mathrm{T}}} = \frac{A_{\mathrm{L}}}{A_{\mathrm{T}}} \exp\left(\frac{-\Delta E_a}{\mathrm{RT}}\right) \tag{2}$$

where the subscripts L and T denote the light isotope (H or D) and the heavy isotope (T) of hydrogen, respectively; k is the microscopic rate constant of the isotopic sensitive step

(the hydride transfer step in this case), and ΔE_a is the difference in the activation energies of that microscopic step between the light and heavy isotopes ($\Delta E_a = E_{aL} - E_{aT}$); A_L/A_T is the isotope effect on the pre-exponential Arrhenius parameter; R is the gas constant and T is the absolute temperature. Table 3-4 summarizes the H/T isotope effects on the Arrhenius parameters of both the WT- and Y209W-catalyzed hydride transfers (H/T, D/T, or H/D isotope effects refer to the same effect and follow the same trend).

Compared with the WT enzyme, the KIE on the hydride transfer of Y209W is more temperature-dependent with slightly larger magnitude in the 5-35 ˚C temperature range, leading to a smaller isotope effect on the pre-exponential parameter (A_L/A_T). However, A_H/A_T is still above the semi-classical limit (Table 3-4), suggesting that Y209W-catalyzed hydride transfer also occurs predominantly *via* quantum mechanical tunneling.[27,30,82,118] Based on the Marcus-like models, these observations suggest that although the mutation is remote from the reaction site, the altered structural and dynamic properties of the mutant slightly change the DAD distribution at the TRS. In contrast, although the active site mutation W80M also produces HETM-dUMP, it shows no effect on the hydride transfer KIE.[39] This further suggests the Y209 residue is connected to the hydride transfer site through a long range of interactions that are important for the hydride transfer.

Dynamic Effects of the Y209W mutation
— Structural and Kinetic Evidence United

To elucidate the structural origin of the observed kinetic effects presented above, we carefully investigated the previously published electron density maps of the WT and Y209W ternary complexes (PDB IDs 2G8O and 4GEV, Figure 3-3),[97] and performed new refinement of the latter. Here we only focus on new perspectives on the structural data in the context of observed kinetics in the current study. For a complete discussion on the crystal structures of various Y209 mutants, we would refer the reader to Ref 97.

Our previous studies showed that the crystal structure of the Y209W-dUMP-CB3717 complex is remarkably similar to the WT ternary complex with the same ligands (Figure 3-3). The difference electron density map of those two structures suggests that several residues exist in two conformations in Y209W, including R127' (R127 from the other subunit of the protein), L143, and C146. The C146 residue is the active site sulfhydryl that nucleophilically attacks the C6 position of dUMP to initiate the catalyzed reaction (Figure 3-7), and its additional conformation in Y209W cannot form this important covalent bond with dUMP (Figure 3-3B). The additional conformation of R127' places its side chain away from the active site, which could allow the reactive thiols to diffuse into the active site to access the reaction intermediate. A previous study with W80G proposed two mechanisms for the formation of HETM-dUMP:[127] (1) the mutation causes premature release of H_4folate, allowing ß-ME to diffuse into the active site and react with the intermediate; or (2) the active site of the W80G mutant is large enough to accommodate ß-ME in addition to H_4folate and the dUMP exocyclic intermediate. The W80G-dUMP-CB3717 crystal structure showed that the L143 side chain is exclusively in a conformation that impinges on the space occupied by the W80 side chain in WT TSase, which exposes the C7 of the exocyclic intermediate to bulk solvent.[127] In contrast, the alternate conformation of L143 in Y209W is similar to its conformation in the WT enzyme, and is only occupied 30% of the time (Figure 3-3A). Although the alternate conformation of R127' expands the active site cavity of Y209W, the residues around the hydride transfer site almost perfectly overlap with their conformations in the WT enzyme, which would not allow coexistence of a thiol and H_4folate around C7 of the exocyclic intermediate. Therefore, it is more probable that the Y209W mutation causes premature release of the H_4folate (*i.e.* hydride source), after which the reactive thiol can attack C7 of the exocyclic intermediate (*i.e.* hydride acceptor). Regardless of the exact mechanism of thiol attacking, the additional conformations of those three residues agree with our kinetic data that suggested a

decreased fraction of the reactive complex, *i.e.* deteriorated "preorganization", for the hydride transfer in Y209W.

The other observable difference in the Y209W ternary complex is that the dUMP phosphate-binding loop (residues 19-25 in ecTSase) shifts 1.0 ± 0.2 Å away from the active site, which is accompanied by higher normalized isotropic B factors in both this loop and dUMP (Figure 3-4).[97] This observation indicates that both the substrate and the phosphate-binding loop are more mobile in the Y209W mutant. Crystal structures of the WT TSase suggested the phosphate-binding loop progressively closes towards the active site and becomes more rigid as the substrate and cofactor bind to the enzyme.[62] Particularly, the highly conserved R21 residue in this loop not only forms H-bond with the phosphate group of dUMP, but also interact with both I264 and L143 (Figure 3-3). Consequently, the mutational effect on the location and mobility of this loop can propagate to the opposite wall of the active site cavity, leading to a "global" impact on the active site. Analysis of the anisotropic B factors revealed that in the WT TSase-dUMP-CB3717 complex, the atomic vibrations of active site residues are highly correlated with each other and, to a less extent, with the ligands, suggesting the protein residues can move concertedly (*i.e.* rigid-body vibrations) during the structural changes in the ligands.[97] In contrast, the atomic vibrations in the Y209W-dUMP-CB3717 complex are much less correlated in several protein segments including the phosphate-binding loop, the C terminus, and the loop containing L143 and C146 (Figure 3-4).

Taken together, our structural and kinetic data indicate the Y209W mutation impairs the hydride transfer by affecting both the conformational fluctuations of specific active site residues, and the rigid-body vibrations of several protein segments that align the active site cavity. These altered protein motions are likely to occur at different timescales and have different activation parameters, which can explain the curvature in the Eyring plot of k_{cat} in Y209W. The Y209W mutation perturbs the location and mobility of the phosphate-binding loop, where R21 propagates these effects to the C146-

containing loop and the C-terminus that are closer to the hydride transfer reaction site. This long range of interactions can explain the unusual kinetics observed in Y209W, such as the reaction intermediate trapped by thiols, and a larger increase in $K_m^{\mathrm{CH_2H_4folate}}$ than in K_m^{dUMP}. Furthermore, the rigid-body vibrations of the protein segments in the WT TSase ternary complex have very small amplitude (*ca*. 0.1 Å), indicating very high frequency that is on the timescale (picosecond) of the proposed reorganization motions in the Marcus-like model (Figure 1-1). Therefore, those rigid-body vibrations may contribute to the heavy atom reorganization that "optimize" the TRS for the hydride transfer in the WT TSase. The disruption of those vibrations in the Y209W mutant suggests defective heavy atom reorganization that generates a slightly different TRS, where the DADs are longer and/or the DAD distribution is wider, leading to marginally temperature dependent KIEs with larger magnitude (Figure 3-2 and Table 3-4).

Conclusions

Whether and how enzyme motions contribute to chemical bond activations is an important contemporary question in enzymology. Mutations remote from the chemical reaction site are of particular interest in addressing this question, since their effect usually requires structural and dynamic perturbations through a long range of interactions in the protein-ligands complex. A "dynamic network of coupled motions" has been proposed for dihydrofolate reductase (DHFR) based on NMR relaxation experiments, genomic analysis, and QM/MM calculations.[23,130-132] This proposal was substantiated by a couple of remote mutations that altered the temperature dependence of the hydride transfer KIE.[108] Recent studies also reported several remote mutations that affected the chemical bond activations catalyzed by human purine nucleoside phosphorylase[133,134] and soybean lipoxygenase-1[135]. The current study integrates kinetic data with high-resolution crystal structures and anisotropic B-factors to analyze the effects of protein motions on different aspects (*e.g*. pre- and re-organization, and H-tunneling at the TRS) of a C-H→C transfer

in a complex catalytic cascade. Our experiments with various thiols trapped the reaction intermediate prior to the hydride transfer in a remote mutant of ecTSase, Y209W. This suggests the mutation deteriorates the protein's ability to preorganize the active site for the hydride transfer, which is further supported by additional conformations of several active site residues in its crystal structure. The poorly preorganized protein environment causes higher penalty of reorganization energy for the hydride transfer, as revealed by our steady state and KIE experiments. Some rigid-body vibrations in the WT crystal structure are lost in the mutant, suggesting potential contribution of these high frequency motions to the reorganization of protein environment for the hydride transfer. The marginal changes in the temperature dependence of hydride transfer KIE implicates slightly altered protein motions that modulate the DADs at the TRS. The remote location of the current mutation and the high structural similarity of its ternary complex to the WT enzyme spotlight the alteration of enzyme dynamics and their role in disrupting mechanistic and kinetic aspects, including the chemical conversion itself. These observations agree with our predictions from QM/MM calculations that some concerted protein motions in ecTSase can enhance the hydride transfer step.[122-124] Future investigations on these concerted motions can examine the possibility of a "dynamic network" for TSase catalysis, and may provide new insights for rational drug designs that target TSase. In addition, these new findings provide another piece of the grand puzzle describing the relationship between motions and chemical reactivity in enzymes.

Experimental Section

Materials and Instruments

[2-^{14}C] dUMP (specific radioactivity 53 Ci/mol) was from Moravek Biochemicals. [^{3}H]$NaBH_4$ (specific radioactivity 15 Ci/mmol) was from American Radiolabeled Chemicals. [^{2}H]$NaBH_4$ (> 99.5% D) was from Cambridge Isotopes. Unlabeled CH_2H_4folate was a generous gift from EPROVA (Switzerland). Ultima Gold

liquid scintillation cocktails were from Packard Bioscience. Liquid scintillation vials were from Research Products International Corp. [2-^{3}H]iPrOH and [2-^{2}H]iPrOH were prepared by reduction of acetone with [^{3}H]$NaBH_4$ and [^{2}H]$NaBH_4$, respectively.[136] Dihydrofolate (H_2folate) was synthesized using Blakely's method.[137] The WT[110] and Y209W[97] ecTSase enzymes were expressed and purified following the previously published procedures. All other materials were purchased from Sigma. The steady state kinetic experiments were performed using a Hewlett-Packard Model 8452A diode-array spectrophotometer equipped with a temperature-controlled cuvette assembly. All the purifications and analytical separations were performed using an Agilent Technologies model 1100 HPLC system with a Supelco Discovery® C18 reverse phase column. The radioactive samples were analyzed using a Packard Flo-One radioactivity detector or a Liquid Scintillation Counter (LSC).

Experimental Details

Synthesis of [6R-^{x}H]CH_2H_4folate for KIE Experiments

The [*6R*-^{x}H]CH_2H_4folate was synthesized by adapting the published procedure[138] with some modification. Briefly, the synthesis is a one-pot preparation that combines two enzymatic reactions and one chemical reaction: (1) alcohol dehydrogenase from *thermoanarobium brockii* (tbADH) catalyzes the reduction of $NADP^+$ by [2-^{x}H]iPrOH to produce [4*R*-^{x}H]NADPH; (2) DHFR catalyzes the reduction of H_2folate by [4*R*-^{x}H]NADPH to produce [6*S*-^{x}H]H_2folate; (3) formaldehyde is added into the reaction mixture to trap [6*S*-^{x}H]H_2folate and form [6*R*-^{x}H]CH_2H_4folate. The previous procedure used DTT in the reaction mixture, whereas we used glucose/glucose oxidase *in situ* oxygen scavenging system to maintain strict anaerobic conditions. The synthesized [*6R*-^{x}H]CH_2H_4folate was purified by reverse phase HPLC (RP HPLC), lyophilized, and stored at -80 °C prior to use.

Formation of Thiol-trapped Intermediates

The final reaction mixtures for the comparison studies (Table 3-1) contained 100 μM dUMP, 200 μM CH_2H_4folate, 2 mM TCEP, 50 mM $MgCl_2$ and 25 mM thiol reagent in 100 mM tris(hydroxymethyl)aminomethane (Tris)/HCl buffer (pH 7.5). The reaction was initiated by adding Y209W ecTSase, and incubated for 150 min at 25 ˚C prior to HPLC analysis. We used [2-^{14}C]dUMP to track the formation of both dTMP and the thio-trapped intermediate, of which the relative amounts were analyzed by HPLC separation followed by Flo-One radioactivity detector. The RP-HPLC separation method and the elution times for the compounds in the reaction mixture are provided in SI (Table 3-5 and Table 3-6).

Steady-State Kinetics

The steady state initial velocities were measured by following the increase of absorbance at 340 nm that indicates the conversion of CH_2H_4folate to H_2folate ($\Delta\varepsilon_{340nm}$ = 6.4 $mM^{-1}cm^{-1}$), using the published procedure for the WT enzyme[35] with modification. The reaction mixture for the mutant contained 2 mM TCEP instead of 50 mM DTT to avoid intermediate trapping by the thiols. The k_{cat} and K_m of CH_2H_4folate were measured with 200 μM dUMP at 5, 15, 25, and 35 ˚C, and the K_m of dUMP was measured with 50 μM CH_2H_4folate at 25 ˚C. The steady state kinetic data at each temperature were analyzed with the least squares nonlinear regression available in KaleidaGraph (Version 4.03). This analysis provided the steady state rate constants of the reaction at four different temperatures, which were fit to the Eyring equation (Eq 3) to evaluate the activation parameters (Figure 3-1B, Table 3-3). Although the activation parameters for 25-35 ˚C were only based on two data points, they provide a reliable qualitative comparison with data in the low temperature range.

$$\ln\left(\frac{k_{cat}}{T}\right) = \frac{-\Delta H^{\ddagger}}{R} \cdot \left(\frac{1}{T}\right) + \frac{\Delta S^{\ddagger}}{R} + \ln\left(\frac{k_B}{h}\right) \quad (3)$$

Observed and intrinsic KIEs on the Hydride Transfer

The competitive method[29,30,102,118] was used to measure the KIE on the hydride transfer step in the temperature range of 5-35 ˚C, following the procedure published for the WT enzyme[35] with modification. For the same reasons described above, the reaction mixture for the mutant replaced DTT with 2 mM TCEP. The Northrop method was used to extract the intrinsic KIEs from the observed values.[29,102]

New Refinement of the Crystal Structure of Y209W-dUMP-CB3717 Complex

Difference density (Fo-Fc)α_{calc} maps, computed with refined coordinates of Y209W ecTSase,[97] were examined for evidence of disorder that would allow solvent to access the active site. At low contour levels, alternate conformations could be identified for L143 and C146 in both active sites and for R127 in one of the active sites. Two conformations were fitted to density for these three residues, and a new water molecule near the dUMP of the most disordered active site was also built into density (Figure 3-4B). Updated coordinates were refined in Phenix against a complete data set between 45.8Å and 1.3Å resolution using a maximum likelihood target function and anisotropic temperature factors for all non-hydrogen atoms. Occupancies for the two conformations of each disordered residue were refined with the constraint that they summed to 1.0. Refinement converged at R=12.79% and R_{free}=15.24%. RMS deviations in bonds and angles were 0.009Å and 1.34°, respectively, and 99% of the residues had backbone (φ,ψ) angles in the most favored regions of the Ramachandran diagram. The clash score (number of steric overlaps > 4Å per 1000 atoms) was 3.92. Figures 3-3 and 3-4 illustrate the differences in the structures and dynamics of the WT and Y209W ternary enzyme

complexes. Figure 3-3 and Figure 3-4B were generated by Pymol v1.5.0.4, and Figure 3-4C was generated by Chimera.[139]

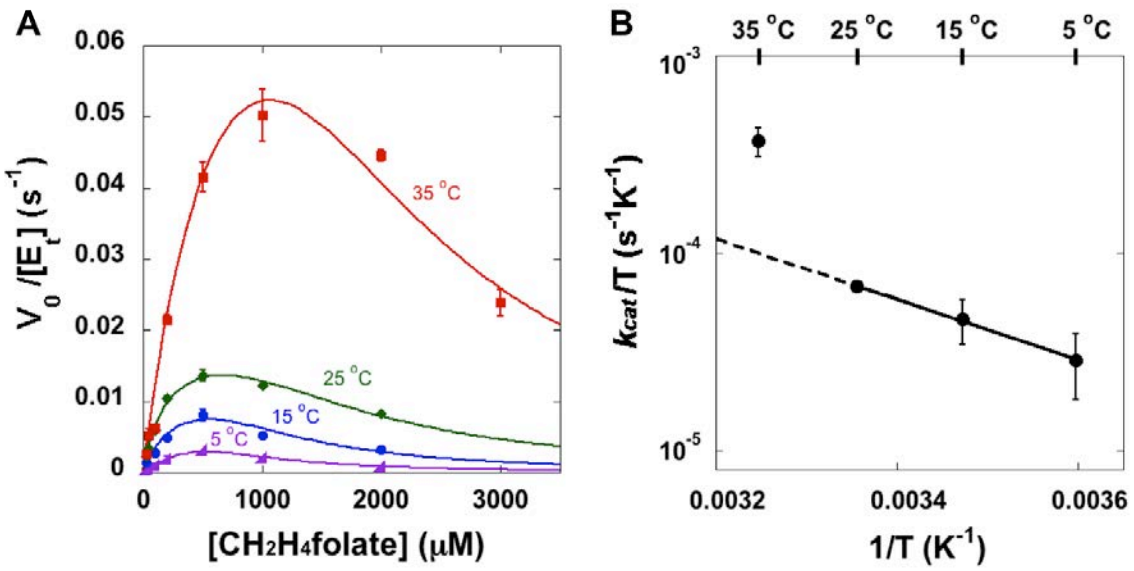

Figure 3-1. Steady state kinetics of Y209W ecTSase.

This figure presents:

(A) Steady state initial velocities of Y209W ecTSase *vs*. the concentration of CH_2H_4folate at 200 μM dUMP. At each temperature, the data were fit to Eq 1 by least-squares nonlinear regression. For clarity purpose, this figure only shows the average with standard deviation for each data point, although all the measurements (at least triplicates for each point) were used in the nonlinear regression for each temperature.

(B) The Eyring plot of k_{cat} is in accordance with a change in the rate-limiting step above 25 ˚C.

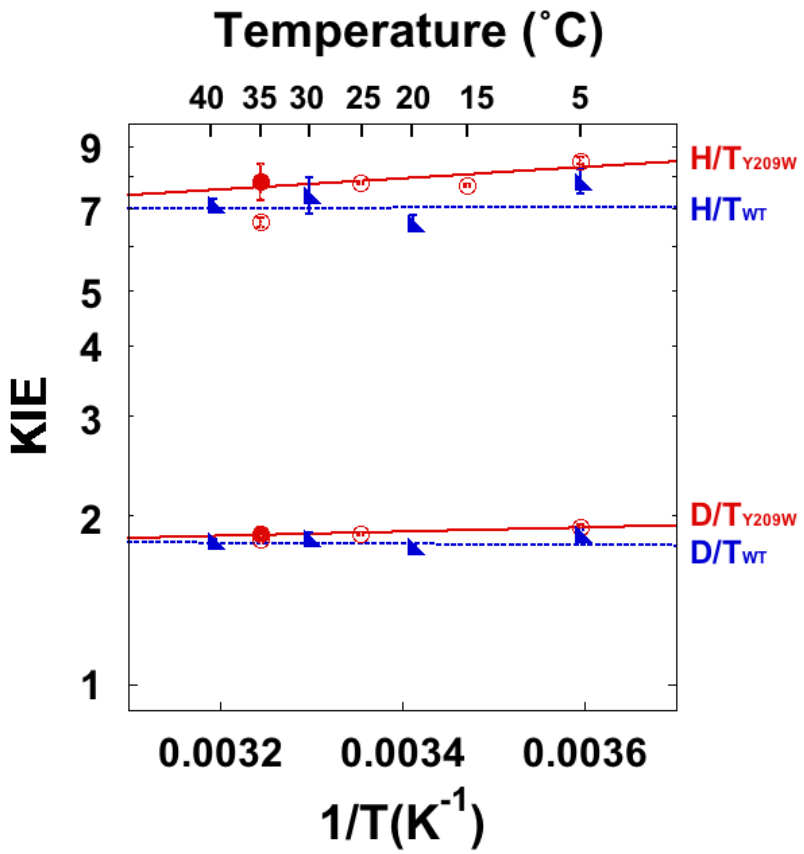

Figure 3-2. KIEs on the hydride transfers in the WT and Y209W ecTSases.

KIEs on the hydride transfers catalyzed by the WT (blue, data from Ref 35) and Y209W (red) ecTSases. The lines represent the least-squares nonlinear regression of the intrinsic KIEs to Eq 2. The empty circles represent the observed KIEs, and filled circles represent the intrinsic KIEs when different from the observed, i.e. at 35 ˚C.

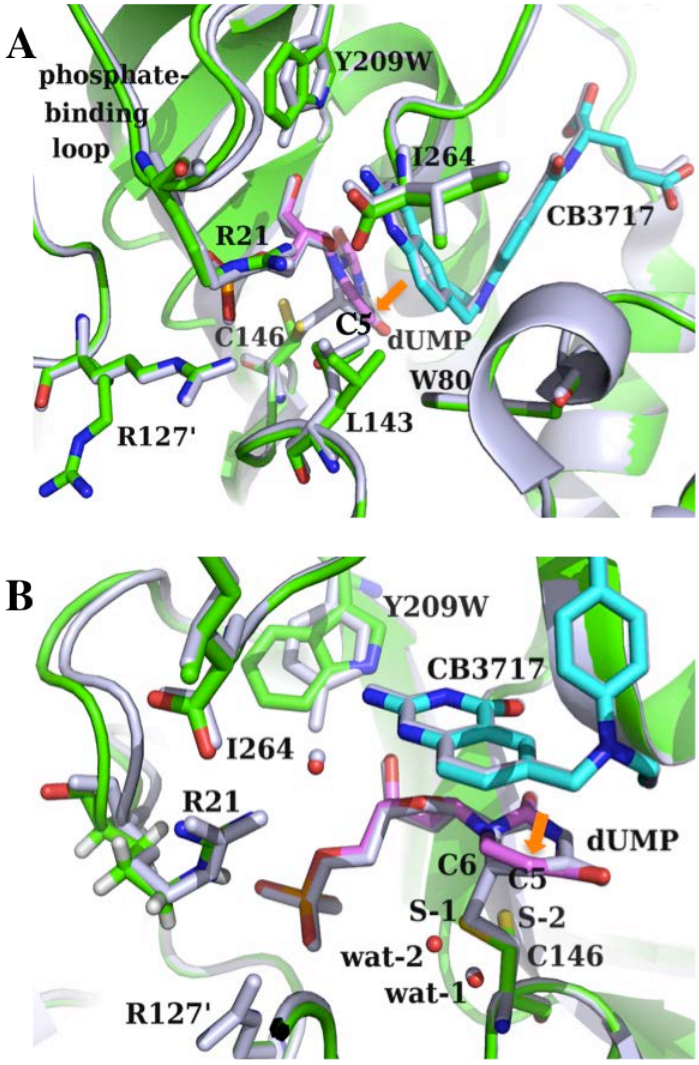

Figure 3-3. Structure perturbation of Y209W mutation on ecTSase.

This figure presents:

(A) Crystal structures of the ternary complexes of the WT (gray; PDB ID 2G8O) and Y209W (green; PDB ID 4GEV) ecTSase with dUMP (magenta) and CB3717 (cyan) are remarkably similar. The mutant shows two conformations for each of the residues R127', L143, and C146. The mutation also causes interesting dynamic effect including the shift-away and increased mobility of the phosphate-binding loop, and the less correlated atomic vibrations of protein residues and ligands. All the catalyzed chemical bond activations happen around the C5 of dUMP (orange arrow).

(B) A closer view of the active site. The additional conformation of C146 (S-2) in Y209W cannot form a covalent bond with dUMP, which is accompanied by the displacement of a nearby water molecule (from wat-1 to wat-2). R21 on this phosphate-binding loop also forms H-bonds with both I264 and the cofactor (through a water molecule).

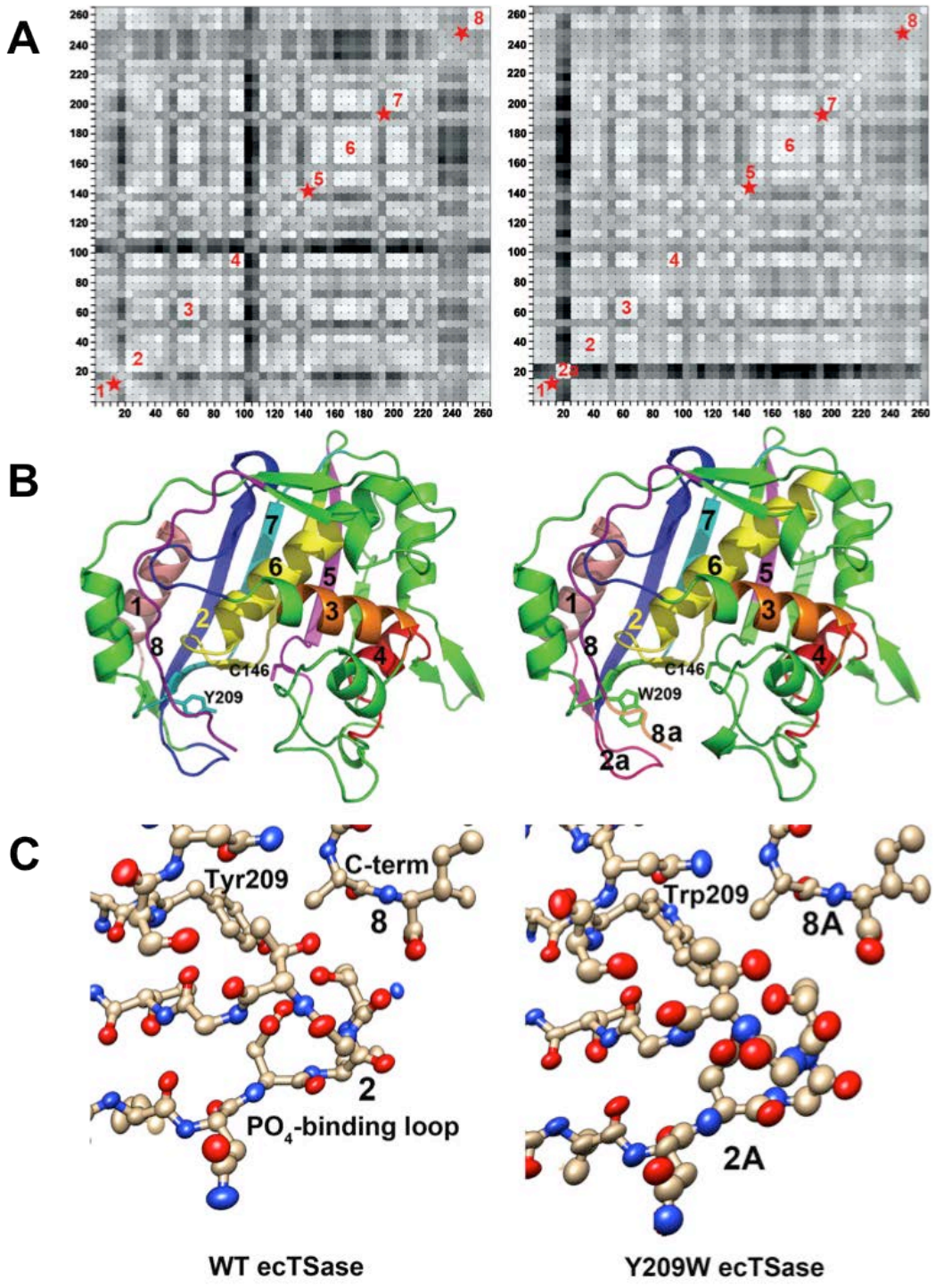

Figure 3-4. Dynamic effects of Y209W mutation on ecTSase.

This figure presents:

(A) Plots showing correlations of anisotropic B-factor displacements between ecTSase atom pairs identified by the (x,y) grid coordinates of the plot (reproduced from Ref 97 with permission form ACS). The left plot is for WT ecTSase and the right plot is for Y209W. Grid points are shaded from white to black with white representing highest correlation, where degree of correlation is determined by similarity of projections of anisotropic displacements along the interatomic vector.[140] Blocks of light colored squares along the diagonals of the plots indicate protein segments that vibrate as rigid bodies. Eight such segments are labeled in the plots, and red stars indicate segments where rigid body movement appears to have been disrupted by the mutation. Segment 2a in the Y209W plot is the phosphate-binding loop, whose vibrations are no longer correlated with the rest of the proteins segments.

(B) Ribbon plots of WT ecTSase (left) and Y209W ecTSase (right). Segments labeled in (A) are labeled and colored. The catalytic cysteine and the mutated residue are shown as sticks.

(C) Plot of the thermal ellipsoids of the phosphate-binding loop for WT (left) and Y209W ecTSase (right). This loop shifts to close the active site cavity during binding of the substrate and cofactor, and it has a key role in orienting the ligands and shielding the cavity from bulk solvent. R21 in this loop makes hydrogen bonds to the phosphate moiety of dUMP and to the protein C-terminus. The thermal ellipsoids are derived from the refined anisotropic B-factors of the structures and the radii of the ellipsoids are proportional to the root-mean-square displacements from the atom positions (see Experimental Details). The B-factors for the loop are larger in the mutant structure, as seen by the larger volumes of the ellipsoids. The thermal vibrations of atoms in the loop are also less well correlated with each other in the mutant, as evidenced by more random orientations of the long axes of the ellipsoids. In addition, the thermal vibrations of the atoms in the loop are no longer correlated with those of other protein segments lining the active site cavity, such as the segments containing S210 and the mutated Y209 or the C-terminal segment. The phosphate-binding loops and C-terminal residues are labeled with the segment numbers from the plots in (A).

Figure 3-4 ——continued

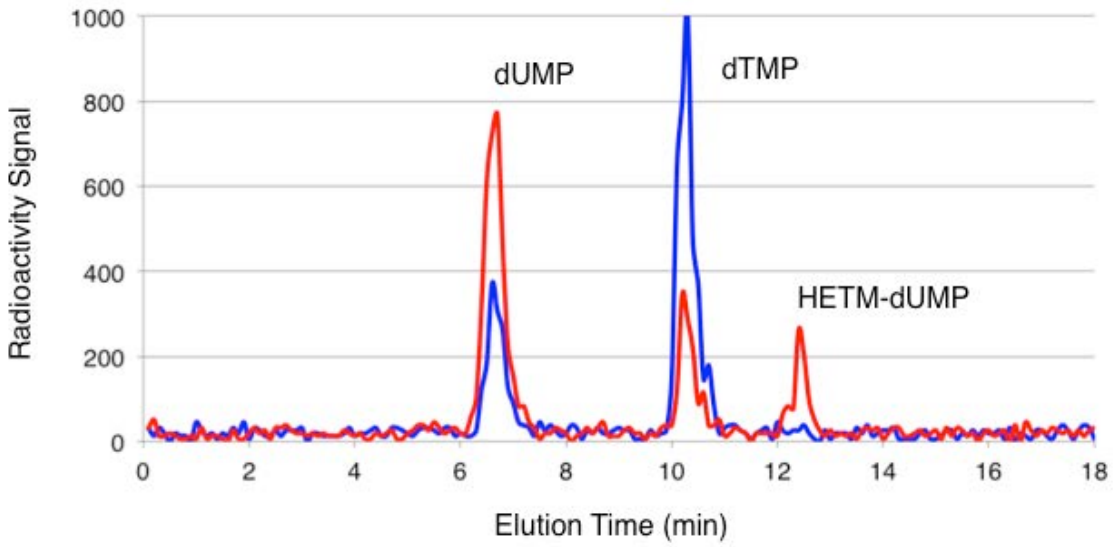

Figure 3-5. HPLC radiograms of the reaction mixtures of WT and Y209W ecTSase.

Representative radiograms of the reaction mixtures of WT (blue) and Y209W (red) ecTSase in the presence of β-mercaptoethanol. The third peak indicates formation of 5-(2-hydroxyethyl)thiomethyl-dUMP (HETM-dUMP) in the reaction mixture of the mutant..

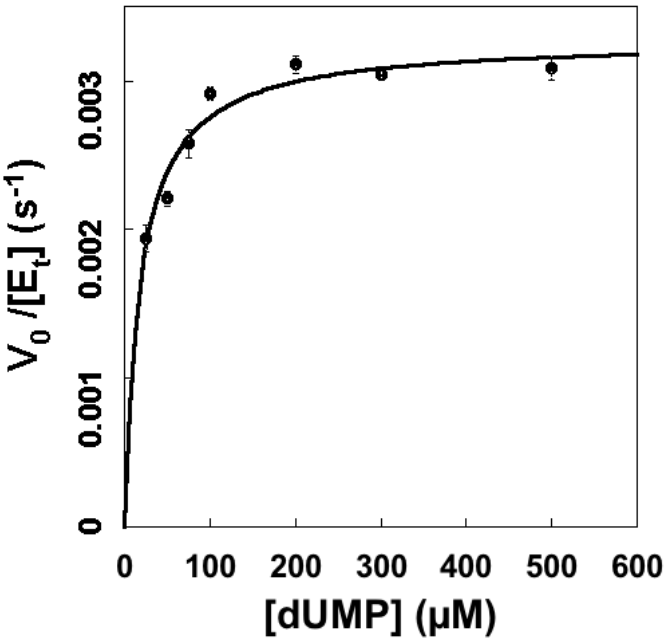

Figure 3-6. Steady state initial velocities of Y209W *vs*. concentrations of dUMP at 25 ˚C.

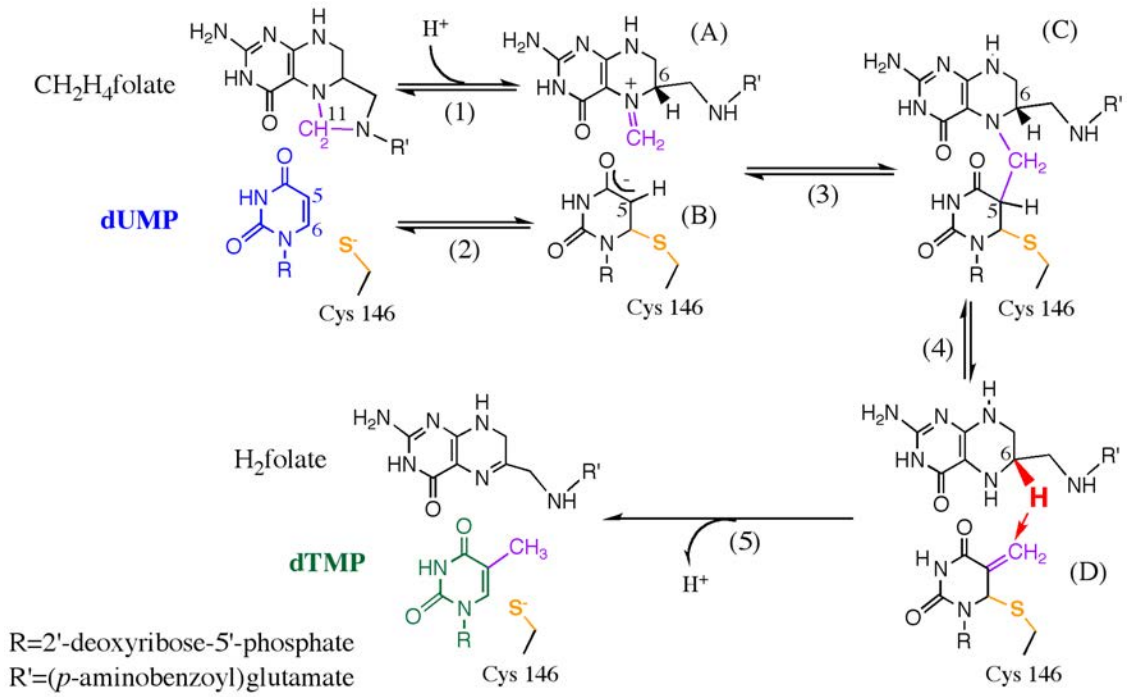

Figure 3-7.The proposed mechanisms for TSase (focus on the hydride transfer).

This reaction involves a series of chemical conversions (1-5) with several intermediates (A-D). All the chemical transformations happen at the “chemical reaction site” near the C146 residue (yellow), which forms the only covalent bond between the protein and the substrate during the catalytic turnover.

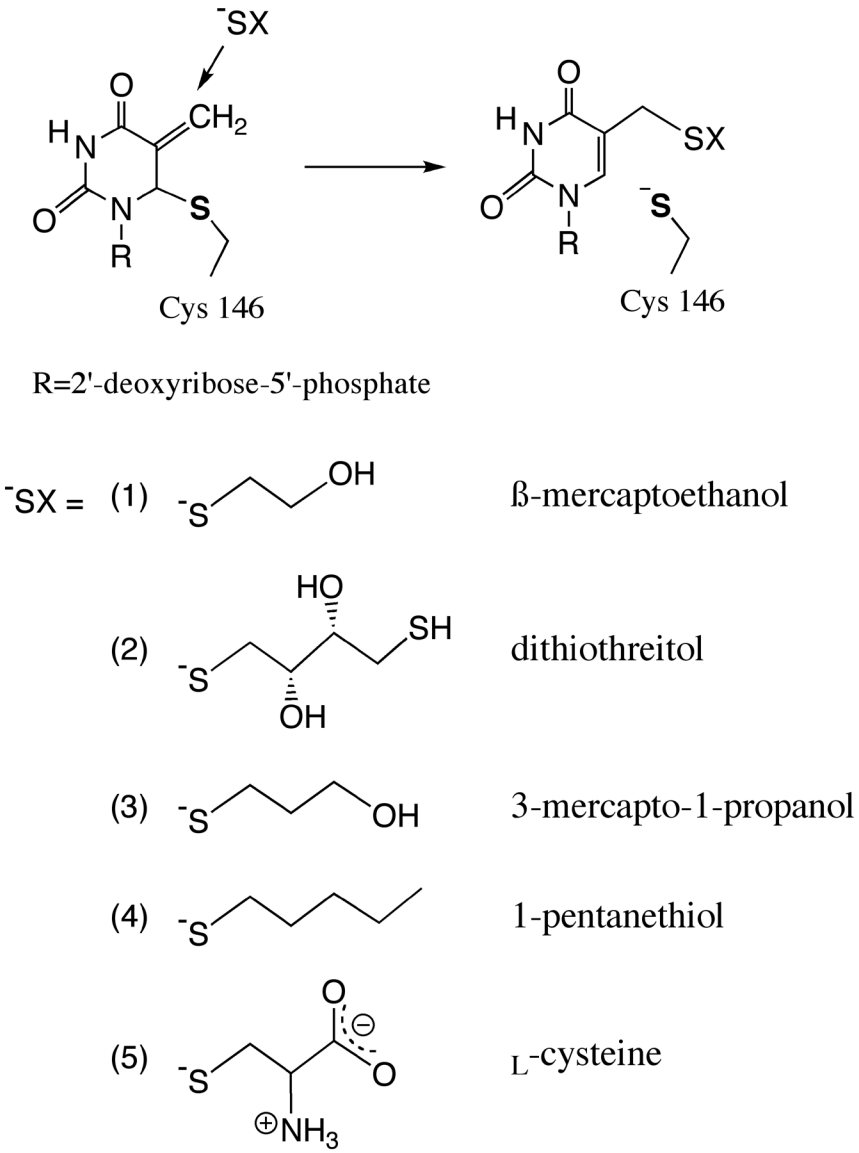

Figure 3-8. Thiols trap the reaction intermediate in Y209W ecTSase.

A variety of thiols (⁻SX) were tested as potential reagents to trap the exocyclic intermediate (Complex D in Figure 3-7) in Y209W ecTSase-catalyzed reaction. This reaction directly competes with the hydride transfer step (step 5 in Figure 3-7).

Table 3-1. Percentage of thiol trapped intermediates in the reaction mixture.

Thiol Reagents	%TI in products
β- mercaptoethanol	73%
dithiolthreitol	70%
3-mercapto-1-propanol	59%
1-pentanethiol	8%
L-Cysteine	0%

Notes:

Competitive formation of dTMP and the exocyclic intermediate trapped by different thiol reagents (trapped intermediate, TI) after 150 min incubation with Y209W at 25 ˚C. The percentage of TI in the products (%TI) reflects how easy each thiol diffuses into the active site to compete with the hydride transfer (step 5 in Figure 3-7). The structure of each thiol is shown in Figure 3-8.

Table 3-2. Steady state kinetic parameters of the WT and Y209W ecTSase at 25 ˚C.

TSase	k_{cat} (s^{-1})	K_m^{dUMP}	$K_m^{CH_2H_4folate}$	$K_m^{dUMP} / K_m^{CH_2H_4folate}$
WT w/ß-ME [a]	8.8 (1)	4.1 ± 0.4 (1)	13.6 ± 0.2 (1)	0.30 (1)
Y209W w/ß-ME [a]	0.05 ± 0.01 (0.005)	118 ± 40 (28.8)	172 ± 26 (12.6)	0.69 (2.3)
Y209W w/TCEP	0.020 ± 0.001 (0.002)	19 ± 2 (4.6)	214 ± 27 (15.7)	0.089 (0.30)

Notes:

The value in the parenthesis below each number is the magnitude of that value relative to the corresponding WT parameter.

[a] Data from Ref 97. A comparison of WT activity with ß-ME and with TCEP found no difference.

Table 3-3. Activation parameters for k_{cat} of WT and Y209W ecTSase.

TSase	temperature range	$\Delta H^{\ddagger}$ kcal/mol	$T\Delta S^{\ddagger}$ at 25 ˚C kcal/mol	$\Delta G^{\ddagger}$ kcal/mol
WT	5-35 ˚C	3.4 ± 0.2	-12.8 ± 0.2	16.2 ± 0.4
Y209W	5-25 ˚C	7.0 ± 0.3	-12.8 ± 0.4	19.8 ± 0.7
	25-35 ˚C	lower limit: *ca*. 30	lower limit: *ca*. 11	N.D.

Table 3-4. Isotope effects on Arrhenius parameters of the hydride transfers catalyzed by the WT and Y209W ecTSase.

	Y209W	WT [a]	S.C. A_L/A_T [b]
A_H/A_T	3.6 ± 0.9	6.8 ± 2.8	0.3 – 1.7
$\Delta E_{a\ H\text{-}T}$ (kcal/mol)	-0.5 ± 0.1	-0.02 ± 0.25	

Notes:

[a] Data from Ref 35.

[b] Semi-classical limits of isotope effects on the preexponential factor.[82,103,141-143]

Table 3-5. HPLC mobile phase gradient.

t (min)	% A	% B	% C
0	100	0	0
8	70	30	0
14	0	0	100
17	0	0	100

Notes:

HPLC mobile phase solutions (flow rate 0.8 ml/min):
A = 20 mM KH_2PO_4/H_3PO_4 buffer (pH = 5.0)
B = 40% methanol, 60% A
C = methanol

Table 3-6. Retention time (min) of the by-products found for the Y209W-catalyzed reaction in the presence of different thiols.

Thiol Reagent	dUMP	dTMP	Thiol-trapped Intermediate
β-mercaptoethanol	6.8	10.2	12.4
DTT			14.0
3-mercapto-1-propanol			14.2
1-pentanethiol			14.2
Cysteine			N/A

Table 3-7. Steady-state kinetic parameters of Y209W ecTSase at different temperatures.

	k_{cat} (s^{-1})	$K_m^{CH_2H_4folate}$ (mM)	$\frac{k_{cat}}{K_m^{CH_2H_4folate}}$ (s^{-1} mM^{-1})	$K_I^{CH_2H_4folate}$ (mM^2)
5 ˚C	0.008 ± 0.003	0.6 ± 0.3	0.013± 0.008	0.5± 0.2
15 ˚C	0.013 ± 0.003	0.3 ± 0.1	0.04 ± 0.02	1.2 ± 0.5
25 ˚C	0.020 ± 0.001	0.21 ± 0.03	0.10 ± 0.01	2.8 ± 0.4
35 ˚C	0.11 ± 0.02	0.8 ± 0.2	0.14 ± 0.04	2.9 ± 0.8

Table 3-8. KIE on the hydride transfer in Y209W.

Temperature ˚C	Observed KIE		$SSE_{obs.}$ [a]
	H/T KIE	D/T KIE	
5	8.5 ± 0.1	1.90 ± 0.02	3.32 ± 0.06
15 [b]	7.68 ± 0.04		
25	7.77 ± 0.04	1.85 ± 0.01	3.33 ± 0.03
35	6.6 ± 0.1	1.81 ± 0.03	3.18 ± 0.09
35 [c] ($KIE_{int.}$)	7.8 ± 0.6	1.85 ± 0.05	

Notes:

[a] The Swain-Schaad exponent for the observed KIEs:

$$SSE_{obs.} = \ln\left(KIE_{obs.}^{H/T}\right) \Big/ \ln\left(KIE_{obs.}^{D/T}\right).$$

The errors of the SSE_{obs} ($\Delta SSE_{obs.}$) are calculated from the errors associated with the observed H/T and D/T KIEs by the error propagation rule:

$$\Delta SSE_{obs} = \sqrt{\left(\frac{\Delta\left(KIE_{obs.}^{H/T}\right)}{KIE_{obs.}^{H/T}} \Big/ \ln\left(KIE_{obs.}^{D/T}\right)\right)^2 + \left(\frac{\Delta\left(KIE_{obs.}^{D/T}\right)}{KIE_{obs.}^{D/T}} \cdot \frac{\ln\left(KIE_{obs.}^{H/T}\right)}{\left[\ln\left(KIE_{obs.}^{D/T}\right)\right]^2}\right)^2}$$

[b] Since the observed KIEs at 5 and 25 ˚C are the same as the intrinsic values (based on SSE_{obs} close to 3.3), it is not necessary to measure the D/T KIE at 15 ˚C.

[c] At 35 ˚C, $SSE_{obs} < 3.3$. Therefore, we used the Northrop method to calculate the intrinsic KIE at this temperature, with SSE_{int} of 3.34. Error propagation in this case has been described elsewhere.[144]

CHAPTER IV

MG^{2+} BINDS TO THE SURFACE OF THYMIDYLATE SYNTHASE AND AFFECTS HYDRIDE TRANSFER AT THE INTERIOR ACTIVE SITE

Introduction

Metal ions are known to stabilize physiologically active conformations of biomolecules by various mechanisms in cells.[145,146] The divalent magnesium cation (Mg^{2+}) is an essential mineral nutrient for all living organisms, which is involved in many cellular functions including energy metabolism, cell growth and proliferation, etc.[147] Owing to the high intracellular magnesium content (i.e. as high as 20 mM),[148] cells can exploit the transport of Mg^{2+} between intracellular compartments to vary local concentrations of Mg^{2+} and regulate enzyme activities.[147,149] Previous studies suggested that the intracellular magnesium content reaches its maximum during the S phase of the cell cycle, concomitant with DNA replication.[150] In exponentially growing *Escherichia coli B* cells, the intracellular concentration of total Mg^{2+} can be higher than 100 mM.[151,152]

One of the enzymes crucial for DNA replication is thymidylate synthase (TSase), which is one of the most conserved enzymes in evolution.[57] TSase catalyzes the reductive methylation of 2'-deoxyuridine-5'-monophosphate (dUMP) to form 2'-deoxythymidine-5'-monophosphate (dTMP), using N^5,N^{10}-methylene-5,6,7,8-tetrahydrofolate (CH_2H_4fol) as the cofactor (Figure 4-1).[61] This reaction is the only intracellular *de novo* source of thymidine (i.e. DNA base T) in nearly all organisms, including bacteria and DNA viruses. In addition, TSase is over-expressed in tumor cells to facilitate the faster DNA replication.[58,59] Consequently, TSase has been a common target for antibiotic and anticancer drugs. Classical drugs that target TSase are structural analogues of either dUMP (*e.g.* 5-flurouracil) or CH_2H_4fol (*e.g.* raltitrexed, also known as ZD1694), which

often interfere with the metabolic pathways of nucleosides/nucleotides or folates, leading to toxicity and development of resistance in cells.[153] Therefore, current drug designs focus on selectively targeting TSase activity in tumor cells, for anticancer drugs, or in specific species, for antibiotic drugs. While the former has learned from the autoregulatory function of TSase, the latter can be aided by careful investigations of its catalytic mechanism.[153,154]

TSase is a homodimer with two active sites, each of which is composed of residues from both protomers, and previous experiments suggested that TSase has "half-of-the-sites" activity, *i.e*. only one active site is competent at a time.[54-56] The large collection of structural and kinetic studies of TSase revealed that protein segments move concertedly throughout the many-step reaction,[62,63] which has attracted experimental and computational examinations of protein motions that contribute to activation of chemical bonds.[35,64,65,67,97,123,124,155] However, the complex catalytic mechanism of TSase makes it difficult to expose information on the microscopic chemical conversions (*e.g.* steps 1-5 in Figure 4-1). We have measured the kinetic isotope effects (KIEs) on the hydride transfer (step 5 in Figure 4-1) in *Escherichia coli* TSase (ecTSase),[35] which is rate limiting for the catalytic turnover in the absence of Mg^{2+}.[98] Similar to H-transfer reactions in many other wild-type (WT) enzymes,[19,35-40] the hydride transfer in ecTSase exhibits a temperature-dependent rate but a temperature independent KIE. The recently-developed Marcus-like model affords an interpretation of those kinetic results, which suggests that protein motions can facilitate an enzymatic H-transfer in three aspects.[19,23,25,27,45-48] First, conformational fluctuations of the protein "pre-organize" an electrostatic environment that is favorable for formation of the "reactive complexes" for the H-transfer step.[19,50-52,119] Secondly, "fine-tuning" of the conformations of reactive complexes further "reorganize" the active site to accommodate structural changes in the substrates going from the reactant state to the tunneling ready state (TRS) of H-transfer. Thirdly, the fluctuation of donor-acceptor distance (DAD) at the TRS affects the H-tunneling

probability. While the DAD fluctuation at TRS determines the magnitude and temperature dependence of the intrinsic KIE, pre- and re-organization affects the rate (and activation parameters) of the H-transfer and thus the "kinetic commitment" factor in experimental KIE measurements.[29,32] To explore the effects of those three categories of protein motions on the hydride transfer, we recently conducted kinetic and structural analysis of a remote mutant of ecTSase, Y209W (9 Å away from the hydride transfer site). This remote mutation affected both the rate and KIE of the hydride transfer through a long range of interactions, suggesting that TSase may exploit a "dynamic network of coupled motions" to facilitate activation of this C-H bond.[65]

Two previous studies reported that Mg^{2+} variably affected the activity of TSase enzymes from different species,[156,157] but the mechanism of those effects has never been investigated. Here we report detailed kinetic and structural analysis of how Mg^{2+} affects the catalytic mechanism of ecTSase, and particularly the hydride transfer step. Our results suggest that, although Mg^{2+} binds weakly to the surface of ecTSase, this interaction stabilizes the productive conformations of both the protein and the bound folate cofactor, thereby accelerating the hydride transfer at the active site (16 Å away).

Results and Discussions

Mg^{2+} Affects the Entropy of Activation on k_{cat}

To investigate the effect of Mg^{2+} on ecTSase activity, we measured the steady-state initial velocities of ecTSase in the absence and presence of 50 mM $MgCl_2$. We chose to use 50 mM Mg^{2+} to be consistent with the concentrations used in previous studies.[156] To assess the potential effects of ionic strength on the protein activity, we conducted a control experiment which measured the initial velocities at 25 ˚C in the absence and presence of 50 mM $CaCl_2$ and found no difference. The cofactor CH_2H_4fol exhibited substrate inhibition at high concentrations in both the absence and presence of Mg^{2+} (Figure 4-2), which is consistent with its unproductive, alternate binding mode

observed in crystal structures.[158] Based on the analysis of initial velocities (details provided in the Experimental Section, ES), the presence of Mg^{2+} affects the cooperativity of CH_2H_4fol binding in the inhibitory mode, suggesting an effect on the interaction between the protein and folate cofactor. This effect is further substantiated by our binding studies (below).

The analysis of initial velocities above provided the first-order rate constant, k_{cat}, of the reaction at four different temperatures, which were fit to the Eyring equation (Eq 1) to evaluate the activation parameters:

$$\ln\left(\frac{k_{cat}}{\mathrm{T}}\right) = \frac{-\Delta\mathrm{H}^{\ddagger}}{R}\cdot\left(\frac{1}{\mathrm{T}}\right) + \frac{\Delta\mathrm{S}^{\ddagger}}{R} + \ln\left(\frac{k_B}{h}\right) \qquad (1)$$

where $\Delta H^{\ddagger}$ is the enthalpy of activation, $\Delta S^{\ddagger}$ is the entropy of activation, T is absolute temperature, and k_B, h, and R are Boltzmann constant, Planck constant, and gas constant, respectively. In the temperature range of 5-35 ˚C, the presence of Mg^{2+} increases k_{cat} by approximately 7-fold (Figure 4-3). The temperature dependence of k_{cat} is linear in both the absence and presence of Mg^{2+}, suggesting that a single kinetic step is rate-limiting for the catalytic turnover in each case. Mg^{2+} reduces the activation energy ($\Delta G^{\ddagger}$, Table 4-1) on k_{cat} by lowering the entropy of activation ($\Delta S^{\ddagger}$), without changing the enthalpy of activation ($\Delta H^{\ddagger}$). These results suggest that Mg^{2+} affects the conformational fluctuations of the active site that constitute the entropic contribution of the catalysis. We also measured the initial velocity of ecTSase with varying concentrations of dUMP (Figure 4-4), and found the presence of Mg^{2+} increases the Michaelis constant of dUMP by *ca*. 5-fold at 25 ˚C (K_m^{dUMP} changed from 0.5 ± 0.1 to 2.4 ± 0.2 μM).

Mg^{2+} Binds Weakly to ecTSase and Affects the Binding Affinity of Both Substrates to the Protein

Mg^{2+} can affect the activity of an enzyme by either chelating with the substrate to form a more active Mg-substrate complex, or binding to the protein to alter its conformations and/or constitute the active site.[149] To determine the functional role of Mg^{2+} in TSase activity, we used an established fluorescence assay[98] to measure the values of dissociation constant (K_d) that describe the interaction between Mg^{2+} and apo-ecTSase, and between Mg^{2+} and the binary ecTSase-dUMP complex. The K_d values were determined to be 27 ± 7 mM for apo-ecTSase and 0.5 ± 0.2 M for ecTSase-dUMP, indicating that Mg^{2+} binds weakly but preferably to the apo-enzyme (Figure 4-5A). These results suggest that Mg^{2+} directly binds to ecTSase to enhance its activity, rather than by chelating with dUMP.

To investigate the effects of Mg^{2+} on the interactions between the substrates and enzyme, we measured the dissociation constants for dUMP (K_d^{dUMP}) binding to apo-ecTSase and to the ecTSase-Mg^{2+} complex, using the fluorescence assay (Figure 4-5B). We also assessed the dissociation constants for CH_2H_4fol ($K_d^{\mathrm{CH_4H_4fol}}$) binding to the ecTSase-dUMP and ecTSase-dUMP-Mg^{2+} complexes,[viii] using the equation derived by Klinman and Matthews[160] (Eq 5 in ES). The results suggest that the presence of Mg^{2+} increases the K_d^{dUMP} value but decreases the $K_d^{\mathrm{CH_4H_4fol}}$ value (Table 4-3), indicating that Mg^{2+} ameliorates the interaction between CH_2H_4fol and the enzyme. The higher affinity of CH_2H_4fol in the presence of Mg^{2+} corroborates the reduction of $T\Delta S^{\ddagger}$ found in the steady-state experiments, since the binding of CH_2H_4fol induces large conformational changes of TSase that close the active-site cavity and properly align the reactants for catalysis.[62,63] Therefore, our kinetic and binding studies suggest that Mg^{2+} stabilizes the

---

[viii] Since the bound dUMP in the active site elaborates a large hydrophobic surface to accommodate cofactor binding, ecTSase binds dUMP and CH_2H_4fol sequentially (Ref 62, 63).

bound CH_2H_4fol and thus reduces the entropic cost for the conformational changes of the protein that lead to formation of the "reactive complex", thereby accelerating k_{cat}.

Mg^{2+} Affects the Rate but not the Intrinsic KIE of Hydride Transfer

Previous studies suggested that the hydride transfer is rate limiting for k_{cat} of ecTSase in the absence of Mg^{2+}.[98] To examine if Mg^{2+} changes the rate-limiting step for the catalytic turnover, we measured the intrinsic KIE as well as the KIE on k_{cat} with *6R*-^{x}H-CH_2H_4fol (^{x}H=H or D) at 25 ˚C in the presence of 50 mM $MgCl_2$ (Figure 4-6). The observed KIE on k_{cat} ($^{D}k_{cat}$) was determined to be equal to the intrinsic KIE (Table 4-4), indicating that the hydride transfer is also rate-limiting for k_{cat} in the presence of Mg^{2+}. Therefore, the observed effects on k_{cat} and the activation energy parameters (Figure 4-3 and Table 4-1) suggest that Mg^{2+} accelerates the rate of the hydride transfer and reduces the entropy of activation on this step.

To investigate the effects of Mg^{2+} on the TRS of the hydride transfer, we measured the temperature dependence of the intrinsic KIE. We measured the observed KIEs on the second-order rate constant $k_{cat} / K_M^{CH_2H_4fol}$ (simplified as k_{cat} / K_M hereafter),[29,124] and used Northrop's method to extract the intrinsic KIEs as described before.[35] In the absence of Mg^{2+}, the observed KIEs are similar to the intrinsic values (Figure 4-7A), implying that the hydride transfer is (at least partially) rate-limiting for k_{cat}/K_M.[35] On the contrary, in the presence of Mg^{2+}, the observed KIEs are smaller than the intrinsic KIEs (Figure 4-7B). This observation suggests that the hydride transfer is no longer rate-limiting for k_{cat}/K_M due to the larger kinetic commitment (C_f in Table 4-6) in the presence of Mg^{2+}.[29,32], which agrees with the accelerated rate of hydride transfer by Mg^{2+} as suggested above. However, the intrinsic KIE on the hydride transfer has the same value as measured in the absence of Mg^{2+}, and remains temperature-independent (Figure 4-7 and Table 4-5). Based on the Marcus-like model, these observations suggest

that Mg^{2+} facilitates protein motions that bring the hydride donor in CH_2H_4fol into proximity with its acceptor in dUMP (*i.e.* pre- and re-organization), but it does not alter the TRS of the hydride transfer.

Structural Insights for Mg^{2+} Binding to ecTSase

Mg^{2+} has not been identified in any published crystal structures of TSase, even though $MgCl_2$ is frequently included in the solutions used for crystallization. It is generally difficult to discriminate Mg^{2+} from a water molecule in X-ray diffraction data, due to the similarity between their electron densities. To investigate the structural origin for our observed kinetic effects, we carefully examined a number of previously solved crystal structures for putative Mg^{2+} ions that were octahedrally-coordinated *via* shorter H-bonds with surrounding water molecules or oxyanions of the protein. A 1.3 Å-resolution crystal structure (PDB ID: 2G8O) of ecTSase ternary complex with dUMP and a cofactor analogue, 10-propargyl-5,8-dideazafolic acid (CB3717), shows such geometry at the binding cleft for the glutamyl (Glu) "tail" of CB3717 (Figure 4-8). Another ternary complex of ecTSase with dUMP and a di-Glu antifolate inhibitor also shows an electron density for octahedrally-hydrated Mg^{2+} near the Glu that is farther from the p-aminobenzoic acid ring of the inhibitor (Finer-Moore and Stroud, unpublished). In agreement with the weak affinity suggested above, Mg^{2+} binds to the surface of ecTSase, and its interaction with the cofactor and protein residues are not conserved in these two structures. Nevertheless, in both structures, Mg^{2+} mediates an H-bond network that tethers the Glu moiety of the cofactor to the backbone carboxylates of a protein loop (Figure 4-8). This loop is involved in the conformational changes of TSase that close the active site upon the cofactor binding.[62,63] Particularly, W83 on this loop forms an H-bond with the C-terminal carboxylic group (residue I264 in ecTSase) as CH_2H_4fol binds to the protein, which helps to immobilize the C-terminus to seal the active site from bulk solvent. This loop also contains W80, which not only orients L143 to protect the active

site cavity but also forms an H-bond with E58, while E58 coordinates the active site water molecules essential for TSase activity.[63,67] Therefore, although Mg^{2+} binds weakly to the surface of TSase, this interaction can stabilize the closed conformations of the ternary enzyme complex, which not only enhances the affinity of CH_2H_4fol but also increases the fraction of "reactive complexes" for the chemical reactions after CH_2H_4fol binding. These structural insights corroborate our kinetic findings that Mg^{2+} accelerates the hydride transfer and reduces the entropy of activation on this step. A similar relay between the protein surface and active site has been observed for the TSase domain of the bifunctional TSase-dihydrofolate reductase enzyme in *Cryptosporidium hominis*. In that case, two nonconserved residues that bind the Glu-tail of CH_2H_4fol are responsible for the faster k_{cat} of this TSase domain than other TSase enzymes.[161] Mutations of those two residues affected the positioning and flexibility of the cofactor, and this effect propagated into the active site and reduced k_{cat} of the TSase domain.[162]

The binding sites of Mg^{2+} revealed by our crystal structures agree with previous observations that Mg^{2+} modulated the selective inhibition of poly-Glu antifolates towards bacterial and viral TSase activities.[156] The residues of TSase that bind the poly-Glu moiety of folate cofactor are not conserved among different species (except for the first Glu nearest the p-aminobenzoic acid ring).[163] In addition, the binding region for the poly-Glu moiety is quite open to solvent, which may allow Mg^{2+} to bind and modulate H-bonds at several locations between the poly-Glu tail and a protein loop as indicated by the current study (Figure 4-8). The residues in the loop of ecTSase whose side chains contribute to the Mg^{2+}-mediated H-bond network include T78 in both ternary complexes and E82 in the di-Glu inhibitor complex. The corresponding residues in human TSase are lysine and alanine, respectively. These differences may preclude formation of analogous Mg^{2+}-mediated H-bond network between human TSase and the cofactor, explaining the lack of sensitivity of human TSase activity to Mg^{2+}. Future studies can exploit our current findings and design species-specific TSase inhibitors, such as antifolate with a poly-Glu

substitute that would create a perfect binding site for Mg^{2+} in a specific TSase enzyme, which may lead to species-specific drugs that target DNA biosynthesis.

Conclusions

The last few decades have brought us to a recognition that protein motions may contribute to the chemical reactions catalyzed by enzymes. Extensive studies of dihydrofolate reductase have provided the proof of concept, where a "network of coupled motions" was suggested to be important for its hydride transfer.[23,108,130-132] It is interesting to examine this concept in more complex enzymatic mechanisms, such as the reaction catalyzed by TSase. TSase exploits progressive conformational changes to assist the binding and orientation of ligands, and to accommodate structural changes in the ligands during the catalyzed chemical reactions.[62,63] Particularly, our recent study of Y209W ecTSase demonstrated that protein motions at various time scales can affect different parameters of the hydride transfer step, suggesting a possible "network of coupled motions" in TSase.[65] The current study has explored how an alteration in the external conditions – the presence vs. absence of Mg^{2+} – affects the kinetics of WT ecTSase through long-range interactions in the protein, particularly focusing on the hydride transfer step. Our crystal structures implicate a binding site for Mg^{2+} near the Glu-moiety of the cofactor, which stabilizes the closed conformation of the ternary enzyme complex of ecTSase. Our kinetic experiments suggest that the binding of Mg^{2+} reduces the entropic cost for protein conformational changes that lead to formation of the reactive complexes, and thereby accelerates the rate of hydride transfer. Since TSase is crucial for DNA replication, these results agree with previously established positive correlation between intracellular magnesium content and proliferating rate of *Escherichia coli* cells.[151,152] The interaction between Mg^{2+} and nonconserved residues of TSase suggests a potential direction in designing antifolates with poly-glutamyl substitutes as species-specific drugs that target DNA biosynthesis.

Experimental Section

Materials and Instruments

[2-^{14}C] dUMP (specific radioactivity 53 Ci/mol) was purchased from Moravek Biochemicals. [*6R*-^{x}H]CH_2H_4folate (^{x}H = D or T) was synthesized according to our published procedure,[65] and unlabeled CH_2H_4folate (^{x}H = H) was a generous gift from EPROVA (Switzerland). Ultima Gold liquid scintillation cocktail reagent was purchased from Packard Bioscience. Liquid scintillation vials were purchased from Research Products International Corp. *Escherichia coli* TSase (ecTSase) enzymes were expressed and purified according to the established procedures.[110] All other materials were purchased from Sigma. The steady-state kinetic experiments were conducted using a Hewlett-Packard Model 8452A diode-array spectrophotometer equipped with a temperature-controlled cuvette assembly. For the competitive KIE experiments, the radioactive materials were separated using an Agilent Technologies model 1100 HPLC system with a Supelco Discovery® C18 reverse phase column, and analyzed with a Liquid Scintillation Counter (LSC). Figure 4-8 was generated with Pymol v1.5.0.4[164] and all other figures with KaleidaGraph (Version 4.03).

Experiments and Data Analysis Details

Steady-State Kinetic Experiments

Our previous experiments measured the steady-state initial velocities of ecTSase in the absence of Mg^{2+} by monitoring the increase of absorbance at 340 nm that indicates conversion of CH_2H_4fol to dihydrofolate ($\Delta\varepsilon_{340nm}$ = 6.4 $mM^{-1}cm^{-1}$).[35] In the current study, we conducted the same experiments in the presence of 50 mM $MgCl_2$. Addition of ecTSase to a final concentration of 20 nM (concentration in terms of dimer, same below) initiated the reaction. Values of k_{cat} and K_m of CH_2H_4fol were measured with 100 μM dUMP at 5, 15, 25, and 35 ˚C, and the K_m value of dUMP was measured with 150 μM

CH_2H_4fol at 25 ˚C. To check the potential effects of ionic strength on the activity of TSase, we also conducted the control experiment at 25 ˚C, in which $MgCl_2$ was replaced by 50 mM $CaCl_2$, and found no effects on the initial velocities.

Analysis of Steady-State Initial Velocities

Analysis of the initial velocities at each temperature employed the least-squares nonlinear regression available in KaleidaGraph (Version 4.03). The initial velocities of ecTSase *vs*. concentration of dUMP can be fit with the standard Michaelis-Menten equation. In contrast, high concentrations of CH_2H_4fol inhibit the activity of ecTSase, and the data were analyzed by the general equation for uncompetitive substrate inhibition (Eq 2), which incorporates Hill coefficients to account for the potential cooperativity in substrate binding:[165]

$$\frac{v}{[\mathrm{E}]_\mathrm{t}} = \frac{k_{cat} + k_{cat(i)}\left(\frac{[S]}{K_I}\right)^x}{1 + \left(\frac{K_M}{[S]}\right)^n + \left(\frac{[S]}{K_I}\right)^x} \tag{2}$$

where $[\mathrm{E}]_\mathrm{t}$ is the total enzyme concentration; [S] is the concentration of the substrate (*e.g.* CH_2H_4fol in this case); $k_{cat(i)}$ accounts for the activity when the substrate binds in the inhibitory mode (*i.e.* if products can still form when the substrate binds in the inhibitory mode); K_M and K_I are the Michaelis constant and inhibition constant of the substrate, respectively; *n* and *x* are Hill coefficients for the cooperativity of substrate binding in the productive mode and inhibitory mode, respectively. Previous crystallographic studies suggested that the alternative binding mode of CH_2H_4fol is unproductive due to improper orientation for the catalyzed reaction, *i.e.* $k_{cat(i)} = 0$.[158] Analysis of the initial velocities using Eq 2 with $k_{cat(i)} = 0$ shows that the integer value of $n = 1$ provides the best fit in both the absence and presence of Mg^{2+}. This result agrees with the previously suggested

"half-of-the-sites" activity for ecTSase, *i.e.* one competent active site per dimer with no cooperativity in the productive binding mode (n = 1).[54-56] To reduce errors on the kinetic parameters in the statistical analysis, we fixed n =1 in the following data analysis, which simplifies Eq 2 to Eq 3:

$$\frac{v}{[\mathrm{E}]_t} = \frac{k_{cat}[\mathrm{S}]}{K_M + [\mathrm{S}]\left(1 + \left(\frac{[\mathrm{S}]}{K_I}\right)^x\right)} \tag{3}$$

Analysis of the initial velocities using Eq 3 shows that the integer value of x =2 provides the best fit in the absence of Mg^{2+}, while x =1 is optimal in the presence of Mg^{2+}. These results implicate that Mg^{2+} alters the interaction between the protein and CH_2H_4fol, which eliminates the cooperativity of CH_2H_4fol binding in the inhibitory mode. Further analysis on the kinetic parameters used x=2 for the initial velocities in the absence of Mg^{2+}, and x=1 in the presence of Mg^{2+}, and the results are presented in Figure 4-2 and Table 4-2.

Equilibrium Dissociation Constants

Equilibrium dissociation constants of the enzyme complexes were measured by titrating Mg^{2+} or dUMP into a solution of ecTSase, following the previously established fluorescence assay.[98] The excitation wavelength was 290nm, and the maximum emission of fluorescence was at 334 nm. Each experiment contained at least a duplicate of datasets. To correct for fluorescence changes that are not associated with the protein, we conducted parallel titrations in which ecTSase was replaced by a quantity of tryptophan with the same initial fluorescence intensity. We also conducted control experiments in which dUMP was titrated into the solution that contained all the reagents except the protein/tryptophan in the absence and presence of Mg^{2+}. Those control experiments did

not produce detectable fluorescence signals, suggesting that the interactions between the ligands (if exist) do not affect the fluorescence intensity measured for the protein.

We measured the dissociation constants that describe the interactions between Mg^{2+} and ecTSase apoenzyme, and between Mg^{2+} and the binary ecTSase-dUMP complex. The initial solution contained 25 mM dithiothreitol (DTT), 1 mM ethylenediaminetetraacetate (EDTA), and 0.8 μM ecTSase pre-incubated with 0 or 100 μM dUMP at 25 ˚C in 100 mM tris(hydroxymethyl)aminomethane (Tris)/HCl buffer (pH 7.5). Titrating a concentrated solution of $MgCl_2$ into the initial solution caused a decrease in protein fluorescence (after correcting for the dilution factor), which indicates protein conformational changes induced by Mg^{2+} binding. Although Mg^{2+} can possibly bind into multiple sites of TSase, we fit the data to the simplest model ("one-site binding", Eq 4) to compare the affinity of this ion for the apoenzyme and the binary complex:

$$I = \frac{I_E K_d + I_{EL}[\mathrm{L}]}{K_d + [\mathrm{L}]} \tag{4}$$

where I is the observed fluorescence intensity; I_E and I_{EL} are the molar fluorescence intensities for the apoenzyme and binary complex, respectively; [L] is the ligand concentration; and K_d is the dissociation constant for L.

We also measured the dissociation constants that describe the interactions between dUMP and apo-ecTSase, and between dUMP and the binary ecTSase-Mg^{2+} complex. The initial solution contained 25 mM DTT, 1 mM EDTA, and 0.8 μM ecTSase pre-incubated with 0 or 50 mM $MgCl_2$ in 100 mM Tris/HCl buffer (pH 7.5). Titrating a concentrated solution of dUMP into the initial solution caused a decrease in protein fluorescence due to dUMP binding. Previous studies suggested dUMP only binds to one active site per ecTSase dimer in the absence of CH_2H_4fol.[98] Thus, we fit the data to the one-site binding model (Eq 4) to evaluate the dissociation constants of dUMP.

Due to the non-specific quenching of fluorescence by formaldehyde (HCHO), which is used to stabilize CH_2H_4fol in solution, we cannot directly measure the dissociation constant of CH_2H_4fol by the fluorescence assay. Instead, we used the equation derived by Klinman and Matthews[160] (Eq 5) to calculate the dissociation constants of CH_2H_4fol:

$$K_d = K_M \cdot \frac{{}^{\mathrm{D}}\left(k_{cat}/K_M\right)_{\mathrm{H}} - 1}{{}^{\mathrm{D}}k_{cat} - 1} \tag{5}$$

where K_M is obtained from the steady state kinetic experiments (Table 4-2); ${}^{\mathrm{D}}k_{cat}$ is H/D KIE measured on k_{cat} by the noncompetitive KIE experiment (Table 4-4); and ${}^{\mathrm{D}}(k_{cat}/K_M)_{\mathrm{H}}$ is the H/D KIE on k_{cat}/K_M, which is calculated from the intrinsic H/D KIE and kinetic commitment factor on the hydride transfer (Table 4-6).

Noncompetitive KIE Experiments

Spencer *et al* have measured the KIEs on k_{cat} at 25 ˚C using the noncompetitive experiments in the absence of Mg^{2+}.[98] We conducted the experiments under the same conditions in the presence of 50 mM $MgCl_2$, with 100 μM dUMP and various concentrations of *6R*-^{x}H-CH_2H_4fol (^{x}H = H or D) in 100 mM Tris/HCl buffer (pH 7.5). Addition of ecTSase to the final concentration of 20 or 80 nM initiated the reaction for *6R*-H-CH_2H_4fol or *6R*-D-CH_2H_4fol, respectively.

Competitive KIE Experiments

Our previous study used the competitive method to measure the KIEs on k_{cat}/K_M, and the temperature dependence of intrinsic KIE on the hydride transfer step in the absence of Mg^{2+}.[35] In the current study, we conducted the experiments under the same conditions in the presence of 50 mM $MgCl_2$. Following the previously published

procedure,[35] we used the modified Northrop method to extract the intrinsic KIE from the observed H/T and D/T KIEs on k_{cat}/K_M (Eq 6):[27,29,32]

$$\frac{{}^{\mathrm{T}}\left(k_{cat}/K_M\right)_{\mathrm{H}}^{-1}-1}{{}^{\mathrm{T}}\left(k_{cat}/K_M\right)_{\mathrm{D}}^{-1}-1}=\frac{\left({}^{\mathrm{T}}k\right)^{-1}-1}{\left({}^{\mathrm{T}}k\right)^{-1/3.34}-1} \tag{6}$$

where ${}^{\mathrm{T}}\left(k_{cat}/K_M\right)_{\mathrm{H}}$ and ${}^{\mathrm{T}}\left(k_{cat}/K_M\right)_{\mathrm{D}}$ are the observed H/T and D/T KIEs on k_{cat}/K_M, respectively; and ${}^{\mathrm{T}}k$ is the intrinsic H/T KIE on the hydride transfer (${}^{\mathrm{T}}k = k_{\mathrm{H}}/k_{\mathrm{T}}$). We have developed an online program, as well as a Mathematica script, to solve Eq 6 numerically for ${}^{\mathrm{T}}k$ at each temperature (http://ccs14.chem.uiowa.edu/faculty/kohen/group/tools.html). Fitting the intrinsic KIE values to the Arrhenius equation (Eq 7) allows analysis of their temperature dependence:[27]

$${}^{\mathrm{T}}\left(k\right)_{\mathrm{L}}=\frac{k_{\mathrm{L}}}{k_{\mathrm{T}}}=\frac{A_{\mathrm{L}}}{A_{\mathrm{T}}}\exp\left(\frac{-\Delta E_a}{\mathrm{RT}}\right) \tag{7}$$

where the subscripts L and T denote a light (H or D) and a heavy (T) isotope of hydrogen, respectively; ΔE_a is the difference in the activation energies of the hydride transfer between the light and heavy isotopes. Since the hydride transfer is irreversible, the comparison between the observed and intrinsic KIEs provides the forward kinetic commitment (C_f) on k_{cat}/K_M (Eq 8).[29,32] Table 4-6 summarizes the observed and intrinsic KIEs, as well as C_f, at the four experimental temperatures in the presence of Mg^{2+}.

$${}^{\mathrm{T}}\left(k_{cat}/K_M\right)_{\mathrm{H}}=\frac{{}^{\mathrm{T}}k+C_{\mathrm{f}}}{1+C_{\mathrm{f}}}$$

$$\Rightarrow \quad C_{\mathrm{f}}=\frac{{}^{\mathrm{T}}k-{}^{\mathrm{T}}\left(k_{cat}/K_M\right)_{\mathrm{H}}}{{}^{\mathrm{T}}\left(k_{cat}/K_M\right)_{\mathrm{H}}-1} \tag{8}$$

Similarly, for H/D KIEs,

$$^{\mathrm{D}}\left(k_{cat}/K_M\right)_{\mathrm{H}} = \frac{^{\mathrm{D}}k + C_{\mathrm{f}}}{1 + C_{\mathrm{f}}} \tag{9}$$

Identifying Mg^{2+} in the Crystal Structures

Divalent Mg^{2+} ion has an identical number of electrons (10) as water and thus is difficult to distinguish in electron-density maps, particularly if the position is partially occupied or the maps are obtained at low resolution. We examined the water molecules in a 1.3 Å-resolution crystal structure of the ternary ecTSase-dUMP-CB3717 complex (PDB ID: 2G8O) for putative Mg^{2+} ions with an approximate octahedral arrangement of hydrogen bonding (H-bonding) partners. A few candidate water molecules were on the periphery of the protein outside the binding region for the ligands, while the only candidate water (*i.e.* putative Mg^{2+}) that can potentially affect catalysis was in the binding groove for the Glu-moiety of the cofactor (Figure 4-8). This putative Mg^{2+} formed H-bonds with five other water molecules and with the backbone carbonyl of N76. Interatomic distances of five of the H-bonds were 2.4 Å, and the sixth was 2.7 Å, which are shorter than the average H-bond length between water molecules. Two of the coordinated water molecules formed H-bonds with the carboxyl oxygen of the Glu of the cofactor, while four of them (including one water that was also H-bonded with the cofactor Glu) formed H-bonds with the protein backbone carbonyl or side chains (Figure 4-8). This water cluster was only seen in the more highly-resolved protomer (*i.e.* with lower isotropic B-factors) of the ecTSase dimer. In contrast, the electron density maps for both protomers of the ecTSase ternary complex with dUMP and a di-Glu antifolate inhibitor has strong, unambiguous density for Mg^{2+} that is octahedrally coordinated with six water molecules in the poly-Glu binding sites (Finer-Moore and Stroud, unpublished results). This density can be fit with the ideal geometry for an octahedrally coordinated

Mg^{2+}, where the distances between Mg^{2+} and coordinated water molecules are approximately 2.1 Å.

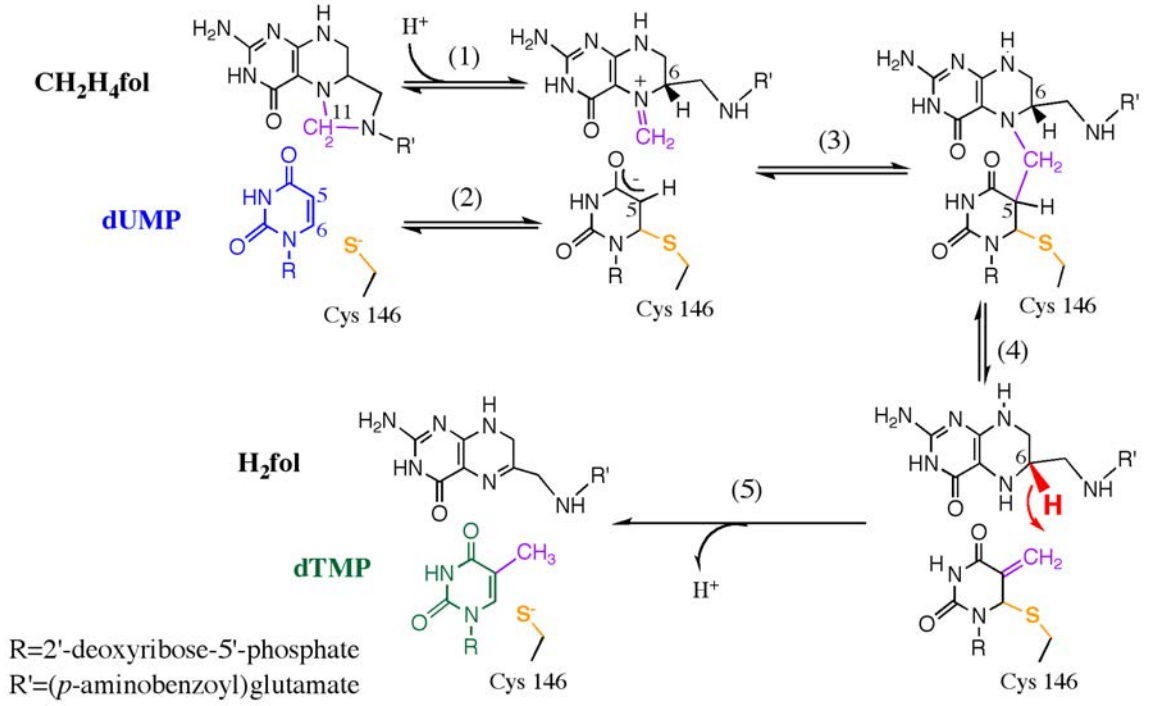

Figure 4-1. The proposed catalytic mechanism of thymidylate synthase.

This reaction involves a series of chemical conversions (1-5), and the hydride (red) transfer (step 5) is rate limiting for the catalytic turnover (see text).

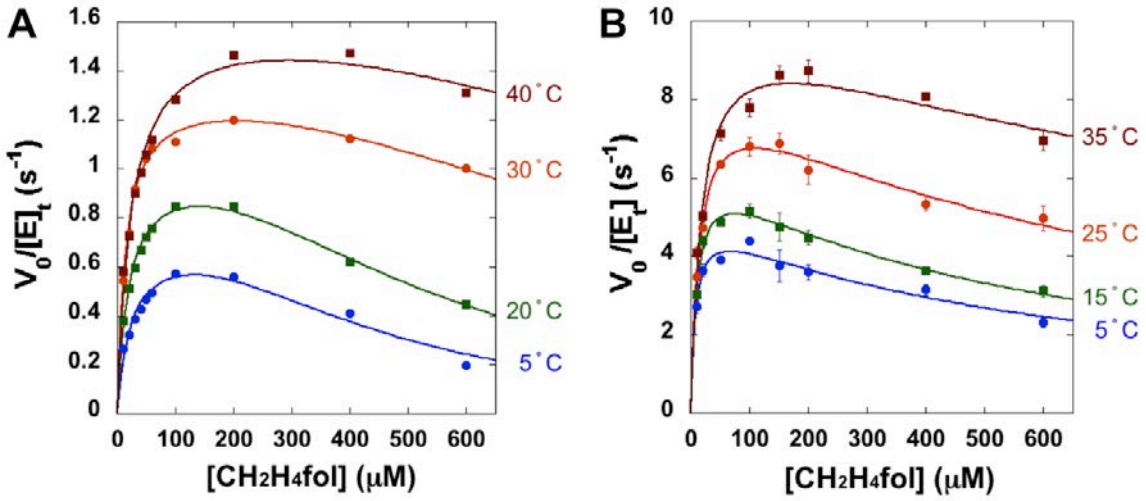

Figure 4-2. Mg^{2+} affects steady state kinetics of thymidylate synthase.

This figure presents the initial velocity of ecTSase-catalyzed reaction *vs*. concentration of CH_2H_4fol, in the (A) absence and (B) presence of 50 mM $MgCl_2$.

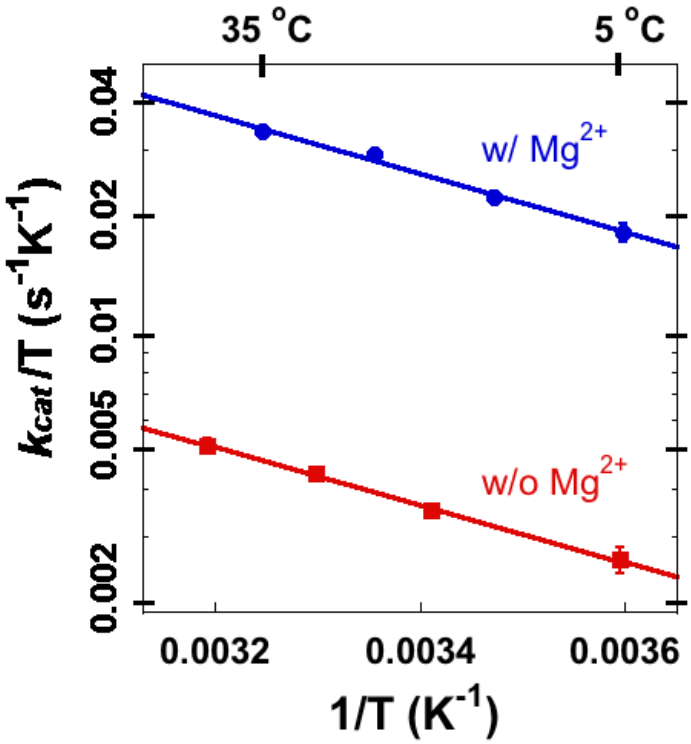

Figure 4-3. Mg^{2+} accelerates k_{cat} by *ca*. 7-fold.

This figure presents the Eyring plots of initial velocity of ecTSase-catalyzed reaction in the absence (w/o, red) and presence (w/, blue) of 50 mM $MgCl_2$ in the temperature range 5-35 ˚C.

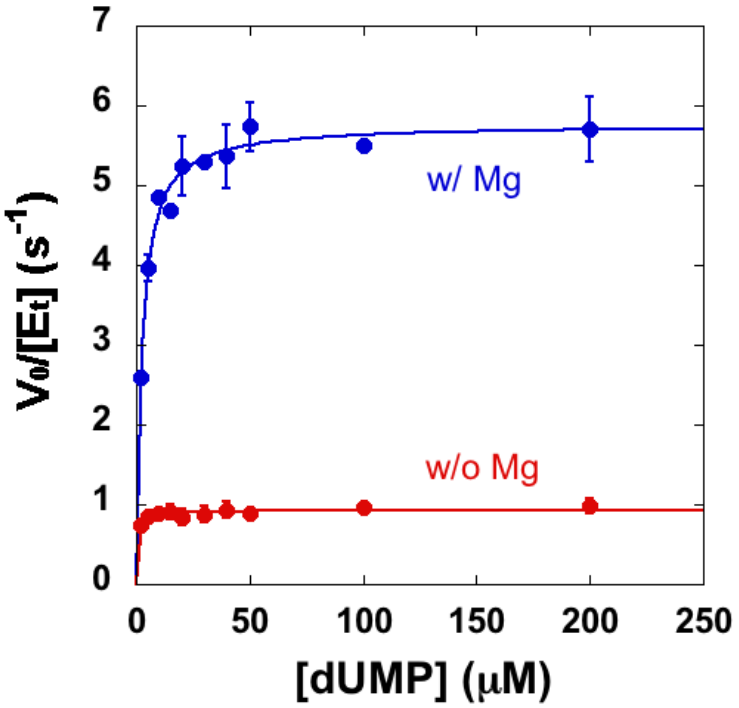

Figure 4-4. Mg^{2+} affects K_M of dUMP.

This figure presents the initial velocity of ecTSase-catalyzed reaction *vs*. concentration of dUMP, in the (A) absence (w/o, red) and (B) presence (w/, blue) of 50 mM $MgCl_2$.

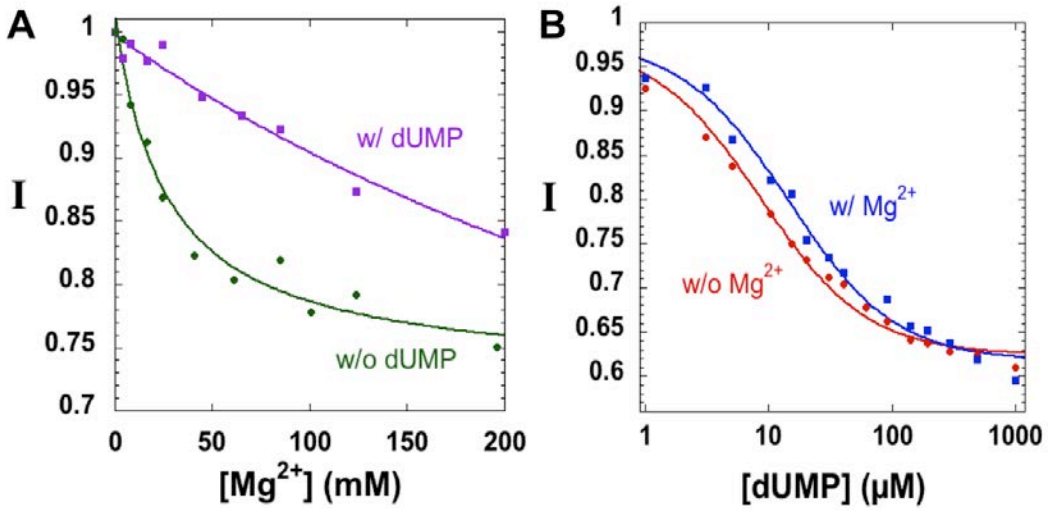

Figure 4-5. Measurements of dissociation constants of ecTSase complexes.

This figure presnts the fluorescence intensity (I, relative to the initial intensity) of ecTSase (A) vs. $MgCl_2$ concentration in the absence (w/o, green) and presence of 100 μM (w/, purple) dUMP; and (B) vs. dUMP concentration in the absence (w/o, red) and presence of 50 mM (w/, blue) of $MgCl_2$.

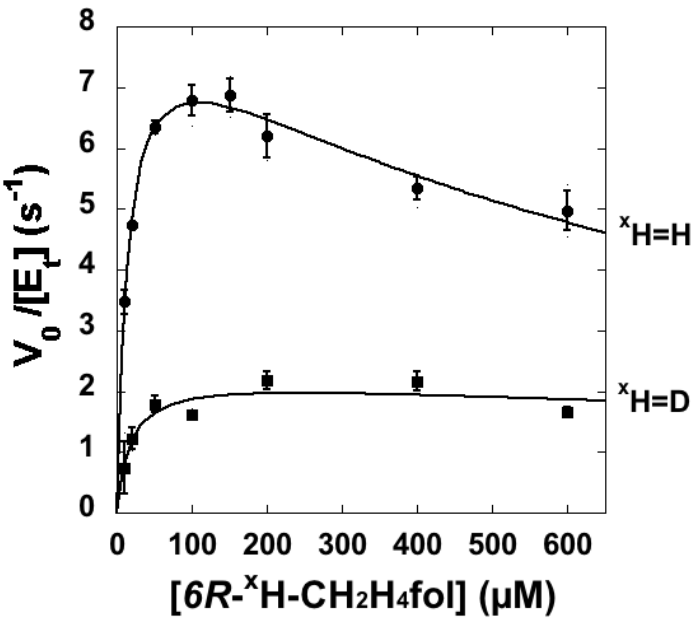

Figure 4-6. Measurements of the KIE on k_{cat} of ecTSase in the presence of Mg^{2+}.

This figure presents the initial velocity of TSase-catalyzed reaction *vs*. concentration of *6R*-^{x}H-CH_2H_4fol (^{x}H = H or D), in the presence of 50 mM $MgCl_2$ at 25 ˚C.

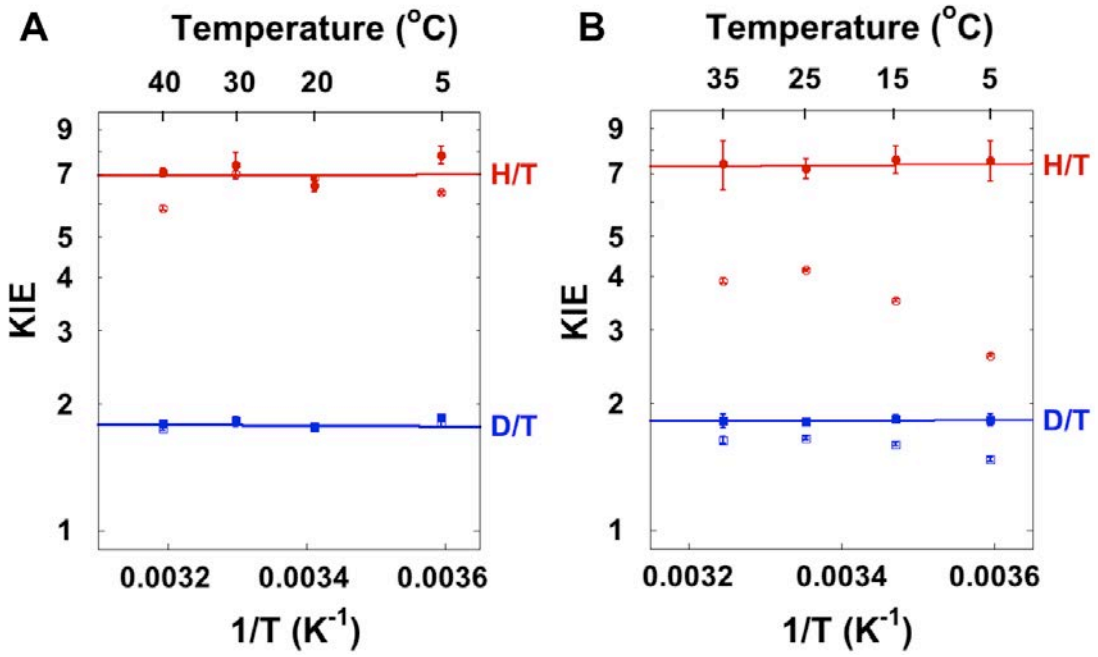

Figure 4-7. The observed and intrinsic KIEs in the absence and presence of Mg^{2+}.

This figure presents the observed KIEs on k_{cat}/K_M (empty symbols) and the intrinsic KIEs (filled symbols) on the hydride transfer in the (A) absence and (B) presence of 50 mM $MgCl_2$. The observed and intrinsic KIE values in the presence of Mg^{2+} are presented in Table 4-6. The lines are nonlinear regression of the intrinsic KIEs to Arrhenius equation (Eq 7 in ES).

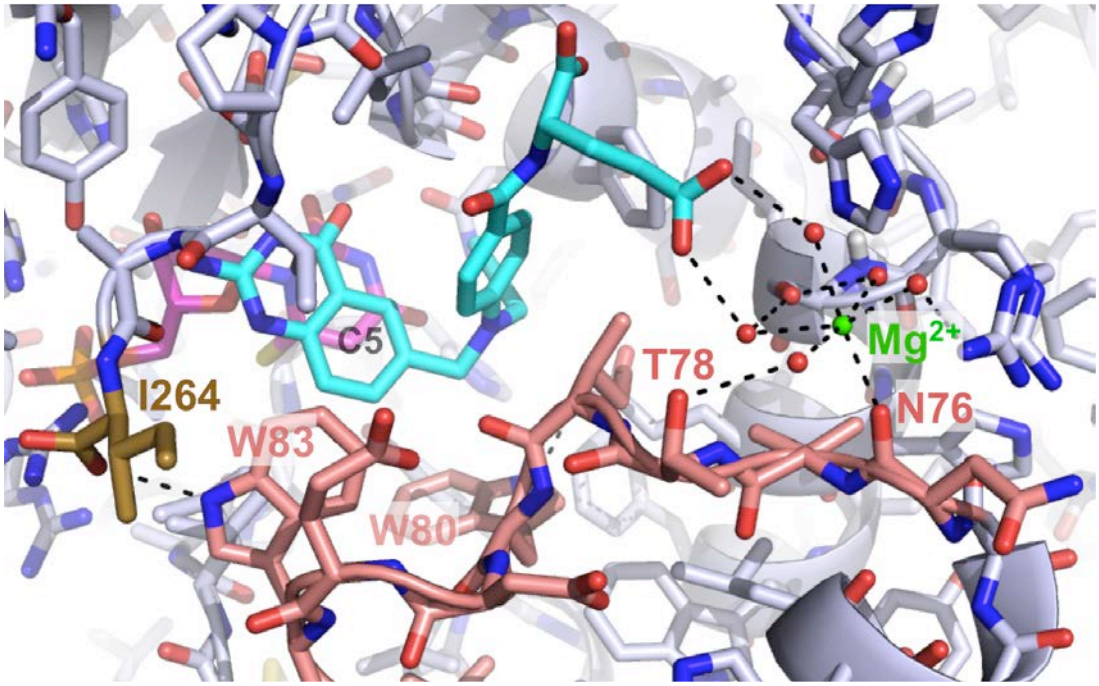

Figure 4-8. The structural evidence for Mg^{2+} binding to ecTSase.

Mg^{2+} (green) binds to the surface of ternary ecTSase-dUMP-CB3717 complex. The cofactor analogue CB3717 is shown in cyan, and the substrate dUMP is shown in magenta. All the catalyzed chemical transformations occur near C5 of dUMP (labeled in black, see Figure 4-1) in the interior active site. Mg^{2+} mediates an H-bond network between the Glu-tail of the cofactor and the backbone carboxylates (*e.g.* N76 and T78) of the loop (residues 76-93 in ecTSase, pink) containing residues W80 and W83, which are important for closing the active site cavity (see text). The C-terminus (I264, brown) is very flexibile in apo-TSase, but it is immobilized by an H-bond with W83 in the ternary complex upon the cofactor binding.

Table 4-1. Mg^{2+} affects the activation parameters of k_{cat} of ecTSase.[a]

TSase	$\Delta H^{\ddagger}$ kcal/mol	$-T\Delta S^{\ddagger}$ at 25 ˚C kcal/mol	$\Delta G^{\ddagger}$ kcal/mol
w/ Mg^{2+}	3.4 ± 0.2	12.8 ± 0.2	16.2 ± 0.4
w/o Mg^{2+} [b]	3.4 ± 0.1	13.9 ± 0.1	17.3 ± 0.2

Notes:

[a] This figure presents activation parameters from fitting k_{cat} of ecTSase to the Eyring equation (Eq 1) in the absence (w/o) and presence (w/) of 50 mM $MgCl_2$. The KIE experiments suggest that the hydride transfer is rate limiting for k_{cat} under both conditions (see text below), thus, the steady-state kinetic experiments actually exposed the activation parameters for the hydride transfer step. The values of k_{cat} are presented in Table 4-2.

[b] Data are from Ref 35.

Table 4-2. Steady state kinetic parameters of ecTSase in the absence and presence of Mg^{2+}.

w/ Mg^{2+} w/o Mg^{2+} [b]	5 °C 5 °C	15 °C 20 °C	25 °C 30 °C	35 °C 40 °C
k_{cat} (s^{-1})	5.1 ± 0.3 0.73 ± 0.06	6.5 ± 0.2 1.02 ± 0.03	8.7 ± 0.2 1.32 ± 0.02	10.3 ± 0.3 1.62 ± 0.06
$K_M^{CH_4H_4fol}$ (μM)	8 ± 1 24 ± 5	11 ± 1 20 ± 2	15 ± 1 14 ± 1	19 ± 2 24 ± 3
$K_I^{CH_4H_4fol}$ (mM)	0.6 ± 0.1 0.43 ± 0.05	0.52 ± 0.05 0.53 ± 0.02	0.76 ± 0.07 1.09 ± 0.07	1.5 ± 0.2 1.5 ± 0.3

Notes:

[a] This table presents the steady state kinetic parameters of ecTSase in the absence (w/o) and presence (w/) of 50 mM $MgCl_2$.

[b] Data are from Ref 35.

Table 4-3. Mg^{2+} affects the Michaelis constants and dissociation constants of the substrates.

	K_M^{dUMP} [a] (μM)	K_d^{dUMP} [b] (μM)	$K_M^{\mathrm{CH_4H_4fol}}$ [a] (μM)	$K_d^{\mathrm{CH_4H_4fol}}$ (μM)
w/ Mg^{2+}	2.4 ± 0.2	14 ± 2	15 ± 1	8 ± 1 [c]
w/o Mg^{2+}	0.5 ± 0.1	8.5 ± 0.9	17 ± 2	17 ± 2 [d]

Notes:

This table presents the Michaelis constants and dissociation constants of dUMP and CH_2H_4fol for ecTSase in the absence (w/o) and presence (w/) of 50 mM $MgCl_2$ at 25 ˚C.

[a] The Michaelis constants are measured by steady-state kinetics (Figures 4-2 and 4-4).

[b] K_d^{dUMP} is measured by the fluorescence assay (Figure 4-5B).

[c] In the presence of Mg^{2+}, ${}^{\mathrm{D}}(k_{cat}/K_M)_{\mathrm{H}}$ is 2.5 ± 0.2 (Table 4-6, Note *b*), ${}^{\mathrm{D}}k_{cat}$ is 3.8 ± 0.3 (Table 4-4), and $K_d^{\mathrm{CH_4H_4fol}}$ is calculated using Eq 5.

[d] In the absence of Mg^{2+}, both ${}^{\mathrm{D}}k_{cat}$ and ${}^{\mathrm{D}}(k_{cat}/K_M)_{\mathrm{H}}$ are equal to the intrinsic H/D KIE on the hydride transfer,[35,98] and thus $K_d^{\mathrm{CH_4H_4fol}}$ is equal to $K_M^{\mathrm{CH_4H_4fol}}$ (Eq 5).

Table 4-4. The observed and intrinsic H/D KIEs in the absence and presence of Mg^{2+}.

6R-^{x}H-CH_2H_4fol		k_{cat} (s^{-1})	$K_M^{CH_2H_4folate}$ (μM)	$K_I^{CH_2H_4folate}$ (mM)	$^{D}k_{cat}$	^{D}k
w/ Mg^{2+}	^{x}H = H	8.7 ± 0.2	15 ± 1	0.76 ± 0.07	3.8 ± 0.3	3.9 ± 0.2 [a]
	^{x}H = D	2.3 ± 0.2	19 ± 5	3 ± 1		
w/o Mg^{2+}					3.7 ± 0.1 [b]	3.8 ± 0.3 [c]

Notes:

This table presents the observed H/D KIEs on k_{cat} ($^{D}k_{cat}$) and the intrinsic H/D KIEs (^{D}k) on the hydride transfer of ecTSase at 25 ˚C, in the absence (w/o) and presence (w/) of 50 mM $MgCl_2$.

[a] Determined as described below (25 ˚C row in Table 4-6).

[b] From Ref 98.

[c] From Ref 35.

Table 4-5. Isotope effects on the Arrhenius parameters of the hydride transfer of ecTSase.[a]

	Mg^{2+} absent [b]	Mg^{2+} present	S.C. A_L/A_T [c]
A_H/A_T	6.8 ± 2.8	6.6 ± 1.3	0.5 – 1.6
$\Delta E_{a\ H\text{-}T}$ (kcal/mol)	0.02 ± 0.25	-0.06 ± 0.12	

Notes:

[a] The intrinsic KIE values were fit to the Arrhenius equation (Eq 7 in ES) to analyze their temperature dependence.

[b] From Ref 35.

[c] Semi-classical limits of the isotope effects on the pre-exponential factor.[34,82,103]

Table 4-6. The observed KIE on k_{cat}/K_M, the intrinsic KIE on the hydride transfer, and C_f in the presence of Mg^{2+}.

	Observed KIE $^{T}(k_{cat}/K_M)_L$		Intrinsic KIE on the hydride transfer [a]			C_f
	H/T	D/T	H/T	H/D	D/T	
5 ˚C	2.59 ± 0.02	1.47 ± 0.02	7.5 ± 0.8	4.0 ± 0.3	1.83 ± 0.06	3.1 ± 0.5
15 ˚C	3.51 ± 0.02	1.60 ± 0.02	7.6 ± 0.6	4.1 ± 0.2	1.83 ± 0.04	1.6 ± 0.2
25 ˚C	4.14 ± 0.02	1.65 ± 0.01	7.2 ± 0.4	3.9 ± 0.2	1.81 ± 0.03	1.0 ± 0.1
35 ˚C	3.91 ± 0.05	1.63 ± 0.03	7.4 ± 0.9	4.0 ± 0.4	1.82 ± 0.07	1.2 ± 0.3

Notes:

[a] The intrinsic H/T KIE is numerically solved from Eq 6 in the main text, and the intrinsic H/D and D/T KIEs are calculated from the intrinsic H/T KIE using the Swain-Schaad relationship.[166]

CHAPTER V

QM/MM CALCULATIONS SUGGEST A UNIQUE MECHANISM FOR THE PROTON ABSTRACTION CATALYZED BY THYMIDYLATE SYNTHASE

Introduction

The cleavage of covalent C-H bonds is one of the most important yet energetically demanding chemical transformations in nature. Many enzymes catalyze C-H bond activations that are critical for the healthy metabolisms and normal growth of biological organisms.[167-169] One of such essential processes in life is DNA synthesis. Among the four DNA nucleotides, 2'-deoxythymidine-5'-monophosphate (dTMP, deoxythymidylate) is the only precursor unique to DNA, which is replaced by uridine-5'-monophosphate (UMP, uridylate) in RNA in most organisms. The only intracellular *de novo* source of dTMP is the reductive methylation of deoxyuridine-5'-monophosphate (dUMP) catalyzed by thymidylate synthase (TSase), which involves a C-H bond activation in the substrate (Figure 5-1). Since TSase is present in most living organisms, and it is overexpressed in tumor cells,[58,59] this enzyme has been an attractive target for both antibiotic and anticancer drugs. Classical drugs that target TSase are precursors of analogues of either the substrate (*e.g.* 5-fluorouracil) or the folate cofactor (*e.g.* 10-propargyl-5,8-dideazafolic acid, also known as CB3717). These drugs often interact with other proteins involved in the metabolic pathways of either nucleosides/nucleotides or folates, leading to toxicity and development of resistance in cells.[170] Therefore, current drug designs focus on selectively targeting TSase activity in tumor cells, for anticancer drugs, or in specific species, for antibiotic drugs. While the former has benefited from studies of the regulatory function of TSase on some oncogenes of mRNA, the latter can be aided by careful inspection of the mechanistic features of TSase.[170,171]

In TSase-catalyzed reaction, the folate cofactor, 5,10-methylene-5,6,7,8-tetrahydrofolate (CH_2H_4folate), donates the methylene and hydride to the substrate dUMP, producing 7,8-dihydrofolate (H_2folate) and dTMP. Figure 5-2 present the traditionally proposed mechanism for this multi-step reaction,[61] which involves activation of two C-H bonds: a C-H→B (B: general base) proton abstraction from C5 of dUMP (step 4 in Figure 5-2), and a C-H→C hydride transfer from $C6^F$ of CH_2H_4folate to the exocyclic-methylene intermediate (step 5). We have studied those two C-H bond activation steps in the wild-type (WT) *Escherichia coli* TSase (ecTSase) by measuring the temperature dependence of their intrinsic kinetic isotope effects (KIEs). The KIE on the hydride transfer is temperature independent[35] while that on the proton transfer is temperature dependent[64], implying a better-organized transition state (TS) for the former. In order to investigate the molecular details underlying those experimental observations, we have studied the catalytic mechanism of WT ecTSase by calculations using the hybrid quantum mechanics/molecular mechanics (QM/MM) potentials.[95,96,123,155,172] Our calculations suggested that the hydride transfer is concerted with cleavage of the covalent bond between C6 of dUMP and S of the C146 residue (noted "C6-S bond" hereafter), which regenerates the free form of the protein (Figure 5-2). Important protein motions progressively accommodate the changes in geometric and electrostatic characteristics of the ligands during the hydride transfer, thereby reducing the free energy barrier. Particularly, a highly conserved arginine residue, R166, approaches C146 as the reaction proceeds, which polarizes the electron density around the S atom to stabilize the TS.[96,123,155] It appears that, owing to the adaptability of the protein environment, the average TS structure is invariant within the examined temperature range (5-40˚C), which leads to a temperature-independent KIE that is consistent with our experimental findings.[172]

In contrast to the well-resolved mechanism for the hydride transfer, the general base that abstracts the proton (H5) from C5 remains unidentified, due to the complicated

network of H-bonds at the active site as indicated by previous structural and kinetic studies,[62,94] Furthermore, the deprotonation of C5 is tightly coupled with the subsequent ß-elimination of the cofactor in WT TSase (step 4 in Figure 5-2),[61,63] making it difficult to expose the intrinsic nature of this C-H bond activation. Earlier work exploited model reactions in solution,[173-175] as well as the tritium release and dehalogenation from C5 of dUMP and analogues in the binary enzyme complexes,[176,177] and proposed that an enol/enolate forms at C5-C4=O4 of dUMP during the proton transfer step. On the contrary, our previous QM/MM calculations with semiempirical AM1 method suggested the deprotonation of C5 leads to cleavage of the C6-S bond, with minimal polarization of the C4=O4 carbonyl.[95] This computational result implicates a new reaction intermediate where the ligands are not covalently attached to the protein, providing new directions for drug designs that target TSase activity.

To further investigate the suggestions from previous calculations, the current study thoroughly explores different proposed mechanisms for the proton transfer step with higher-level QM/MM calculations (Figure 5-3). We first calculated the potential energy profiles of different proposed mechanisms, and then studied the free energy profile to delineate features of the TS for the proton transfer. Our calculations not only provide the molecular details underlying previous experimental observations, but also suggest future experiments that can examine the proposed mechanisms.

Results and Discussion

Proton Transfer Mechanism

In order to resolve the proton transfer mechanism, we thoroughly explored the potential energy surface (PES) of this reaction using various combinations of distinguished reaction coordinates (DRCs). Although experiments were unable to isolate the deprotonation of C5 from the subsequent ß-elimination of the cofactor in WT TSase,[63] our 2D-PES mapping suggests that cleavage of the C7-N5^{F} bond only occurs

after deprotonation of C5 and protonation of $N5^F$. Figure 5-4 summarizes three major proposed mechanisms that our calculations have investigated. In the traditional mechanism proposed by Carreras and Santi (Mechanism I),[61] the C4=O4 carbonyl forms an enol with C5 during the deprotonation step, which then transfers the proton to $N5^F$ through a water molecule and becomes an enolate. The following cleavage of C7-$N5^F$ generates H_4folate, which finally donates a hydride to the exocyclic methylene intermediate (Complex D). In addition, Hardy *et al*. found 5-deazatetrahydrofolate cannot stimulate TSase-catalyzed tritium release, and thus proposed $N5^F$ is the general base that deprotonates C5 (Mechanism II).[178] The structure of the intermediate after the proton transfer step (step II.1) is similar to the one in Mechanism I (after step I.2), but the $N5^F$ atom has a different chirality (see structures in Figure 5-6). Therefore, the potential energy profiles for the subsequent C7-$N5^F$ cleavage are different in those two mechanisms. Both Mechanisms I and II involve formation of enol/enolate at C5-C4=O4, which are in accordance with the classical catalytic mechanism proposed for abstraction of an α–proton adjacent to a carbonyl group.[179] In contrast, our previous AM1/MM PES calculations suggested that an active site water molecule (wat47) abstracts H5 from C5, leading to cleavage of the C6-S bond (Mechanism III).[95] This protonated water molecule then transfers a proton to $N5^F$, followed by S re-attacking C6 to eliminate H_4folate. Calculations of the potential of mean force (PMF, below) suggest that an oxocarbonium cation $C4^+$-O4H (or its resonance form C4=$O4H^+$) can form after the deprotonation of C5 and cleavage of C6-S bond (the structure in the parenthesis in Figure 5-4), without affecting the free energy surface for the proton transfer (see Computation Details). We located a TS and the corresponding reactant and product structures for this mechanism and found it has the same potential energy barrier as Mechanism III. In forming the oxocarbonium, the deprotonation of C5 and protonation of O4 are mediated by wat47, which is the proton abstractor in Mechanism III. Consequently, this mechanism can be

described by the same DRC as Mechanism III (i.e. $d_{C5\text{-}H5}$ - $d_{H5\text{-}Ow}$ and $d_{C6\text{-}S}$) and can be considered as the same mechanism that exploits the lability of the C6-S bond.

Figure 5-5 plots the potential energy profiles of the three proposed mechanisms in Figure 5-4. Our results suggest that Mechanism III is the lowest energy path and thus the most probable mechanism for the proton transfer. Among these examined mechanisms, only Mechanism III presents the hydride transfer step as the highest potential energy barrier, which agrees with previous experimental observations that the hydride transfer is rate limiting for the catalytic turnover.[35,98] Although an enol could form in Mechanism III, the cleavage of C6-S bond plays the essential role in lowering the activation energy barrier for the deprotonation of C5.

Since calculations using the semiempirical AM1 Hamiltonian usually over-estimate the energy barriers for chemical bond cleavages/formations, we employed B3LYP/6-31G(d,p) method to calculate a TS and the corresponding reactant and product structures for the first step of each proposed mechanism (Figure 5-6). The potential energy profiles calculated with B3LYP/MM methods are also presented in Figure 5-5. The B3LYP/MM calculations significantly reduced the heights of the activation energy barriers, but did not change the trend when comparing different proposed mechanisms, which authenticates the use of the much cheaper AM1/MM method in in this case.

Free Energy Profile of the Deprotonation of C5

Our previous experiments found different temperature dependences of KIEs on the proton and hydride transfer steps,[35,64] and our calculations have revealed important mechanistic features for the latter.[96,122-124] In order to afford a good starting point to compare the nature of those two C-H bond activations, we calculated the PMF of the deprotonation of C5, using the antisymmetric combination of the distances describing the proton transfer as the DRC (DRC = $d_{C5\text{-}H5}$ - $d_{H5\text{-}Ow}$, where Ow refers to the oxygen atom of wat47). The obtained free energy profile describes an endothermic chemical reaction

(ΔG = 13.5 kcal·mol^{-1}), with an activation free energy ($\Delta G^{\ddagger}$) of 25.5 kcal·mol^{-1} (Figure 5-7A).

We analyzed the important interatomic distances that changed along the DRC in this PMF calculation (Figure 5-7B). While the proton is transferred from the donor to the acceptor ($d_{C5\text{-}H5}$ and $d_{H5\text{-}Ow}$), the distance between the donor and acceptor ($d_{C5\text{-}Ow}$) reaches the minimum value at the TS. Figure 5-8 provides additional analysis of key geometric parameters around C5 of dUMP, which confirms formation of an intermediate double bond (C5=C6) after the deprotonation of C5 and elimination of the S anion from C6. An interesting observation is that R166 approaches C146 ($d_{S\text{-}H_{R166}}$) during the proton transfer to stabilize the S anion upon the C6-S cleavage ($d_{C6\text{-}S}$), which is similar to the findings of calculations on the hydride transfer.[96,122-124] However, different from the hydride transfer step, the C6-S bond is fully broken (4.5 Å) before the proton transfer reached the TS, suggesting the C6-S distance is an important component of the real reaction coordinate of this reaction. In order to better understand the proton transfer mechanism, we calculated the 2D-PMF using the C6-S bond distance as an additional dimension of the DRC (Figure 5-9A).

Our previous PMF calculations on the hydride transfer found one TS that was invariant at temperatures from 5 to 40 ˚C.[96,124] In contrast, the 2D-PMF surface for the proton transfer is more complex with multiple saddle points for different reaction paths (TSA, TSB, and TSC in Figure 5-9A). Each saddle point represents a collection of transition structures, which all together compose the ensemble-averaged TS that is probed by experiments for the proton transfer step. Since TSA, TSB, and TSC have similar free energies, the reaction goes through these three subsets of TS with comparable probabilities at 25 ˚C. Based on this complex free energy surface, a change in temperature could alter the distribution among the possible reaction paths, leading to different geometric properties of the ensemble-averaged TS. These 2D-PMF results provide a possible explanation for the temperature dependent KIE on the proton transfer

measured experimentally,[64] which contrast the simpler 2D-PMF surface[96] and the temperature independent KIE[35,124] found for the hydride transfer. The complexity of the free energy surface for the proton transfer most likely arises from the mobility of the proton acceptor – a water molecule – in the versatile network of H-bonds at the active site of TSase. In contrast, the hydride is transferred between two C atoms of the ligands, and is very sensitive to the orientations of dUMP and CH_2H_4folate.[35,62,63,65,67] This dissimilarity is probably the major determinant for the difference in temperature dependences of KIEs on those two C-H bond activations.

In addition, the 2D-PMF calculations revealed conformational changes in both dUMP and CH_2H_4folate after the deprotonation of C5 (Figure 5-9C), which are accompanied by rotations of protein residues and rearrangement of the H-bond network at the active site. These changes not only bring the protonated wat47 to a favorable location and orientation for the subsequent protonation of $N5^F$, but also destabilize the S anion to prepare C146 for the next nucleophillic attack onto dUMP during the cleavage of C7-$N5^F$. These synchronized motions of the protein, ligands, and solvent molecules provide an explanation for the previous experimental observations that the deprotonation of C5 is tightly coupled with ß-elimination of the cofactor in WT TSase.[61,63] Further analysis of the global network of H-bonds that accommodates those local changes is an interesting future direction that may reveal important long-range interactions in TSase activity.

Compared with the 2D-PMF results, the 1D PMF calculations (Figure 5-7) provided a TS equivalent to TSA (Figure 5-9), thus providing a similar magnitude for the free energy activation barrier. The 1D PMF calculations revealed important features for the proton transfer, i.e. the cleavage of C6-S bond and the interaction between R166 and C146. Beyond those features, the 2D-PMF calculations also exposed the multi-path nature and other interesting information for the proton transfer step. This comparison

suggests 2D-PMF calculations are valuable in studying a complex system whose reaction coordinate involves many degrees of freedom.

The Labile C6-S Bond

C146 is the nucleophile that attacks C6 of dUMP to initiate TSase-catalyzed reaction (step 1 in Figure 5-2). This C6-S bond was proposed to remain intact until the last chemical transformation in the catalytic turnover -- the hydride transfer step (step 5 in Figure 5-2).[63] The deprotonation of C5 of dUMP can occur in solution (e.g. with high concentrations of L-cysteine or other non-enzymatic catalysts)[112,180,181] as well as in the binary TSase-dUMP complex (Complex A in Figure 5-2)[177], and evidence suggested those reactions occur *via* formation of enol/enolate at C5-C4=O4.[61] In the ternary enzyme complex, the binding of CH_2H_4folate induces conformational changes in the protein as well as formation of a new C-C bond at C5 (Complex C in Figure 5-2). These changes may impose geometric strain on the uracil ring of dUMP and make the C6-S bond weaker, which would increase the acidity of the C5-H5 and facilitate the deprotonation.[182] Therefore, the formation of methylene bridge with the folate cofactor alters the reaction coordinate for the proton transfer step, which then occurs *via* a mechanism different from the model reactions in solution and the off-pathway deprotonation of C5 in the binary complex. Once the C6-S bond is broken after the proton transfer step, the question remains whether and when this labile bond forms again during the catalytic turnover. We examined the possibility of the subsequent C7-$N5^F$ cleavage (step III.3 in Figure 5-4) without reforming the C6-S bond and found a much higher energy barrier (33 kcal/mol with AM1/MM method), indicating that the S anion attacks C6 to assist ß-elimination of the cofactor. Furthermore, our previous calculations suggest that the cleavage of C6-S bond also lowers the activation energy barrier for the hydride transfer step. Therefore, the lability of C6-S bond is an important strategy of TSase to catalyze multiple chemical transformations.

We scrutinized all the available electron density maps for the crystal structures of ecTSase on the Protein Data Bank (http://www.rcsb.org/) and found the electron density between C6 and S is very diffuse in almost all the ternary complexes with dUMP and folate analogues (e.g. PDB IDs 2G8O, 1KZI, and 3BHL). These observations agree with our calculations and suggest that the conformations of the ternary enzyme complex allow the C6-S bond to be labile in catalyzing the chemical transformations of the ligands. Since the C6-S bond is the only proposed covalent bond between TSase and the ligands during the catalyzed reaction, our calculations implicate new reaction intermediates that are not covalently attached to the protein, providing new directions for drug designs that target DNA biosynthesis.

Functionalities of Several Key Residues in the Proton Transfer

Different from many other enzymes that use specific protein residues as the general acid/base, both experiments[94,183-185] and computations[95] suggested that TSase exploits active site water molecules as the proton donors/acceptors in various steps during the catalytic turnover. To examine the functionalities of active site residues, we conducted molecular dynamics (MD) simulations with the reaction intermediate (Complex C in Figure 5-2) in several single site mutants of ecTSase (see Computational Details). The results suggest that the network of H-bonds in TSase rearranges in response to the mutation, which could partially recover the functionalities of the mutated residue. This suggestion agrees with saturation mutagenesis studies that concluded only five protein residues[ix] are essential to TSase activity.[63] Our calculations found that four of

[ix] While the sequence of TSase has several hundreds of amino acids, there are only five residues essential for the catalytic activity: E58, Y94, C146, R166, and D169 (the numbering refers to ecTSase).

those five essential residues are involved in the proton transfer step, including C146, R166, E58, and Y94, where the particular roles of C146 and R166 have been discussed above.

Although a water molecule (wat47 in Figure 5-3) is the direct acceptor of the proton abstracted from C5, several protein residues can modulate the basicity of this water to influence the reaction. Particularly, the negatively charged E58 forms the largest number of H-bonds with other active site residues and water molecules, and thus is critical to the entire H-bond network at the active site. In the reactant state of the proton transfer step, E58 is connected to wat47 *via* H-bonds through another water molecule (Figure 5-9C, R). The conformational fluctuations of protein environment enable formation of a direct H-bond between E58 and wat47, which increases the basicity of wat47 for the proton abstraction and then brings the protonated wat47 to a favorable position for the subsequent protonation of $N5^F$ (Figure 5-9C). These results agree with previous experiments that found mutations on E58 caused moderately slower deprotonation of C5 and dramatically slower ß-elimination of the cofactor, leading to accumulation of the ternary enzyme complex.[178]

In addition, the Y94 residue was postulated to act as the general base to deprotonate C5,[186,187] based on its proximity to the fluorine of 5-fluoro-dUMP (5F-dUMP) in the crystal structure of the ternary TSase-(5F-dUMP)-CH_2H_4folate complex.[182] Our calculations suggest that Y94 is connected to the S of C146 *via* H-bonds through a water molecule (wat80 in Figure 5-3) before and during the proton transfer step (Figure 5-9, R, D, and TS states). However, once the proton is transferred to wat47, Y94 replaces R166 to form a direct H-bond with C146, which is involved in the rearrangement of active site H-bonds that moves the protonated wat47 to a favorable position for the next step. Since Y94 stabilizes the S anion to a lesser extent than the positively charged R166, this rearrangement also prepares C146 for the next nucleophillic attack onto C6 of dUMP to facilitate elimination of the cofactor. These results corroborate the suggestion from our

recent experiments that Y94 is not the general base to deprotonate C5, but rather plays an important role in the steps between the proton transfer and hydride transfer.[94]

Although H147 is not one of the five essential residues, it is highly conserved and was proposed to assist the enol formation at C5-C4=O4 during the proton transfer (step I.1 in Figure 5-4).[94] During our 600 ps MD simulation of the WT reaction intermediate (Complex C in Figure 5-2), H147 was connected to O4 *via* H-bonds through a water molecule rather than directly. We calculated a TS and the corresponding reactant and product structures for the mechanism where H147 donates a proton to O4 to facilitate the enol formation during the deprotonation of C5. The results suggest this mechanism has a lower activation energy barrier than Mechanisms I and II, but still higher than Mechanism III. Among all the simulated active site mutants, the H147V mutation of ecTSase caused the largest displacements of atoms in C146 and in the 2'-deoxyribose-5'-phosphate moiety of dUMP. These displacements are accompanied by variations in the H-bonds around the C6-S bond, while the residues around O4 of dUMP are marginally affected. These results suggest that, in contrast to the traditional proposal, H147 is most likely involved in coordinating active site water molecules together with E58 and other residues, which maintains the proper conformations of C146 and dUMP for the deprotonation of C5 and cleavage of C6-S.

Future Directions to Verify the Proposed Mechanisms

Our calculations not only delineate the molecular mechanisms underlying many previous experimental observations but also provide new insights that can be examined by future experiments. Particularly, our results suggest the C6-S bond breaks during the deprotonation of C5, which is different from the traditionally proposed mechanisms (Figure 5-4). It was previously suggested that examination of the H147 mutational effects on the proton transfer can assist in distinguishing between the proposed traditional mechanisms.[94] However, our calculations indicate that H147 is involved in mediating the

H-bond network at the active site, which can affect the lability of C6-S bond. Therefore, the experimentally measured H147 mutational effects would require more careful interpretation. Furthermore, our calculations suggest that an oxocarbonium cation could form at C5-C4=O4, although it does not play an important role in reducing $\Delta G^{\ddagger}$ of the proton transfer. Accordingly, we suggest that future experiments shall focus on verifying the cleavage of C6-S bond during the proton transfer, rather than formation of the enol/enolate, to distinguish between the proposed mechanisms. A most convincing experiment would be to chemically trap any of the proposed intermediates (H, J, or K in Figure 5-4) using the quenching experimental assay similar to the one recently developed for the flavin-dependent thymidylate synthase.[221] Further calculations are underway to estimate the stability of these proposed intermediates. In addition, the C146S mutant of ecTSase can form a stiffer C6-O bond upon the initial nucleophillic attack, which would increase the energy barrier for the proton abstraction from C5. Future experiments can measure the intrinsic KIE on the proton transfer step in C146S ecTSase to examine the proposed mechanism. Our calculations also indicate that R166 is critical in stabilizing the S anion of C146 during the proton transfer, while E58 and Y94 are important for the H-bond rearrangements at the end of this step. These indications corroborate previous experimental results of E58 and Y94 mutations. Future experiments can investigate the R166 mutational effects on the kinetics and KIEs of the proton transfer to verify the proposed mechanism.

Conclusions

Understanding the catalytic mechanisms of enzymes has been a focus of biochemistry research for the past few decades. The current study used QM/MM calculations to investigate a proton transfer catalyzed by ecTSase, which is one of the two C-H bond activations in the reaction mechanism. Experimental evidences suggested that

the analogous proton transfer occurs in solution and in the binary enzyme complex TSase-dUMP *via* formation of an enol/enolate in the substrate. In contrast, our calculations indicate that ecTSase uses a different strategy, i.e. the labile C6-S bond between the protein and substrate, to catalyze the proton transfer step during the turnover for dTMP production. The cleavage of C6-S bond during the proton transfer leads to new reaction intermediates that are not covalently bound to ecTSase, revealing a potential target for mechanism-based antibiotic drug design. In addition, the calculations suggest that the proton transfer has a complex free energy surface, indicating a highly variable ensemble-averaged TS that may account for the temperature dependent KIE observed in our previous experiments.[64] The comparison between the results of 1D- and 2D-PMF calculations of the proton transfer suggests that important protein motions are part of the reaction coordinate and should be included in the DRC in the simulations to obtain the complete information for the reaction mechanism. Collective protein motions rearrange the network of H-bonds at the active site to accommodate the structural changes in the ligands during and after the proton transfer. Particularly, the positively charged R166 approaches C146 to make it a better leaving group, thereby stabilizing the TS of the proton transfer step. After that step, the conformational changes in the active site prepare the C146 residue and the protonated water for subsequent chemical steps in the catalyzed reaction. Importantly, while protein motions play unequivocal roles in both the proton and hydride transfer steps in TSase-catalyzed reaction, the dissimilarity in their intrinsic nature may account for the different temperature dependences of KIEs on these two C-H bond activations. These results not only illustrate the functionalities of specific protein residues that reconcile previous experimental observations, but also suggest future directions for experiments to verify the proposed mechanisms. The synchronized conformational changes in the ligands and protein residues provide another example for the indispensable roles of protein motions in enzyme-catalyzed chemical reactions.

Computation Details

Computation Model

The starting point for the calculations was a X-ray crystal structure solved for ecTSase (PDB code 1TLS),[182] which had both 5F-dUMP and CH_2H_4folate bound at the active site of each protomer. We used PyMOL[164] to replace the fluorine with a hydrogen atom at C5 of dUMP, and to add hydrogen atoms to both ligands; and we used fDYNAMO[188,189] to add hydrogen atoms to the protein with a defined pH of 7.5. To account for the influence of local protein environment, we used the empirical *PROPKA*3 program to recalculate the pK_a values of the titratable protein residues to verify their protonation states.[190] To neutralize the overall charge of the system, we added 22 counter ions (Na^+) to the system at optimal electrostatic positions, at least 10.5 Å away from the periphery of the protein and 5 Å away from each other, using a regular grid of 0.5 Å. Finally, we used a pre-relaxed water box (100 × 80 × 80 $Å^3$) to solvate the system by removing the water molecules that had their oxygen atoms within 2.8 Å of the nonhydrogen atoms.

The hybrid QM/MM calculations require division of the whole system into a QM part and a MM part.[53] This work examines the proton abstraction from the substrate, which can be largely affected by the network of H-bonds in the protein. Therefore, initial calculations on the PESs used a QM region of 157 atoms (Figure 5-10), which contained all the residues involved in the H-bond network in the proximity of the active site. Further studies examined the effects of various QM regions, and the results suggested that the smaller QM region (57 atoms) in Figure 5-3 was sufficient for calculations on the main proposed mechanisms (Figure 5-4). This QM region was used for the final calculations presented in the Results and Discussions, unless otherwise specified (*e.g.* 77 atoms were included in the PMF calculations). The remaining 60769 atoms were simulated by MM, including the rest of the protein and ligands, the crystallized and

solvent water molecules, and the sodium counter ions. Link (hydrogen) atoms were added at the boundary between QM and MM regions to satisfy the valence of the QM/MM frontier atoms.[53,191] Base on the "half-of-the-sites-activity" proposed for ecTSase,[54,56] the calculations only modeled one active site in the QM region, leaving the second active site (ligands removed) in the MM region.

The QM region used the Austin Model 1 (AM1) method,[192] or the density functional theory with the Becke, three-parameter, Lee-Yang-Parr (B3LYP) exchange-correlation functional and the 6-31G(d,p) basis set,[193,194] to investigate different proposed mechanisms (Figure 5-4). The MM region used the OPLS-AA force field[195] for the protein and ligand atoms, and the TIP3P force field[196] for water molecules. The nonbonding interactions were simulated using periodic boundary conditions and a switching function with a cutoff radius in the range of 14.5–16 Å. All the MD simulations were performed using the canonical ensemble (NVT, with a reference temperature of 298 K) and the Langevin–Verlet integrator with a time step of 1 fs.[197]

Molecular Dynamics

After setting up the model, we optimized the complete system using the Adopted Basis Newton Raphson (ABNR)[198] method with the backbone of the protein frozen, followed by MD simulations for 600 ps.[197] Analysis of the final structures and the time evolution of the root mean square deviation (RMSD) suggested the system was equilibrated (Figure 5-11). The last structure from this 600ps MD simulation was fully optimized again to serve as the reaction intermediate (Complex C in Figure 5-2) for the PES calculations. The main interactions between the active site residues and water molecules in the final optimized structure resemble those proposed by Stroud and Finer-Moore.[63] Due to the large dimensions of the system, all the residues farther than 25 Å from the QM center were kept frozen (a total of 53425 out of 60826 atoms) for the following PES and PMF calculations.

We also conducted MD simulations of several active site mutants to explore their impacts on the reaction intermediate for the proton transfer (Complex C in Figure 5-2). Particularly, our calculations with the WT ecTSase revealed important roles for C146, R166, E58, and Y94 during the proton transfer (see Results and Discussions); therefore, we conducted MD simulations of C146S, R166K, E58Q, and Y94F mutants. We also simulated the mutant H147V, because this His residue was proposed to stabilize the intermediate in the traditional proposed mechanism for the proton transfer, while *B. subtilis* TSase has a Val residue as the natural variance for this position. We used PyMOL[164] to introduce the mutation to the final optimized structure of the WT reaction complex. Afterwards, the resulting mutant complexes were optimized, relaxed for 600 ps, and finally optimized again, following the same procedure as for the WT reaction intermediate.

Potential Energy Surface

We generated the QM/MM PESs for the proton transfer in the WT ecTSase using the final optimized WT reaction intermediate. Previous experiments suggested that the whole network of H-bonds contribute to the general base for the deprotonation of C5. After a careful inspection of the protein structure around the active site, we found that two water molecules can serve as the direct acceptor for H5 transfer, both H-bonded with Y94 (wat47 and wat80 in Figure 5-3). However, due to the proximity of wat80 to C146, wat80 is inclined to protonate the S anion of C146 after it accepts H5. Therefore, all the calculations presented in this paper used wat47 as the proton acceptor. In order to correctly evaluate the potential energy barriers for different proposed mechanisms, we scanned the AM1/MM PESs for the reaction with the corresponding interatomic distance, when describing a bond cleavage/formation, or antisymmetric combination of two distances, when describing an atom transfer, as the DRC. The 2D-PES scanning for each proposed mechanism provided saddle point structures that were used in the calculations

of stationary-point location and characterization of TS structures. The obtained TS structure and corresponding intrinsic reaction coordinate (IRC, i.e. the vibrational mode with an imaginary frequency) were then used to optimize to the reactant and product structures. To authenticate the AM1/MM results, we also used B3LYP/6-31G(d,p) method to calculate the TS structures for the first step of each proposed mechanism, followed by calculations with the IRC and full optimization of the corresponding reactants and products. These PES calculations followed the micro-macro iterations scheme [199] that is incorporated in the fDynamo library,[188,189] as described in our previous publications.[95] In our calculations, the core space contained all the QM atoms, and the environment space included all the MM atoms, and the Hessian matrix was only explicitly calculated for the core atoms.

Potential of Mean Force (PMF)

To obtain the free energy profile for the proton transfer, we employed the umbrella sampling approach and the weighted histogram analysis method (WHAM)[200,201] to calculate the PMFs with AM1/MM. We followed the same procedure in our previous calculations on the hydride transfer,[95,96] and used an umbrella force constant of 2500 $kJ \cdot mol^{-1} \cdot Å^{-2}$ (597 $kcal \cdot mol^{-1} \cdot Å^{-2}$) for each window. Each window carried out 5 ps of relaxation and 10 ps of production with a time step of 0.5 fs. In all PMF windows, the resulting structure had a total energy fluctuation lower than 0.6%, a kinetic energy fluctuation lower than 1%, and a change in temperature lower than 3 K over the production period of time (i.e. the last 10 ps). In order to confirm good overlaps between trajectories in adjacent PMF windows, we plotted all the sampled values on the DRC and also checked all the resulting structures to make sure trajectories in adjacent windows have similar structures.

We first calculated the PMF using the antisymmetric combination of distances describing the proton transfer, $d_{C5\text{-}H5}$-$d_{H5\text{-}Ow}$, as the DRC. This DRC was varied from -1.50

to 1.50 Å, with a window width of 0.05 Å, generating 60 windows. The starting structure for all the windows in this 1D-PMF calculation was a TS structure located in the PES calculations. In order to obtain a more precise TS for the proton transfer (see Results and Discussions), we calculated a 2D-PMF using the interatomic C6-S distance as the additional dimension of the DRC. The starting structures for the 2D-PMF windows were the optimized structures in the PES scanning with the same DRC constrained at the corresponding values. There were 45 simulation windows along the $d_{C5\text{-}H5}$-$d_{H5\text{-}Ow}$ coordinate (from -1.48 to 1.82 Å with a window width of 0.075 Å) and 31 simulation windows along the $d_{C6\text{-}S}$ coordinate (from 1.8 to 4.8 Å with a window width of 0.1 Å), generating 1395 windows. The trajectories in some windows for the 2D-PMF calculations resulted in formation of enol at C4=O4 of dUMP after the deprotonation of C5 and cleavage of C6-S bond, due to the proximity of the protonated wat47 to O4 during the simulation. When this happened, the resulting structures were swapped between adjacent windows and the simulations in those windows were repeated. Analyzing the results with alternative trajectories for those few windows (i.e. enol at O4 or protonated wat47) produced the same 2D-PMF surface (Figure 5-9). The contour plot of the 2D-PMF results was generated with Surfer (R) Version 8.04 from Golden Software, Inc.

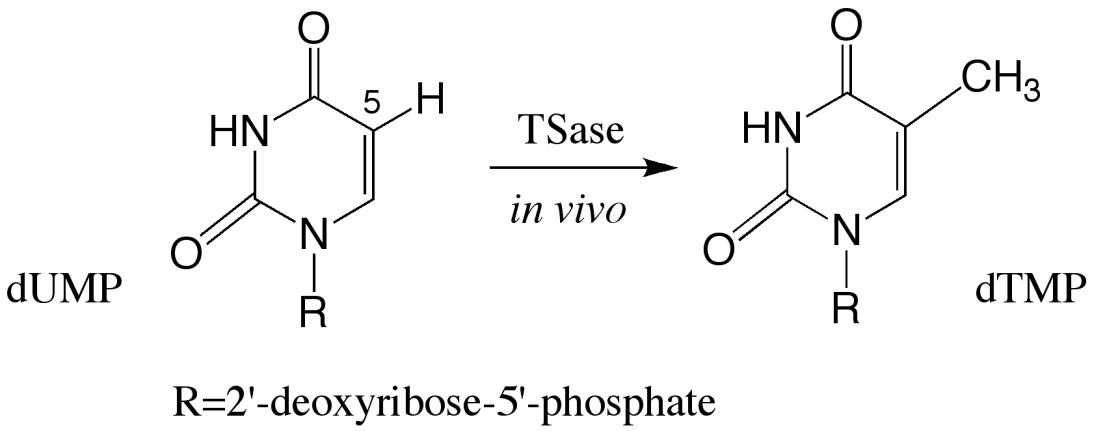

Figure 5-1. The overall reaction catalyzed by TSase.

Thymidylate synthase (TSase) catalyzes the reductive methylation of dUMP to produce dTMP *in vivo*, where the C-H bond at the C5 position of the pyrimidine is replaced by a C-C bond to a methyl group.

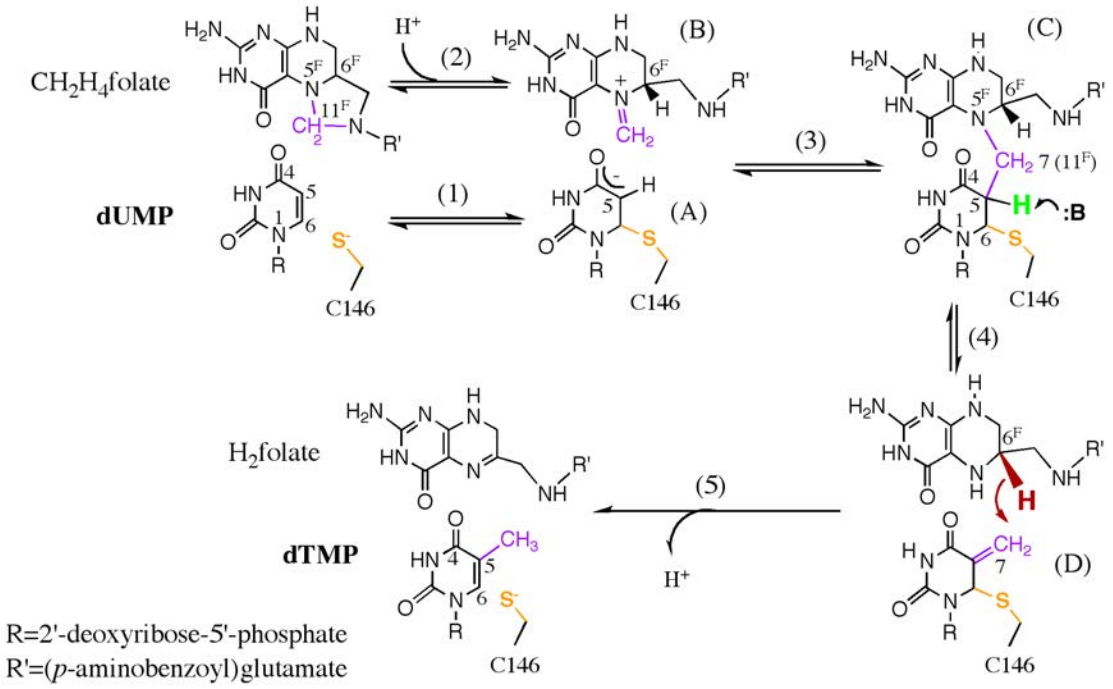

Figure 5-2. The traditionally proposed reaction mechanism for TSase.

The numbering of atoms on CH_2H_4folate is marked with an F superscript (^{F}) to discriminate from those on the nucleotides. The proton abstraction (green) and C7-N5^F cleavage (purple) steps are tightly coupled in WT TSase and thus is represented by one step (step 4). The following hydride transfer (dark red) is rate limiting for the catalytic turnover[35,98] and has been carefully investigated in our previous calculations[124] (step 5).

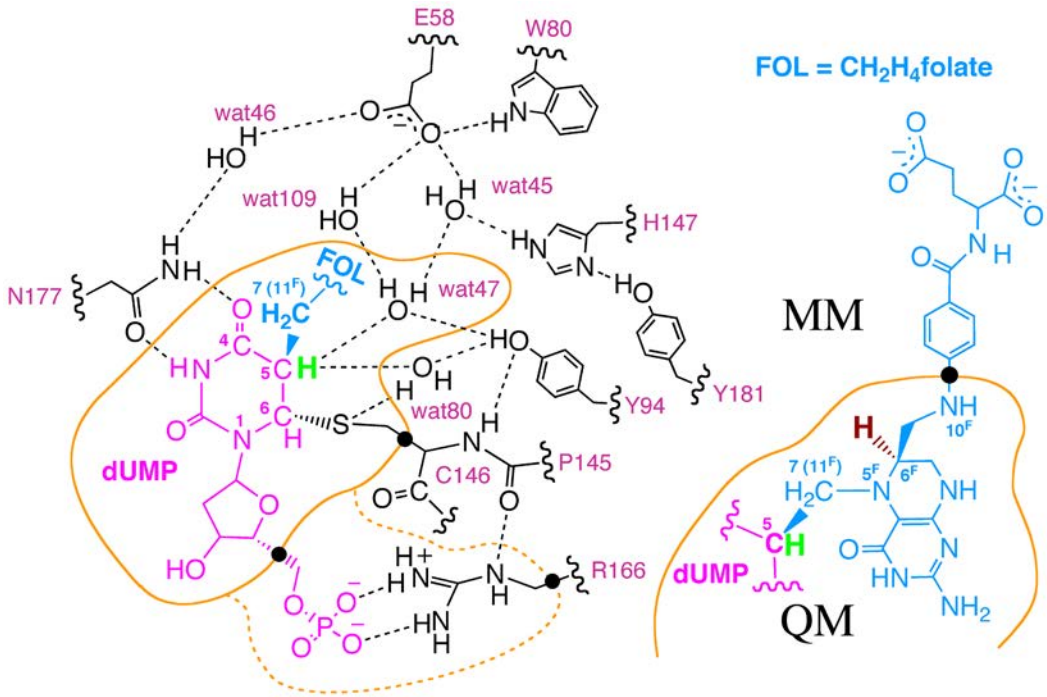

Figure 5-3. The QM regions used for calculations on the proton transfer in ecTSase.

This figure illustrates the complex H-network in the proximity of the active site of ternary ecTSase-dUMP-CH_2H_4folate complex (Complex C in Figure 5-2). This study focuses on the proton (green) abstraction from C5 of dUMP, and compares the computational results with the rate-limiting hydride (dark red) transfer studied in our previous calculations.[124] The QM region for the PES calculations included 57 atoms and 3 hydrogen link atoms (black dots) on the boundary between the QM and MM regions. The QM region for the PMF calculations included 77 atoms (additional atoms in the dashed orange curve) and 3 hydrogen link atoms. For the reader's convenience, the color code in this figure matches the color code for the structures in Figures 5-6 and 5-9.

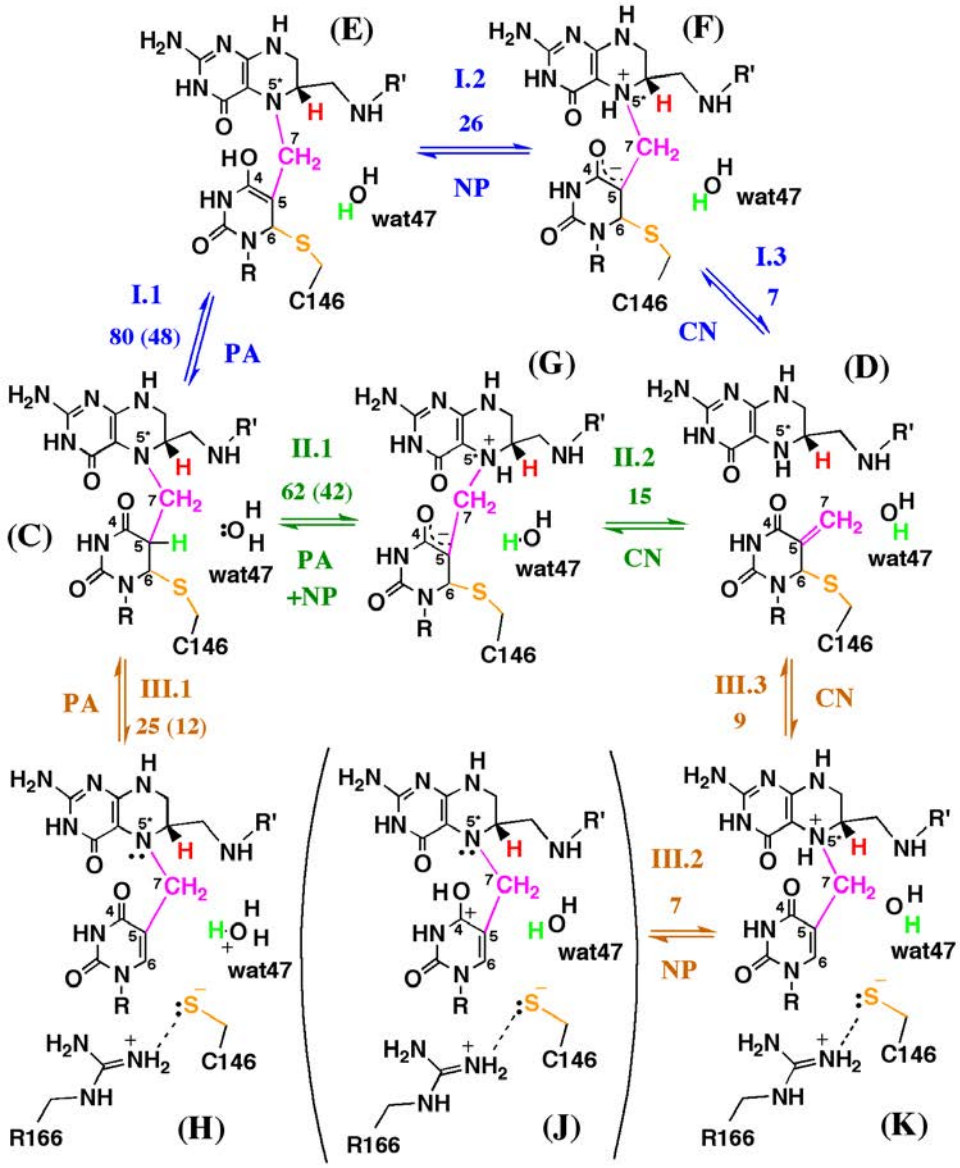

Figure 5-4. Three major proposed mechanisms for the proton transfer in ecTSase.

Our calculations examined three proposed mechanisms for conversion of Complex C to Complex D (step 4 in Figure 5-2) in ecTSase-catalyzed reaction. This conversion involves the proton abstraction from C5 (PA), $N5^F$ protonation (NP), and C7-$N5^F$ cleavage (CN). The combinations of Roman and Arabic numbers (I.1, I.2, …) represent the proposed steps of each mechanism as described in the text, for which the activation energy barriers (kcal/mol) calculated with the AM1 or B3LYP (in parenthesis) method are presented by the numbers near the reaction arrows. The PMF calculations suggest that residue R166 stabilizes the S anion upon the cleavage of C6-S bond in Mechanism III.

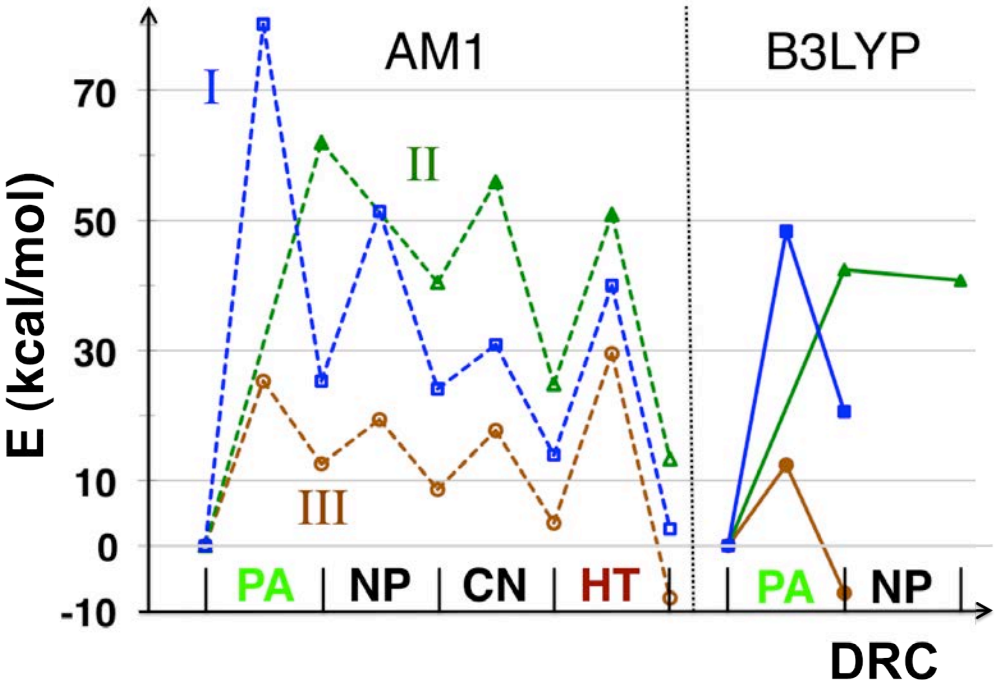

Figure 5-5. Results of PES calculations on the proton transfer.

The PES calculations on the major proposed mechanisms (Figure 5-4) suggest the cleavage of C6-S bond lowers the activation energy barrier for the proton transfer step (Mechanism III). The energy profile for the hydride transfer (HT) is adopted from Ref 95. The horizontal axis is the DRC for each chemical step as described in Computation Details. Dashed lines (left panel) present the energy profiles calculated with AM1/MM, and solid lines (right panel) present the energy profiles calculated with B3LYP/MM on the first step of each mechanism.

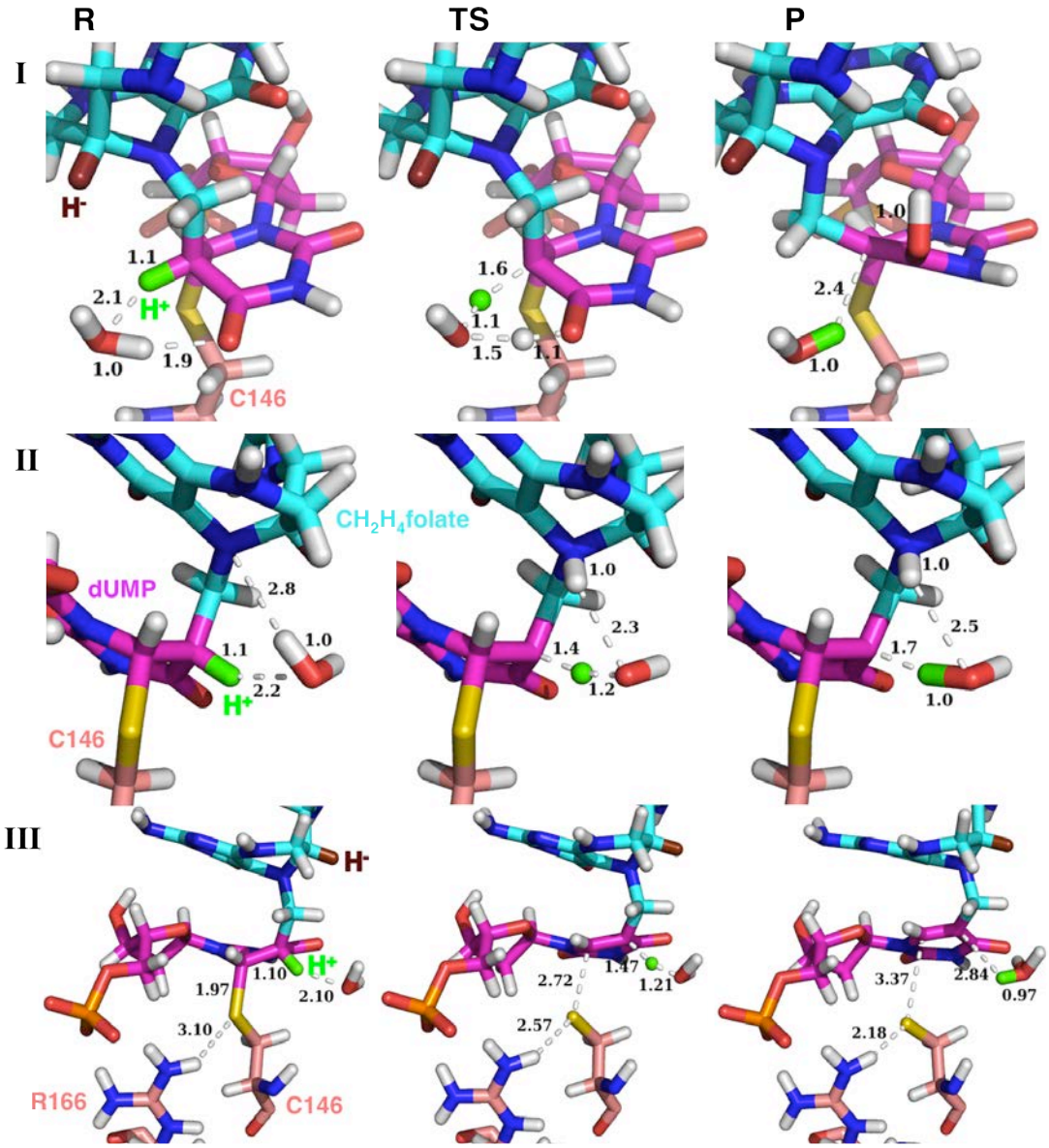

Figure 5-6. Representative structures from the B3LYP/MM calculations.

This figure presents the optimized structures with the B3LYP/MM method for the reactants (R), transition state (TS), and products (P) of the deprotonation of C5 in Mechanisms I, II, and III (Figure 5-4). Although the specific geometric parameters are different from the corresponding structures calculated with AM1/MM (e.g. compare Table 5-1 and Table 5-2), the B3LYP/MM calculations substantiate the conclusion that the deprotonation of C5 is concerted with the cleavage of C6-S bond (Mechanism III), which is assisted by the strong H-bond formed between R166 and C146.

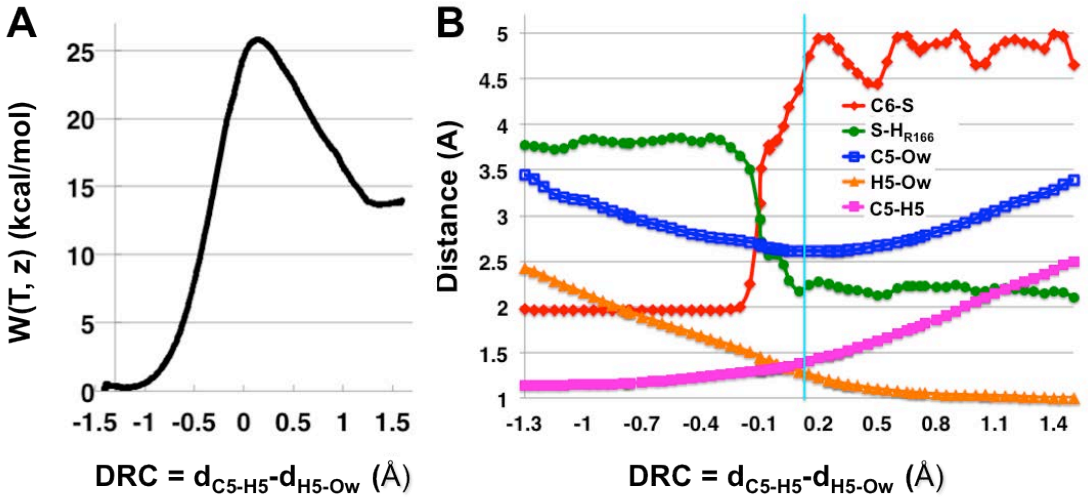

Figure 5-7. Results of 1D PMF calculations.

The AM1/MM PMF calculated at 25 ˚C provides:

(A) the free energy profile for the deprotonation of C5 (step III.1 in Figure 5-4); and

(B) changes in interatomic distances along the DRC. Atom labels: C5, H5, and C6 refer to the atoms on dUMP; S--the S atom of C146; H_{R166}--the H atom of R166 that is closest to S (see the structures in Figure 5-9); Ow--the O atom of wat47. The cyan line indicates the average value of the DRC at the TS.

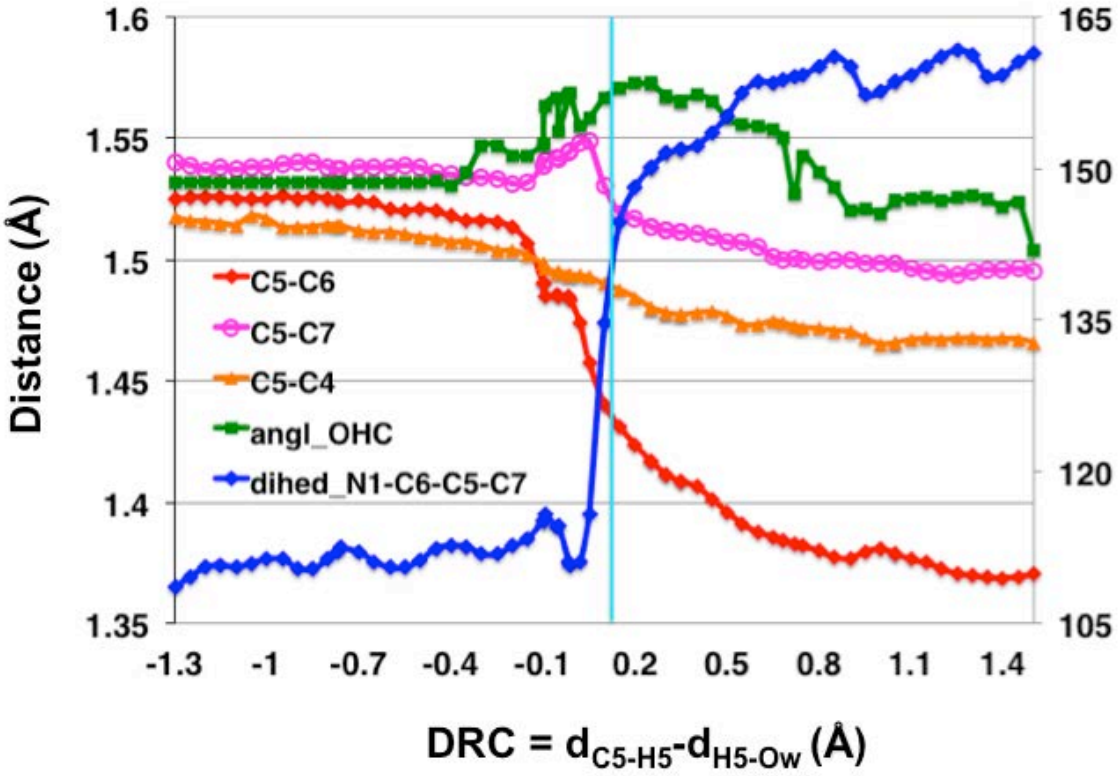

Figure 5-8. Changes in the substrate structure during the proton transfer.

Changes in the geometric parameters near C5 on the uracil ring of dUMP during the deprotonation of C5, analyzed with the 1D AM1/MM PMF calculation results. The C5-C6 bond length decreases from 1.53 Å to 1.37 Å, and the dihedral of N1-C6-C5-C7 increases from 106˚ to 164˚, both suggesting the deprotonation leads to a double bond formation on C5-C6 that is concomitant with the cleavage of the C6-S bond (Figure 5-7). Subtle decreases are also observed for the C5-C7 and C5-C4 bond lengths. The angle of C5-H5-O_{wat47} (agl_OHC, green) reaches the maximum near the TS (vertical cyan line).

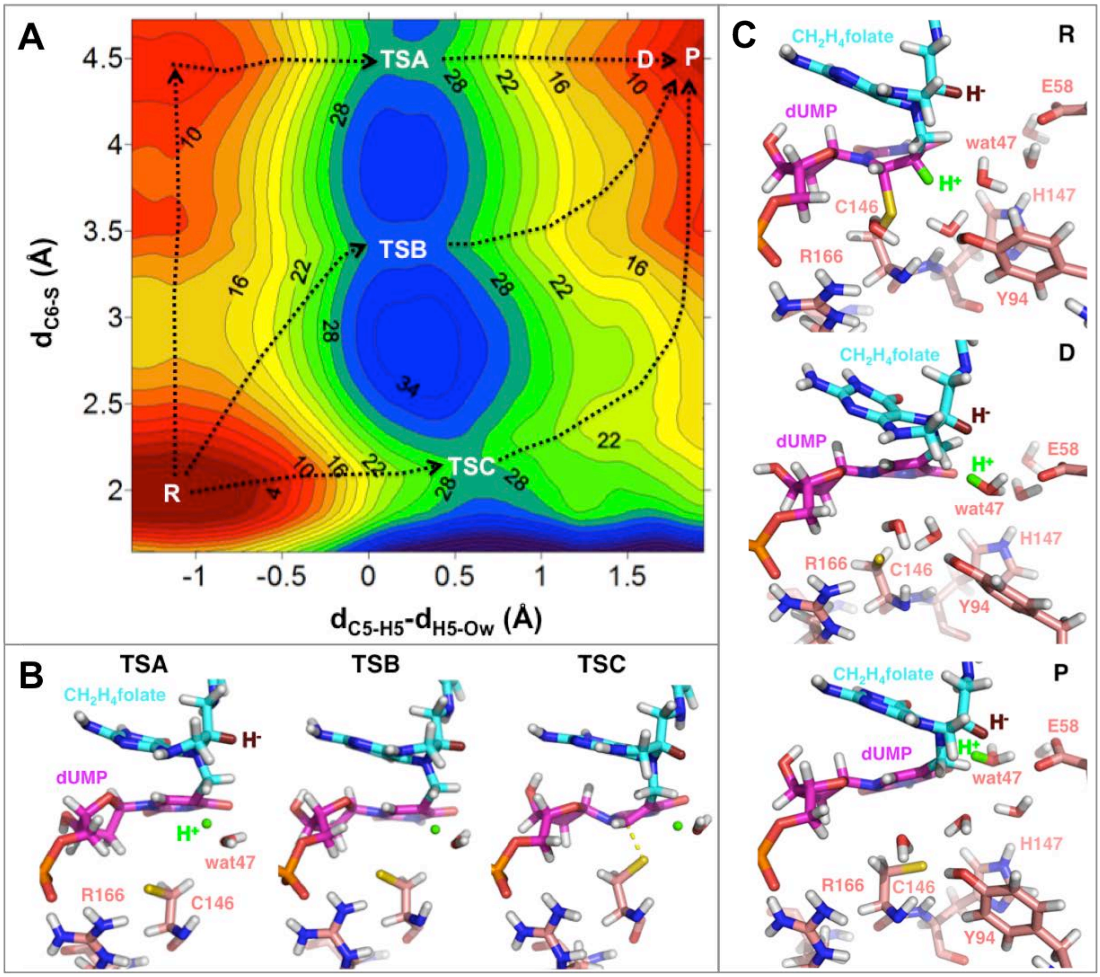

Figure 5-9. Results of 2D-PMF calculations.

This figure presents:

(A) The 2D-PMF calculation used the C6-S bond distance (d_{C6-S}, vertical axis) and the antisymmetric combination describing the C-H→O proton transfer (d_{C5-H5} - d_{H5-Ow}, horizontal axis) as the DRC. There are various reaction paths (exemplified by the black dotted lines) with three subsets of TS structures for the proton transfer (labeled as TSA, TSB, and TSC on the plot). TSA, TSB, and TSC present similar free energy barriers (28.5, 31.0, and 26.5 kcal/mol, respectively, with *ca*. 3 kcal/mol errors for each number due to the limitation of AM1/MM PMF method) relative to the reactant state (R). The C6-S bond is fully broken (4.5 Å) in the product state (P), suggesting a reaction intermediate where the ligands are not covalently attached to the protein.

(B) Representative structures for the three subsets of TSs. Only residues R166 and C146 are shown for the protein for clarity. R166 forms a strong H-bond (2.1 Å, Table 5-1) with C146 to stabilize the S anion in TSA and TSB. For the reader's reference, the transferred proton is in green and the hydride to be transferred later is in dark red.

(C) Representative structures for the R and P states, and a representative structure (D) along the reaction path before the system reaches P. Only the protein residues discussed in the text are shown for clarity. After the proton transfer step, the protein rearranges the H-bond network (from D to P states) to relocate the protonated water and to destabilize the S anion, making the active site favorable for the subsequent chemical steps (see text). Table 5-1 provides structural analyses of the six states labeled in this figure.

Figure 5-9 ——continued

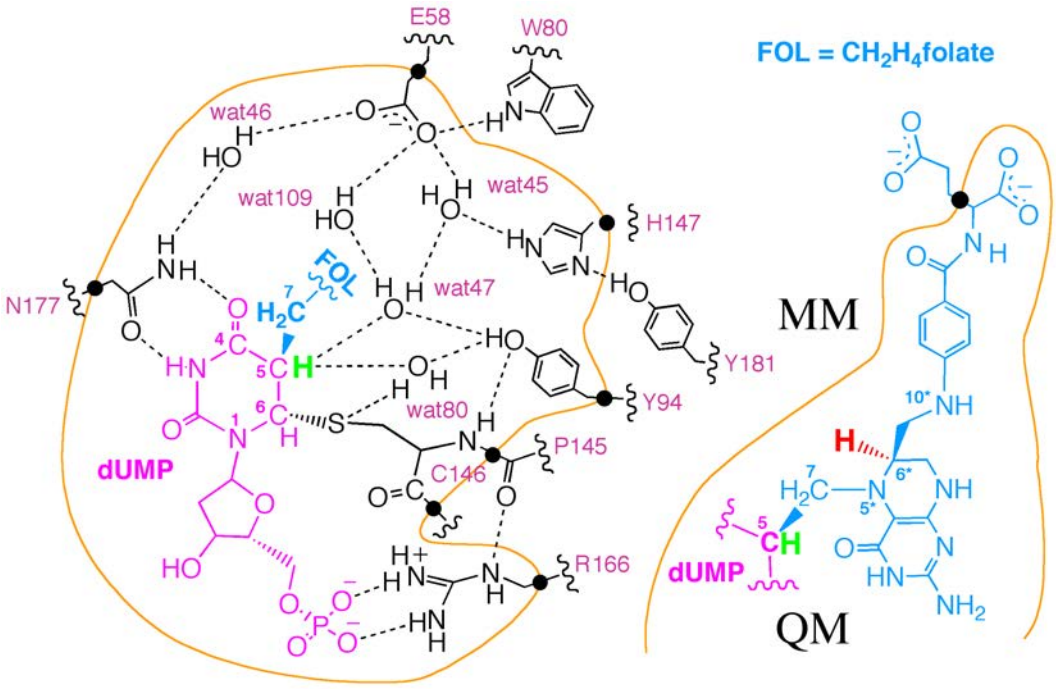

Figure 5-10. Larger QM regions used in initial calculations.

The initial AM1/MM PES calculations in this work used a large QM region containing all the residues involved in the H-bonds network in the proximity of the active site. This QM region included 157 atoms (within the yellow curve) and 8 hydrogen link atoms (black dots) at the boundary between the QM and MM regions. Further studies examined the effects of various QM regions on the reaction energy profiles, and the results suggested that the smaller QM region (57 atoms) in Figure 5-3 was sufficient for calculations on the proposed mechanisms (Figure 5-4).

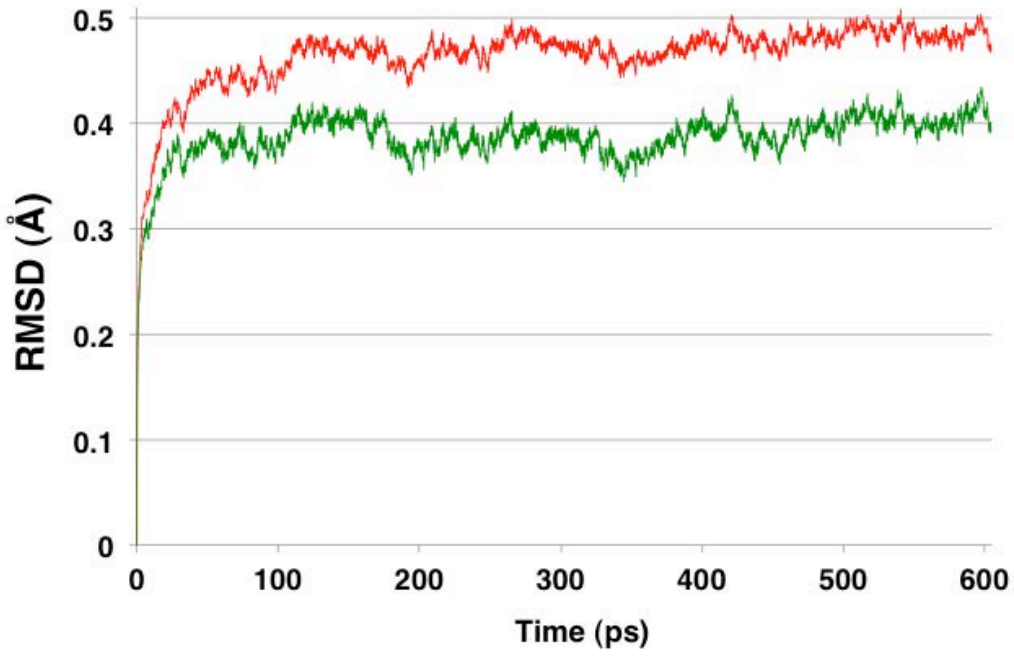

Figure 5-11. The system reaches equilibrium during 600 ps MD simulations.

Time evolution of the root mean square deviation (RMSD) of the positions of atoms during the 600 ps of AM1/MM MD simulations of the WT ecTSase reaction intermediate (Complex C in Figure 5-2). The green curve corresponds to the RMSD measured only on the backbone of the protein while the red curve corresponds to the RMSD measured on all the non-hydrogen atoms of the protein. The time evolutions of the RMSD for the examined mutants are similar to this plot.

Table 5-1. Structural changes during the proton transfer (AM1/MM PMF).

Geometric Variable	R	TS			D	P
		TSA	TSB	TSC		
C5(dUMP)-H5(dUMP)	1.14 ± 0.03	1.40 ± 0.03	1.40 ± 0.03	1.78 ± 0.04	2.61 ± 0.04	2.78 ± 0.04
H5(dUMP)-Ow(wat47)	2.49 ± 0.04	1.27 ± 0.03	1.31 ± 0.03	1.07 ± 0.03	1.04 ± 0.03	1.05 ± 0.03
C5(dUMP)-Ow(wat47)	3.30 ± 0.09	2.62 ± 0.06	2.60 ± 0.06	2.78 ± 0.07	3.59 ± 0.07	3.73 ± 0.09
C6(dUMP)-S(C146)	2.09 ± 0.03	4.50 ± 0.03	3.40 ± 0.03	2.19 ± 0.04	4.51 ± 0.03	4.41 ± 0.03
S(C146)-H(R166)	4.6 ± 0.3	2.1 ± 0.1	2.1 ± 0.2	5.0 ± 0.3	2.1 ± 0.1	5.2 ± 0.3
S(C146)-H(Y94)	3.4 ± 0.2	3.8 ± 0.2	4.3 ± 0.1	2.5 ± 0.2	3.9 ± 0.2	1.9 ± 0.1
C5(dUMP)-C6(dUMP)	1.52 ± 0.02	1.44 ± 0.02	1.45 ± 0.02	1.43 ± 0.03	1.38 ± 0.02	1.38 ± 0.02
C4(dUMP)-O4(dUMP)	1.24 ± 0.02	1.24 ± 0.01	1.25 ± 0.02	1.26 ± 0.02	1.26 ± 0.01	1.25 ± 0.01
Angle C5-H5-Ow	127 ± 6	157 ± 10	149 ± 8	154 ± 9	158 ± 9	152 ± 12
Dihedral N1-C6-C5-C7 (all atoms on dUMP)	115 ± 5	150 ± 6	136 ± 6	130 ± 5	161 ± 5	171 ± 5

Notes:

This table compares the key distances (Å), angle (˚) and dihedral (˚) in the reactant state (R), several different TSs (TSA, TSB, and TSC), a pseudo-product state along the reaction path (D), and product state (P) of the proton transfer step calculated with the 2D AM1/MM PMF at 25 ˚C (Figure 5-9).

Table 5-2 Structural changes during the proton transfer (B3LYP/MM PES).

Geometric Variable	R	TS	P
C5(dUMP)-H5(dUMP)	1.10	1.47	2.84
H5(dUMP)-Ow(wat47)	2.10	1.21	0.97
C5(dUMP)-Ow(wat47)	3.09	2.64	3.20
C6(dUMP)-S(C146)	1.97	2.72	3.37
S(C146)-H(R166)	3.10	2.57	2.18
S(C146)-H(Y94)	4.57	4.56	4.75
C5(dUMP)-C6(dUMP)	1.54	1.44	1.37
C4(dUMP)-O4(dUMP)	1.22	1.23	1.27
Angle C5-H5-Ow	148.2	159.4	103.1
Dihedral N1-C6-C5-C7	95.3	123.4	155.9

Notes:

This table compares key distances (Å), angle (˚) and dihedral (˚) in the structures of the reactant, TS, and product of the proton transfer step calculated with B3LYP/MM (Figure 5-4, step III.1). The structures are presented in Figure 5-6, path III.

CHAPTER VI

OXIDASE ACTIVITY OF A FLAVIN-DEPENDENT THYMIDYLATE SYNTHASE

Introduction

Thymidylate synthases (TSs, encoded by the *thyA* and *tym*S gene[x]) catalyze the reductive methylation of 2'-deoxyuridine-5'-monophosphate (dUMP) to form 2'-deoxythymidine-5'-monophosphate (dTMP) in nearly all eukaryotes including humans. This reaction employs N^5, N^{10}-methylene-5,6,7,8-tetrahydrofolate (CH_2H_4folate) as both the methylene and the hydride donor,[61] producing 7,8-dihydrofolate (H_2folate), as illustrated in Figure 6-4. The product, H_2folate, is reduced to 5,6,7,8-tetrahydrofolate (H_4folate) by dihydrofolate reductase (DHFR, encoded by the *folA* gene), and then methylenated back to CH_2H_4folate. Thus, the genomes of *thyA*-dependent organisms have always been found to contain *folA* as well, forming a TS-DHFR coupled catalytic cycle that is essential for thymidine biosynthesis.

Since 2002, *thy*X, a new gene that encodes for flavin-dependent thymidylate synthases (FDTSs), has been identified in a number of microorganisms, including some severe human pathogens.[69-72] FDTS is a homotetramer with four identical active sites, each of which is formed at an interface of three of the four subunits.[202] This is quite different from the structure of classical TS, which is a homodimer with one active site per subunit.[61] Recent studies have suggested that the catalytic mechanisms of TS and FDTS also differ substantially.[76,203-205] Since dTMP is a vital metabolite for DNA biosynthesis, this newly discovered enzyme is a promising target for novel antibiotics that could be designed to selectively inhibit FDTS activity with potentially low toxicity for humans.

---

[x] The gene that encodes TS (EC 2.1.1.45) in mouse, rat, and human is currently named *tym*S rather than *thy*A.

In order to direct future drug design, the molecular mechanism by which FDTS catalyzes thymidylate synthesis must be clarified to reveal the enzyme-substrate complexes and intermediates present along the reaction pathway. In contrast to classical TS, FDTS takes the hydride from reduced nicotinamides or other reductants, while CH_2H_4folate serves as the methylene donor only and produces H_4folate instead of H_2folate,[69,71,72] as illustrated in Figure 6-5. This explains the absence of both *thyA* and *folA* in the genomes of some *thyX*-dependent organisms.[206] Preliminary mechanistic studies have demonstrated that the FDTS mechanism is substantially different from the common bi-functional enzymes with both TS and DHFR activities.[203-205] During the reductive half reaction, reduced nicotinamide adenine dinucleotide 2'-phosphate (NADPH) reduces the non-covalently bound flavin adenine dinucleotide (FAD) cofactor to its reduced form ($FADH_2$); during the oxidative half reaction, the enzyme catalyzes the transfer of the methylene group from CH_2H_4folate to dUMP, while $FADH_2$ serves as the reducing agent to produce dTMP. Several proposed kinetic mechanisms suggested that the product of the reductive half reaction (nicotinamide adenine dinucleotide 2'-phosphate, $NADP^+$) leaves before CH_2H_4folate binds to the enzyme.[203-205] This putative kinetic mechanism, however, remains to be experimentally tested.

Like many other flavoenzymes, FDTS can function as an NADPH oxidase, consuming molecular oxygen (O_2) and producing $NADP^+$ and hydrogen peroxide (H_2O_2). Our recent studies revealed a close connection between the synthase activity (dUMP → dTMP) and oxidase activity (O_2 → H_2O_2) of FDTS [207,208]. Several aspects of the proposed mechanism, however, have not been experimentally confirmed thus far. In the present paper, we report pre-steady state and steady state studies on the oxidase activity of FDTS from *Thermotoga maritima*, and elucidated the binding and release features of its synthase substrates NADPH, CH_2H_4folate, and dUMP.

Results and Discussion

Initial Velocity Studies of FDTS Oxidase Activity

Previous studies suggested that NADPH binds to the FDTS-FAD complex, and that after the flavin is reduced the product of the reductive half reaction, $NADP^+$, dissociates before the initiation of the oxidative half reaction.[203-205] This proposed mechanism was examined by measuring the steady state initial velocities of FDTS oxidase activity while varying NADPH concentrations at several O_2 concentrations (8 μM, 20 μM, 50 μM, 210 μM, 1 mM). These experiments were conducted in the presence of saturating concentrations of dUMP, to ensure examination of the dUMP-activated form of the enzyme [207,208]. The results revealed that in the absence of CH_2H_4folate, FDTS oxidase activity exhibits Michaelis-Menten kinetics for O_2 with an unusually small K_m. The apparent K_m values of O_2 with 100 μM NADPH were determined to be 7 ± 1 μM at 37 ^oC, and 29 ± 2 μM at 65 ^oC. This may imply that either the enzyme has a binding site for O_2, or, more likely, that an O_2 independent step becomes rate limiting as the concentration of O_2 increases.[209]

The double reciprocal Lineweaver-Burk plot (1/rate *vs*. 1/[substrate]) of FDTS oxidase activity shows an intersecting pattern (Figure 6-1), which suggests a sequential kinetic mechanism. If the product $NADP^+$ left the enzymatic complex before O_2 binds, these lines would have been parallel (i.e., Ping Pong mechanism[210,211]). The data were globally fit to a bi-substrate sequential mechanism (Eq 1, from Ref 211) to estimate the kinetic parameters:

$$\frac{v}{[\mathrm{E}]_\mathrm{t}} = \frac{k_{cat}[\mathrm{A}][\mathrm{B}]}{K_{ia}K_b + K_a[\mathrm{B}] + K_b[\mathrm{A}] + [\mathrm{A}][\mathrm{B}]} \tag{1}$$

where [A], [B], and $[E]_t$ are the concentrations of NADPH and O_2, and total concentration of enzyme active sites, respectively; K_a is the Michaelis constant of

NADPH, K_b is the Michaelis constant of O_2; and K_{ia} is the dissociation constant of the substrate from the enzymatic complex. The kinetic parameters determined from this global fitting are: k_{cat}= 0.0830 ± 0.0002 s^{-1}, K_a = 522 ± 2 μM, K_{ia} = 3.61 ± 0.06 mM, K_b = 1.12 ± 0.02 μM.

Assessment of the Rate of Product $NADP^+$ Release by Examination of the $FADH_2$-$NADP^+$ Charge-Transfer Complex

The progress of the reductive half reaction was monitored by recording UV-Vis spectra continuously in anaerobic single turnover experiments. The decrease of absorbance at 450 nm follows the reduction of enzyme-bound FAD. When NADPH is used as the reducing agent, the spectra also show an increase in the absorbance of a wide absorbance band (550-900 nm) with an isosbestic point at 510 nm (Figure 6-2, *a*). This wide band is not observed during FAD reduction by dithionite, and is identified as a charge-transfer complex between the reduced flavin and the oxidized nicotinamide.[212-214] The first-order rate constant of the formation of the charge-transfer complex was determined to be identical to that of FAD reduction (Figure 6-2, *a*, Inset), which, together with the isosbestic point, indicates that the two changes occur simultaneously and represent the same process. This observation demonstrates the stability of the enzyme bound $FADH_2$-$NADP^+$ complex that is formed during the reductive half reaction, and suggests a close proximity of the oxidized nicotinamide ring to the reduced isoalloxazine ring. This observation is significant since no other structural information is currently available regarding the binding site of the nicotinamide cofactor.

After the completion of the reductive single turnover experiment, the rate of $NADP^+$ release from the FDTS-$FADH_2$-$NADP^+$-dUMP complex was measured by following the disappearance of the charge-transfer band while no change was observed at 450 nm (Figure 6-2, *b*). The rate constant of $NADP^+$ release was determined to be

0.00135 ± 0.00005 s^{-1} at 37 ^{o}C (Figure 6-2, *b*, Inset). In comparison, the first order rate constant of $FADH_2$ oxidation by O_2 was determined to be 0.131± 0.010 s^{-1} at 0 ^{o}C in the oxidative single turnover experiment. Thus, $NADP^+$ release from the enzyme is at least 2 orders of magnitude slower than $FADH_2$ oxidation by O_2, indicating that $NADP^+$ has a very high affinity for the reduced enzyme. This suggests that $NADP^+$ does not leave the FDTS-$FADH_2$-$NADP^+$-dUMP complex at the end of the reductive half reaction, but rather remains bound to the enzymatic complex during the oxidative half reaction. This observation supports the sequential mechanism suggested above from steady state kinetic measurements. Neither the rate of FAD reduction nor that of $FADH_2$-$NADP^+$ formation is dependent on dUMP concentrations, which confirms our previous suggestion that dUMP does not influence the reductive half reaction.[208]

Assessment of $NADP^+$ Binding to the Oxidized Enzyme from Product Inhibition Studies

Since $NADP^+$ appears to bind tightly to the reduced enzyme, it is of interest to assess its binding to the oxidized enzyme. Additionally, product inhibition studies can discriminate between the steady state ordered and random mechanisms, which is not easy to do *via* initial velocity measurements in the absence of products.[210,211] Therefore, the effect of $NADP^+$ on initial velocities was examined by measuring the steady state initial velocities of FDTS oxidase activity with 100 μM NADPH at both saturating (210 μM) and sub-saturating (10 μM) concentrations of O_2. These measurements show no observable inhibition up to the solubility limit of ~550 mM $NADP^+$ under the experiment conditions. Regardless of the enzymatic complex from which $NADP^+$ dissociates, the lack of any inhibitory effect corroborates the low affinity of $NADP^+$ for the oxidized enzyme, despite its high affinity for the reduced enzyme.

Inhibition of FDTS Oxidase Activity by CH_2H_4folate

CH_2H_4folate appears to inhibit FDTS oxidase activity, and addition of 400 μM CH_2H_4folate completely suppresses this activity under atmospheric concentration of O_2 (210 μM). In order to investigate the nature of inhibition of FDTS oxidase activity by CH_2H_4folate, steady state initial velocities were measured while varying CH_2H_4folate concentrations at several O_2 concentrations (8 μM, 12.5 μM, 20 μM, 210 μM, 1 mM), in the presence of a saturating concentration of dUMP. The initial velocities under atmospheric concentration of O_2 were also studied in the absence of dUMP, and although the rates are slower (in accordance with Ref 208), dUMP does not seem to affect the nature of CH_2H_4folate inhibition of the oxidase activity. To examine the relation between CH_2H_4folate and O_2, and to ascertain the binding constant of CH_2H_4folate to the reduced and dUMP-activated enzyme, we used a simplified model in which CH_2H_4folate is treated as a dead-end inhibitor[210,211] of the oxidase activity. The Supporting Information (SI) examines and verifies the validity of this simplification.

To determine the inhibition pattern of CH_2H_4folate toward O_2, initial velocities were analyzed by the secondary slope and intercept replots of the Lineweaver-Burk double reciprocal plot (Figure 6-3, *a*).[211] The slope of the double reciprocal plot increases linearly with the concentration of CH_2H_4folate (Figure 6-3, *b*), while the intercept is independent of the concentration of CH_2H_4folate (Figure 6-3, *c*). According to this analysis, CH_2H_4folate appears to be a competitive inhibitor of O_2 in FDTS oxidase activity. The initial velocities were thus fit to the competitive inhibition model to estimate the kinetic parameters:[210,211]

$$\frac{v}{[\mathrm{E}]_\mathrm{t}} = \frac{k_{cat}[\mathrm{S}]}{K_m\left(1+\frac{[\mathrm{I}]}{K_I}\right)+[\mathrm{S}]} \tag{2}$$

where k_{cat} is the first-order rate constant, describing the maximal reaction rate per enzyme active site; [S], [I], and $[E]_t$ are the concentrations of O_2, CH_2H_4folate, and total concentration of enzyme active sites, respectively; K_m is the Michaelis constant of O_2, and K_I is the inhibition constant of CH_2H_4folate. The kinetic parameters determined from this fitting were: $k_{cat} = 0.0127 \pm 0.0004\ s^{-1}$, $K_m = 7 \pm 1\ \mu M$, $K_I = 1.9 \pm 0.3\ \mu M$. The inhibition pattern was also analyzed by globally fitting the initial velocities to the mixed-type inhibition model,[210] which is a general equation for competitive, non-competitive, or un-competitive inhibition. The results also suggest that the inhibition is best described by the competitive pattern. A detailed analysis is presented in the SI. In summary, the observed competitive inhibition of CH_2H_4folate towards O_2 indicates that CH_2H_4folate and O_2 indeed compete for the same enzymatic complex (FDTS-$FADH_2$-$NADP^+$-dUMP).

The sequential binding order of NADPH and O_2 in FDTS oxidase activity, together with the competitive inhibition pattern between O_2 and CH_2H_4folate, suggests that the binding order of NADPH and CH_2H_4folate in FDTS synthase activity is also sequential. This conclusion disagrees with the kinetic schemes proposed in previous studies, in which $NADP^+$ leaves before the oxidation of $FADH_2$.[203-205] A recent kinetic study on the synthase activity of FDTS from *Mycobacterium tuberculosis* corroborates our data.[215] The presence of $NADP^+$ in complexes during the oxidative half reaction is important in various attempts to mimic these complexes, which may assist in the design of inhibitors and drugs as well as in the crystallization of the long sought enzymatic complexes with nicotinamide cofactors and/or folate derivatives.

The inhibition constant ($K_I = 1.9 \pm 0.3\ \mu M$) obtained from this experiment is a direct measure of the dissociation constant of CH_2H_4folate from the FDTS-$FADH_2$-$NADP^+$-dUMP-CH_2H_4folate complex. This measurement affords a good estimate of the binding constant of CH_2H_4folate to the FDTS-$FADH_2$-$NADP^+$-dUMP complex ($1/ \approx 0.5\ \mu M^{-1}$), which reflects the high affinity of CH_2H_4folate for the reduced and dUMP-activated enzyme. This complex seems to be unique to FDTS, therefore such information

may assist in rational design of inhibitors and drugs. This is significant because hitherto no specific inhibitors or drugs targeting FDTS have been identified. The current finding may also direct efforts towards crystallization of complexes of FDTS with $FADH_2$, dUMP, $NADP^+$, and folate derivatives under anaerobic conditions. Solving structures with nicotinamide and folate entities would help identify the binding sites of both NADPH and CH_2H_4folate, and provide important structural information for FDTS studies.

Kinetic Scheme

Based on the results presented in this report and in previous studies,[203-205,207,208] thymidylate synthesis catalyzed by FDTS follows a sequential kinetic mechanism with respect to all its substrates, as illustrated in Figure 6-6. The reaction is composed of a reductive half reaction and an oxidative half reaction, and $NADP^+$ only leaves the enzymatic complex after the oxidation of flavin. Since dUMP acts as an activator for the oxidative half reaction, but not for the reductive half reaction,[207,208] we propose that it binds at the beginning of the oxidative half reaction. After dUMP binds to and activates the enzyme, CH_2H_4folate and O_2 compete for the reduced and dUMP-activated enzymatic complex. No direct evidence has been shown so far to support the exact order of product release after the oxidation of $FADH_2$, so Figure 6-6 follows a "first come, last leave" principle.

Conclusions

The oxidase activity of *tm*FDTS was exploited to probe several aspects of the kinetic mechanism of FDTS-catalyzed thymidylate synthesis. CH_2H_4folate and O_2 appear to be competitive substrates of FDTS, supporting the notion that both compete for the same reduced form of the enzyme (i.e., the FDTS-$FADH_2$-$NADP^+$-dUMP complex). The binding constant of CH_2H_4folate to the reduced form of the enzyme is determined to be rather large ($1/K_I = 0.5$ μM), suggesting a tightly bound reactive FDTS-$FADH_2$-$NADP^+$-

dUMP-CH_2H_4folate complex. Binding constants of a substrate to a pre-activated enzyme are usually difficult to measure. We developed a method to assess such a binding constant, by studying an alternative activity of the enzyme where the substrate of interest acts as an inhibitor (or competitive substrate, see SI). The high binding affinity of CH_2H_4folate to the reactive enzymatic complex, and the observation that the oxidase activity of FDTS is faster than the synthase activity, implies that steps following CH_2H_4folate binding are rate-limiting for the oxidative half reaction of FDTS synthase activity. These results agree with previous observations that the presence of CH_2H_4folate slows the consumption of NADPH under aerobic conditions.[204] Additionally, the oxidase activity of FDTS calls for caution when studying the synthase activity under aerobic conditions, which has been the case in many previous studies.[69,72,204,205,215,216] Aerobic experiments where non-saturating CH_2H_4folate concentrations were used may need to be revisited, while the results of kinetic measurements with saturating concentrations of CH_2H_4folae should be valid, as the oxidase activity of the FDTS would be completely suppressed.

In contrast to the suggestions from previous studies,[203-205] our data indicate that the product of the reductive half reaction, $NADP^+$, does not leave the enzymatic complex after the reductive half reaction (in accordance with Ref 215). The findings identify a potentially stable complex of reduced FDTS with dUMP, $NADP^+$, and folate derivatives (Figure 6-6). The existence of such complexes may lead to new directions in inhibitor and drug design as well as direct attempts to gain structural information of FDTS complexes with folates and nicotinamides. The lack of such information is currently a major obstacle to understanding FDTS in general.

Experimental Section

Materials

All chemicals were purchased from Sigma-Aldrich, USA, unless otherwise specified. Formaldehyde solution (37.3% by weight) was purchased from Fisher Scientific, USA. CH_2H_4folate was a generous gift from Eprova Inc., Switzerland. All chemicals were used as purchased without further purification. *Thermotoga maritima* FDTS (*tm*FDTS) enzyme was expressed and purified as previously described.[202]

Methods

Analytical Methods.

A Varian Cary 300 Bio UV-Vis spectrophotometer was used for concentration determinations and steady state kinetic measurements. A Hewlett-Packard 8453 series diode-array UV-Vis spectrophotometer was used in single-turnover experiments. All the measured velocities were normalized by the concentration of enzyme active sites. All the reported concentrations refer to the final reaction mixture. FDTS concentration refers to its active site concentration as determined from 450 nm absorbance of bound FAD ($\varepsilon_{450\ nm}$ = 11,300 $M^{-1}cm^{-1}$,[207]). To analyze the data from steady state initial velocity measurements, kinetic parameters were assessed from least-square non-linear regression of the data to the appropriate rate equation with Grafit 5.0. For graphical presentation and further analysis, we used the Lineweaver-Burk double reciprocal plot and secondary replots to further discriminate the kinetic patterns.[211]

Steady State Kinetic Measurements.

Initial velocities of FDTS oxidase activity were measured with the coupled horseradish peroxidase (HRP, type VIA)/Amplex Red assay, by following the oxidation of Amplex Red by H_2O_2 as indicated by the increase of absorbance at 575 nm ($\varepsilon_{575\ nm}$ = 67,000 $M^{-1}cm^{-1}$) [217]. Experiments were performed at 37 ºC in 200 mM

tris(hydroxymethyl)aminomethane (Tris)/HCl buffer (pH=7.9), with 100 μM dUMP (to ensure examination of the dUMP-activated enzyme[208]), 50 μM Amplex Red, 1 unit/ml HRP, and 2 μM FDTS. Reactions were initiated by addition of FDTS. The final volume of the reaction mixture was 210 μl. Three different Tris/HCl buffers were prepared: (i) buffer under atmospheric concentration of O_2 (210 μM), (ii) buffer under 1 atm of purified argon, ([O_2] = 0), and (iii) buffer saturated with O_2 (1 atm of pure oxygen, [O_2] = 1050 μM). In order to obtain various O_2 concentrations, different combinations of these buffers were mixed in preparation of each experiment. Air-tight syringes were used to transfer the solutions under anaerobic conditions controlled by a dual manifold Schlenk line. Control experiments were performed under Ar atmosphere with the same experiment techniques, where no oxidase activity was observed.

The apparent Michaelis constant of O_2 at 100 μM NADPH was determined with O_2 concentrations ranging from 2 to 990 μM. The binding order of NADPH and O_2 was studied by varying the NADPH concentration from 10 to 400 μM over an O_2 concentration range of 8 μM - 1 mM. The product inhibition by $NADP^+$ was examined with 100 μM NADPH at both saturating (210 μM) and sub-saturating (10 μM) O_2 concentrations. $NADP^+$ concentrations ranged from 0 to its solubility limit (~550 mM) in 200 mM Tris/HCl buffer (pH=7.9) at 37 ºC. The inhibition of FDTS oxidase activity by CH_2H_4folate was studied by varying the CH_2H_4folate concentration from 0 to 100 μM over an O_2 concentration range of 8 μM - 1 mM. This inhibition study was conducted in the presence of fixed concentrations of NADPH (100 μM) and formaldehyde (10 mM, to stabilize CH_2H_4folate).

<u>$FADH_2$ Oxidation by O_2.</u>

Single-turnover experiments of the oxidative half reaction were conducted to examine the oxidation of the enzyme bound $FADH_2$ by O_2. Experiments were performed at 0 ºC in 200 mM Tris/HCl buffer (pH=7.9) with a dUMP concentration range of 0-1

mM. 10 μM FDTS-bound FAD was first reduced to $FADH_2$ by titrating with one equivalent of sodium dithionite[218] under anaerobic conditions. The anaerobic conditions were controlled by the Schlenk line. Reactions were then initiated by addition of O_2-containing buffer ($[O_2]$=14 μM in the final reaction mixture). The final volume of the reaction mixture was 300 μl. $FADH_2$ oxidation was followed by increase of absorbance at 450 nm ($\varepsilon_{450\ nm}$=11,300 $M^{-1}cm^{-1}$).[207] Data from each time course were fit to an exponential equation to obtain the rate constant for this reaction.

Formation of the $FADH_2$-$NADP^+$

Charge-Transfer Complex.

In order to examine the formation of the $FADH_2$-$NADP^+$ charge-transfer complex, single-turnover experiments were conducted on the reductive half reaction under anaerobic conditions (Ar) maintained by a glucose/glucose oxidase (type X) O_2-consuming system [208]. Experiments were performed at 37 ºC in 200 mM Tris/HCl buffer (pH=7.9) with 10 mM glucose, 100 units/ml glucose oxidase, 200 μM NADPH, and 10 μM FDTS, at various concentrations of dUMP (0-200 μM). Reactions were initiated by addition of NADPH stock solution. The final volume of the reaction mixture was 300 μl. The reduction of FAD and the formation of the $FADH_2$-$NADP^+$ complex were followed by changes in the absorbance at 450 nm [207] and in the charge-transfer band from 550 to 900 nm[212-214], respectively. Data from each time course were fit to an exponential equation to obtain the rate constant for this process.

Supporting Information

This supporting information presents the details of two analytical procedures we employed: (i) Determination of the inhibition pattern of CH_2H_4folate, which is treated as a dead-end inhibitor for FDTS oxidase activity; and (ii) Examination and validation of the assumption that using the inhibition constant from item i leads to direct assessment of

the binding constant of CH_2H_4folate to the reduced and dUMP-activated enzymatic complex.

Analysis of the Inhibition Pattern of

FDTS Oxidase Activity by CH_2H_4folate

The traditional analysis to determine the inhibition pattern[211] has been shown in the Results and Discussion section. Here we present an alternative way to analyze the same data. The inhibition pattern of CH_2H_4folate is examined by fitting the steady state initial velocities to the mixed-type inhibition model (Eq 3). As presented below, this general model can distinguish between various patterns of dead-end inhibition with a single substrate and a single inhibitor:

$$\frac{v}{[\mathrm{E}]_\mathrm{t}} = \frac{k_{cat}[\mathrm{S}]}{K_m\left(1+\frac{[\mathrm{I}]}{K_I}\right)+[\mathrm{S}]\left(1+\frac{[\mathrm{I}]}{\alpha K_I}\right)} \tag{3}$$

where k_{cat} is the first-order rate constant of the reaction when [S] approaches infinity and [I] approaches zero; [S], [I], and $[\mathrm{E}]_\mathrm{t}$ are the concentrations of O_2, CH_2H_4folate, and total concentration of enzyme active sites, respectively; K_m is the Michaelis constant of O_2; and K_I is the inhibition constant of CH_2H_4folate. The coefficient α is the ratio between the dissociation constants of the inhibitor from the enzyme (EI) and from the enzyme-substrate complex (ESI), which reflects the difference in the inhibitor's affinities for these two different enzymatic complexes. The magnitude of α discriminates between various types of inhibition:[210] when $\alpha \ll 1$, the inhibition is un-competitive; when $\alpha \sim 1$, it is non-competitive; and when $\alpha \gg 1$, it is competitive. Fitting our data to Eq 3 yields a value for α that is much larger than unity ($\alpha = 101 \pm 46$, Table 6-1), thus the second term of the denominator approaches [S], and the mixed inhibition model (Eq 3) is reduced to the competitive inhibition model (Eq 2).

The F-test (a statistical test of validity of going from a complicated model to a simpler one[219]) suggests that the mixed-type inhibition (Eq 3) does not provide a statistically better fitting than the competitive inhibition (Eq 2). Furthermore, kinetic parameters for both fittings were determined to be identical within experimental error (Table 6-1). In accordance with the linearized analysis presented in the main text, the current analysis indicates that the inhibition of FDTS oxidase activity by CH_2H_4folate is best described by a competitive pattern.

Estimating the Binding Constant of CH_2H_4folate to The Reduced and Dump-Activated Enzymatic Complex from its Apparent Inhibition Constant

The analysis of data from the inhibition study of FDTS oxidase activity with CH_2H_4folate, presented above, treated CH_2H_4folate as a dead-end inhibitor. Yet, when the reduced complex is activated by dUMP,[208] CH_2H_4folate is actually an alternative substrate competing with O_2. This part of the SI examines the validity of treating CH_2H_4folate as a dead-end inhibitor to assess its binding constant to the reactive enzymatic complex.

The initial velocity of the oxidase activity, in the presence of CH_2H_4folate, can be best described by the equation for a bi-substrate system with an alternative second substrate:[210]

$$\frac{v}{[\mathrm{E}]_\mathrm{t}} = \frac{k_{cat}[\mathrm{B}]}{K_{m_\mathrm{B}}\left(1+\frac{K_{ia}}{[\mathrm{A}]}+\frac{[\mathrm{I}]}{K_{m_\mathrm{I}}}+\frac{K_{ia}[\mathrm{I}]}{K_{ii}[\mathrm{A}]}\right)+[\mathrm{B}]\left(1+\frac{K_{m_\mathrm{A}}}{[\mathrm{A}]}\right)} \tag{4}$$

where [A], [B], [I] and $[\mathrm{E}]_\mathrm{t}$ are the concentrations of NADPH, O_2, and CH_2H_4folate, and total concentration of enzyme active sites, respectively; K_{m_A}, K_{m_B}, and K_{m_I} are the Michaelis constants of NADPH, O_2, and CH_2H_4folate, respectively; K_{ia} is

the dissociation constant of NADPH from the FDTS-FAD-NADPH-dUMP complex, and K_{ii} is the dissociation constant of CH_2H_4folate from the FDTS-$FADH_2$-$NADP^+$-dUMP-CH_2H_4folate complex (i.e., the reciprocal of its binding constant to the reactive FDTS-$FADH_2$-$NADP^+$-dUMP complex). Eq 5 can be derived from Eq 4:

$$\frac{v}{[\mathrm{E}]_\mathrm{t}} = \frac{k_{cat}[\mathrm{B}]}{K_{m_\mathrm{B}}\left(1+\frac{K_{ia}}{[\mathrm{A}]}+\frac{[\mathrm{I}]}{K_{m_\mathrm{I}}}+\frac{K_{ia}[\mathrm{I}]}{K_{ii}[\mathrm{A}]}\right)+[\mathrm{B}]\left(1+\frac{K_{m_\mathrm{A}}}{[\mathrm{A}]}\right)}$$

$$= \frac{\dfrac{k_{cat}}{1+\dfrac{K_{m_\mathrm{A}}}{[\mathrm{A}]}}[\mathrm{B}]}{K_{m_\mathrm{B}}\dfrac{1+\dfrac{K_{ia}}{[\mathrm{A}]}+\dfrac{[\mathrm{I}]}{K_{m_\mathrm{I}}}+\dfrac{K_{ia}[\mathrm{I}]}{K_{ii}[\mathrm{A}]}}{1+\dfrac{K_{m_\mathrm{A}}}{[\mathrm{A}]}}+[\mathrm{B}]}$$

$$= \frac{\dfrac{k_{cat}}{1+\dfrac{K_{m_\mathrm{A}}}{[\mathrm{A}]}}[\mathrm{B}]}{K_{m_\mathrm{B}}\dfrac{1+\dfrac{K_{ia}}{[\mathrm{A}]}}{1+\dfrac{K_{m_\mathrm{A}}}{[\mathrm{A}]}}\left(1+\dfrac{\dfrac{[\mathrm{I}]}{K_{m_\mathrm{I}}}+\dfrac{K_{ia}[\mathrm{I}]}{K_{ii}[\mathrm{A}]}}{1+\dfrac{K_{ia}}{[\mathrm{A}]}}\right)+[\mathrm{B}]}$$

$$= \frac{\dfrac{k_{cat}}{1+\dfrac{K_{m_\mathrm{A}}}{[\mathrm{A}]}}[\mathrm{B}]}{K_{m_\mathrm{B}}\dfrac{1+\dfrac{K_{ia}}{[\mathrm{A}]}}{1+\dfrac{K_{m_\mathrm{A}}}{[\mathrm{A}]}}\left(1+\dfrac{\dfrac{[\mathrm{I}]}{K_{m_\mathrm{I}}}+\dfrac{K_{ia}[\mathrm{I}]}{K_{ii}[\mathrm{A}]}}{1+\dfrac{K_{ia}}{[\mathrm{A}]}}\right)+[\mathrm{B}]}$$

$$= \frac{\dfrac{k_{cat}}{1+\dfrac{K_{m_A}}{[A]}}[B]}{K_{m_B}\dfrac{1+\dfrac{K_{ia}}{[A]}}{1+\dfrac{K_{m_A}}{[A]}}\left(1+\dfrac{[I]}{\left(1+\dfrac{K_{ia}}{[A]}\right)\Big/\left(\dfrac{1}{K_{m_I}}+\dfrac{K_{ia}}{K_{ii}[A]}\right)}\right)+[B]}$$

$$= \frac{k'_{cat}[B]}{K'_{m_B}\left(1+\dfrac{[I]}{K'_I}\right)+[B]} \tag{5}$$

Eq 5 has the same form as Eq 2, where

$$k'_{cat} = \frac{k_{cat}}{1+\dfrac{K_{m_A}}{[A]}} \tag{6}$$

$$K'_{m_B} = K_{m_B}\frac{1+\dfrac{K_{ia}}{[A]}}{1+\dfrac{K_{m_A}}{[A]}} \tag{7}$$

$$K'_I = \frac{1+\dfrac{K_{ia}}{[A]}}{\dfrac{1}{K_{m_I}}+\dfrac{K_{ia}}{K_{ii}[A]}} \tag{8}$$

Therefore, with a fixed concentration of substrate A (NADPH), fitting our data to Eq 2 provides the estimated values for the parameters k'_{cat}, K'_{m_B}, and K'_I. To test whether K'_I, which is K_I in eq 2, can represent K_{ii}, which is the dissociation constant of CH_2H_4folate from the reduced enzymatic complex, eq 8 is transformed to eq 9:

$$K_I^{'} = \frac{1 + \frac{K_{ia}}{[\mathrm{A}]}}{\frac{1}{K_{m_1}} + \frac{K_{ia}}{K_{ii}[\mathrm{A}]}} = K_{ii} \frac{1 + \frac{K_{ia}}{[\mathrm{A}]}}{\frac{K_{ii}}{K_{m_1}} + \frac{K_{ia}}{[\mathrm{A}]}} \tag{9}$$

Under the conditions of our experiments ([NADPH] = 100 μM),

$$\frac{K_{ia}}{[\mathrm{A}]} >> 1, \text{ and } \frac{K_{ii}}{K_{m_I}} << 1, \text{ so } \frac{K_{ia}}{[\mathrm{A}]} >> \frac{K_{ii}}{K_{m_I}}.$$

Thus, Eq 9 is therefore reduced to Eq 10:

$$K_I^{'} \approx K_{ii} \frac{\frac{K_{ia}}{[\mathrm{A}]}}{\frac{K_{ia}}{[\mathrm{A}]}} = K_{ii} \tag{10}$$

Thus, the apparent $K_I^{'}$ value for CH_2H_4folate determined in the inhibition study is a reasonable estimate of the dissociation constant (K_{ii}) of CH_2H_4folate from the FDTS-$FADH_2$-$NADP^+$-dUMP-CH_2H_4folate complex.

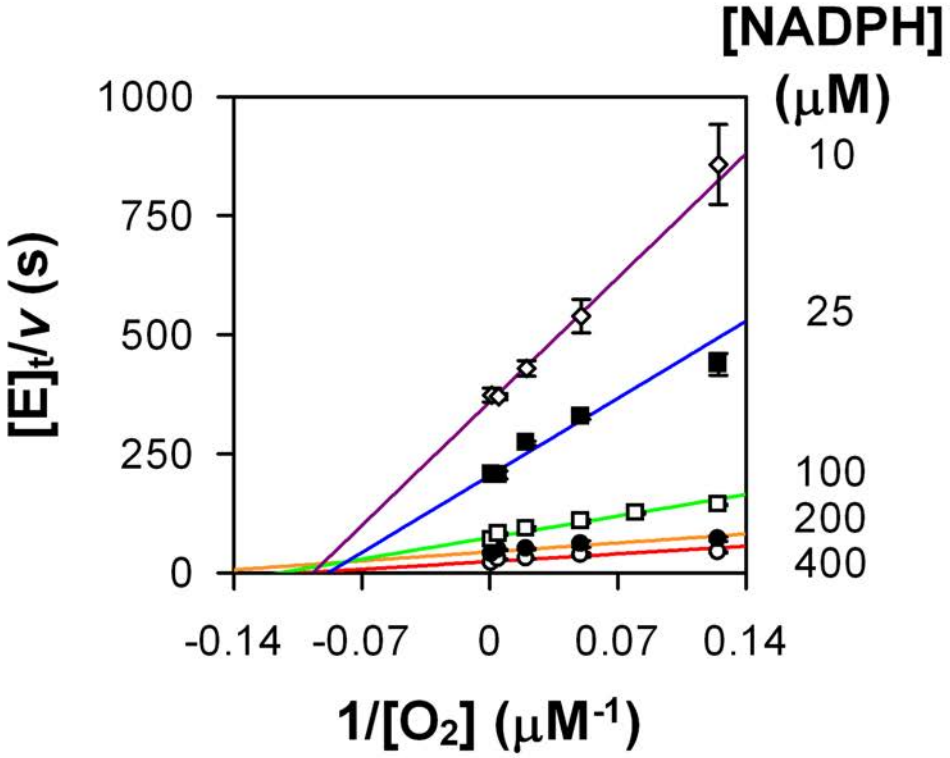

Figure 6-1. Steady state sequential mechanism of FDTS oxidase activity.

Data are presented as a Lineweaver-Burk double reciprocal plot. Experiments were performed at 37 ºC. NADPH concentrations used were (○, red line) 400 μM, (●, orange line) 200 μM, (□, green line) 100 μM, (■, blue line) 25 μM, and (◇, purple line) 10 μM.

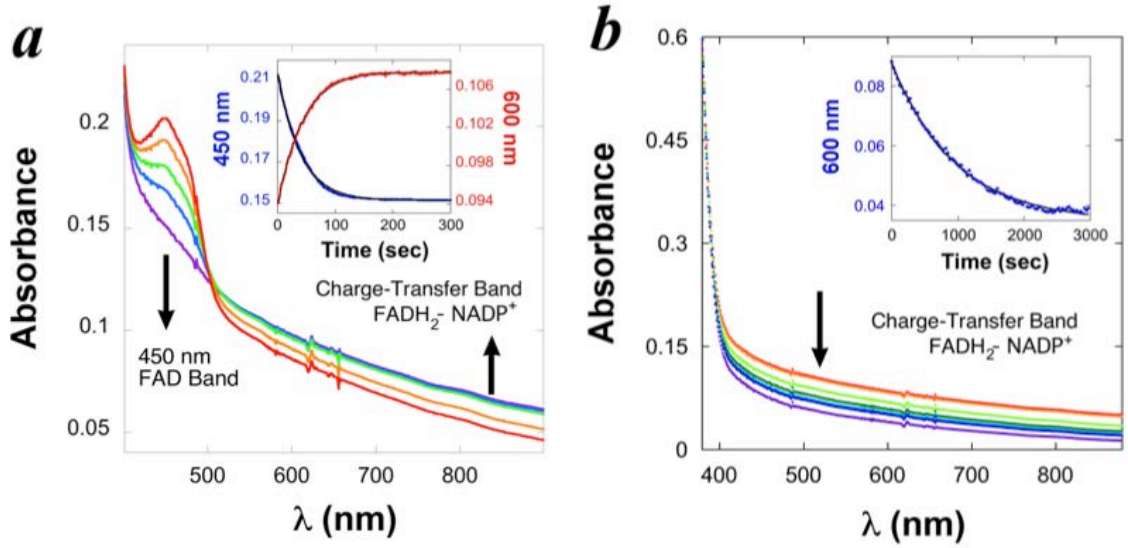

Figure 6-2. The kinetics of $FADH_2$-$NADP^+$ charge-transfer complex during the reductive half reaction of FDTS.

This figure presents:

a. Spectra of 10 μM (active site concentration) *tm*FDTS-FAD being reduced anaerobically by 200 μM NADPH in 200 mM Tris/HCl buffer (pH 7.9) at 37 ºC. Each spectrum was sampled at a different time during one single-turnover experiment. The absorbance of FAD (450 nm) decreases as the charge-transfer band of the $FADH_2$-$NADP^+$ complex (550 - 900 nm) increases. Inset**:** A typical time course of the enzyme-bound FAD reduction by NADPH. The decrease of absorbance at 450 nm is presented as red traces, and the increase of the charge-transfer band from 550 nm to 900 nm is presented as blue traces. Fitting each time course (black curves in the inset) to an exponential equation yields a first-order rate constant, both equal 0.025 ± 0.002 s^{-1}.

b. Continuation of the experiments described in panel a., but the first spectrum was recorded after the last one in panel a., and the spectra were recorded in intervals of 30 min. The wide charge-transfer band disappears slowly while the enzyme remains reduced and with no change in total enzyme concentration (as judged from absorbance at 230-300 nm range). The decrease in charge transfer bend is interpreted as $NADP^+$ release. The inset presents the exponential fitting (black curve) of the time course of absorbance change at 600 nm (blue traces). The first-order rate constant of disappearance of the charge-transfer band was determined to be 0.00135 ± 0.00005 s^{-1}.

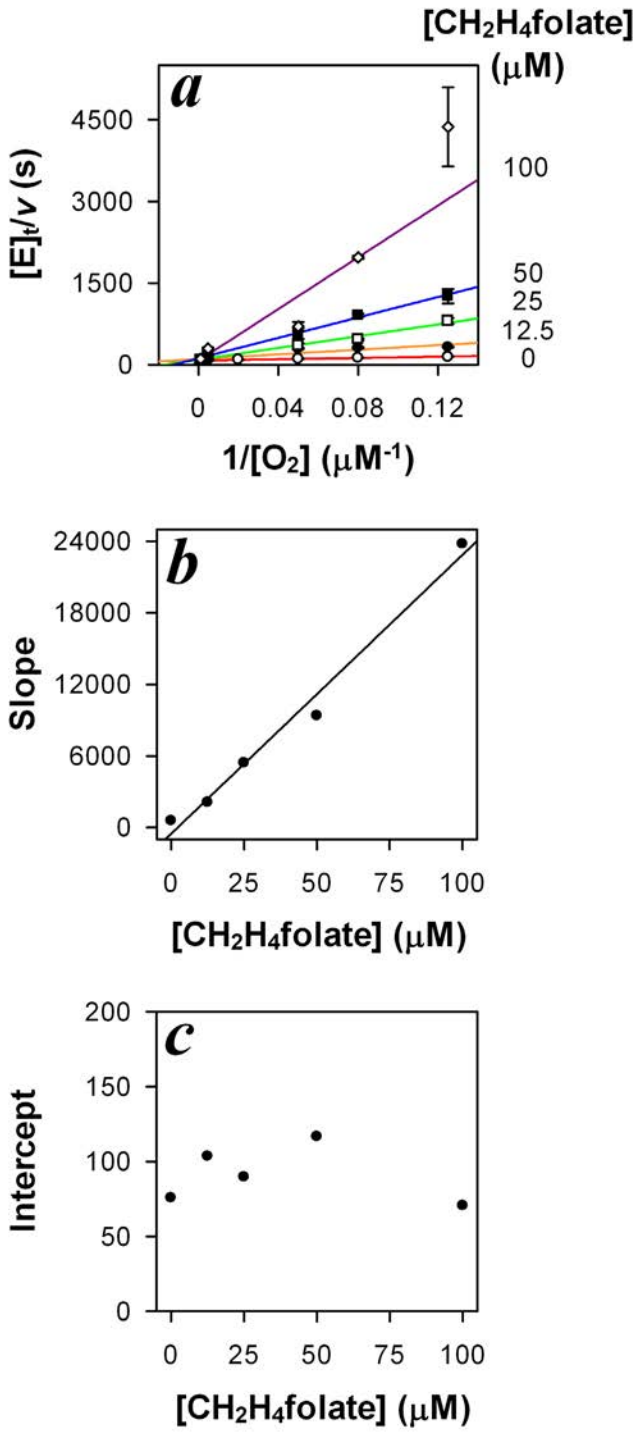

Figure 6-3. Competitive inhibition of FDTS oxidase activity by CH_2H_4folate.

This figure presents:

a. The Lineweaver-Burk double reciprocal plot (1/rate vs. 1/[O_2]). CH_2H_4folate concentrations used were (○, red line) 0 μM, (●, orange line) 12.5 μM, (□, green line) 25 μM, (■, blue line) 50 μM, and (◇, purple line) 100 μM.

b. The secondary slope-replot of the Lineweaver-Burk plot (*a*), which increases linearly with [CH_2H_4folate].

c. The secondary intercept-replot of the Lineweaver-Burk plot (*a*), which is independent of [CH_2H_4folate]. Experiments were performed at 37 ^{o}C.

Figure 6-3 ——continued

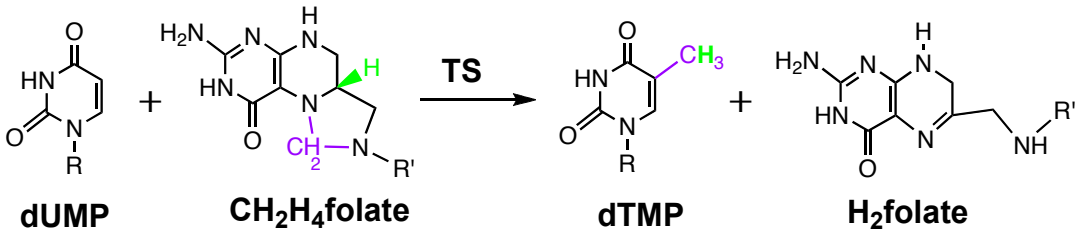

Figure 6-4. The reaction catalyzed by classical TSase.

R is 2'-deoxyribose-5'-phosphate and **R'** is *p*-aminobenzoyl-glutamate.

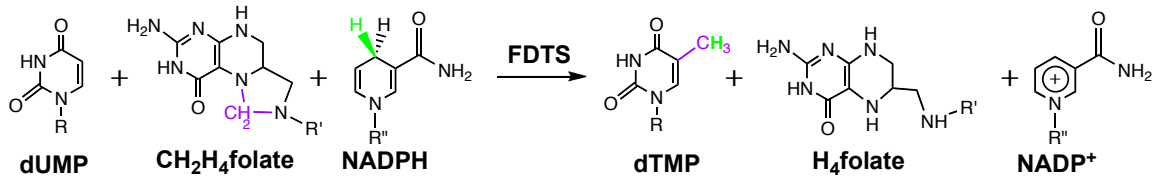

Figure 6-5. The reaction catalyzed by FDTS.

R is 2'-deoxyribose-5'-phosphate, **R'** is *p*-aminobenzoyl-glutamate, and **R"** is adenine-2'-phosphate-ribose-5'-pyrophosphate-ribose.

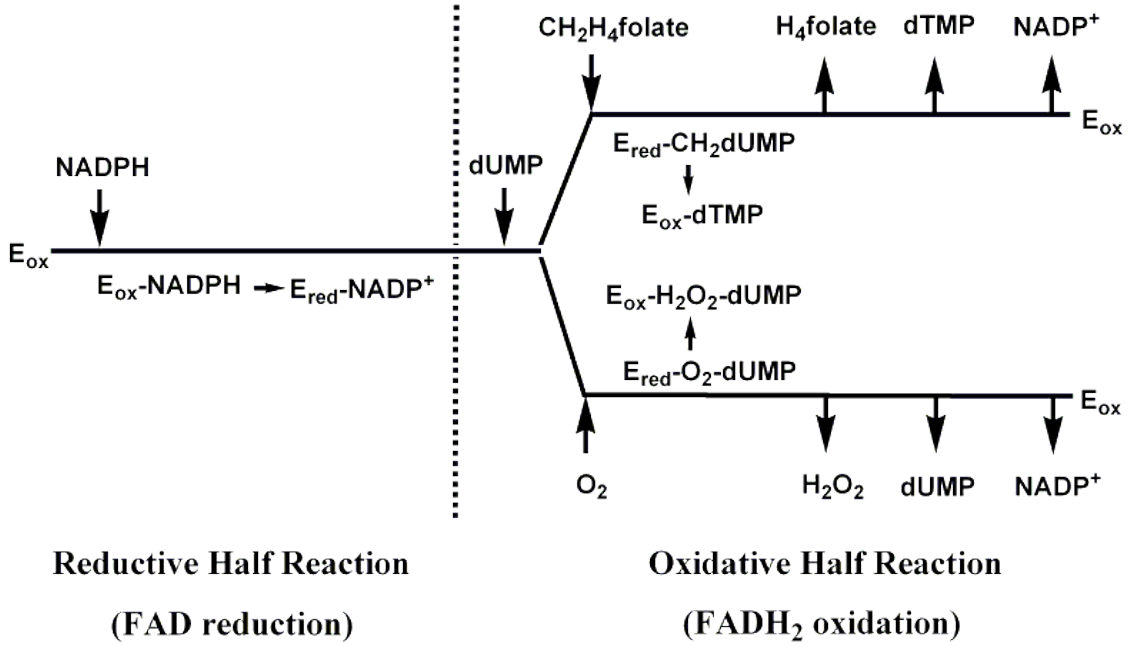

Figure 6-6. The proposed binding and release kinetic mechanism for FDTS.

E_{red} and E_{ox} represent the reduced and the oxidized enzymatic complexes, respectively. Adopted from Ref 208. All the arrows represent reversible process but the formation of dTMP that appears to be irreversible.

Table 6-1. Kinetic parameters for FDTS.

Model Parameter	Competitive [a]	Mixed-type [b]
k_{cat} (s^{-1})	0.0127 ± 0.0004	0.0134 ± 0.0005
K_m (mM)	7 ± 1	8 ± 1
K_I (mM)	1.9 ± 0.3	2.5 ± 0.4
α	NA	101 ± 46

Notes:

The kinetic parameters determined from the fittings of data for the inhibition of FDTS oxidase activity by CH_2H_4folate to competitive and mixed-type inhibition (Eq 2 and Eq 3, respectively).

[a] Fitted to Eq 2.

[b] Fitted to Eq 3.

CHAPTER VII

SUMMARY, IMPACT, AND FUTURE DIRECTIONS

The relationship between protein structure, motions, and catalytic activity is an evolving perspective in enzymology. An interactive approach, where experimental and theoretical studies examine the same catalytic mechanism, is instrumental in addressing this issue. My dissertation has presented a series of studies of thymidylate synthase (TSase) using various techniques, including steady state kinetics, temperature dependence of kinetic isotope effects (KIEs), site-directed mutagenesis, X-ray crystallography, and quantum mechanics/molecular mechanics (QM/MM) calculations. My PhD research has focused on examining two C-H bond activations in *Escherichia coli* TSase (ecTSase) to illustrate how protein motions affect "simple" H-transfer steps in a complex reaction mechanism. We found that the KIE on the rate-limiting hydride transfer is temperature independent while that on the faster proton transfer is temperature dependent. Based on the phenomenological Marcus-like model, these results suggest that the hydride transfer has a better-organized tunneling ready state (TRS) than the proton transfer, invoking the question how TSase behaves differently in reaching the TRSs of these two H-transfers. Our QM/MM calculations revealed that the movements of protein residues are synchronized with structural changes in the ligands during both H-transfers, and the difference in the temperature dependences of KIEs probably arise from the dissimilarity in their intrinsic nature, i.e. C-H→C hydride transfer between substrates vs. C-H→O proton transfer to a mobile water molecule (Figure 7-1.II). Compared with the hydride transfer, the proton transfer has a more complex free energy surface with multiple subsets of transition state (TS) structures, which corroborates the interpretation by the Marcus-like model. Our QM/MM calculations with TSase demonstrate the ability of high-level simulations to not only interpret previous experimental results at molecular details, but also provide guidance for future experiments to examine the computational

outcomes. Besides the accomplished work in Chapters II – VI, we also investigated the details of mechanistic steps between the proton and hydride transfers by QM/MM calculations (steps 5 and 6 in Figure 7-1.II), which suggest that protein motions play unequivocal roles in all those mechanistic steps.[68] In addition, we studied properties of the molecule CH_2H_4folate, which is the cofactor for TSase and an important folate metabolite *in vivo*. We found that the stability of CH_2H_4folate is dependent on its own concentration, and are currently performing molecular dynamics (MD) simulations to understand this phenomenon.[220] The experimental-theoretical interactive approach taken in this project has not only assisted in understanding the catalytic mechanisms of TSase, but also provided insights into the relationship between protein structures, motions, and catalytic activity.

Our calculations suggest a new reaction mechanism for the proton transfer, which involves cleavage of the only covalent bond formed between ecTSase and ligands during the catalyzed reaction (i.e. the C6-S bond, Figure 7-1). Future experimental efforts shall examine the transient cleavage of C6-S bond during the proton transfer to authenticate the proposed new mechanism. Our calculations indicate R166 is critical in stabilizing the S anion of C147 during the proton transfer, while Y94 is important for the H-bond rearrangements at the end of this step. Therefore, experimental studies of the effects of R166 and Y94 mutations on the kinetics and KIEs of the proton transfer can also examine the proposed new mechanism. In addition, it might be possible to chemically trap the proposed new reaction intermediate that is not covalently attached to ecTSase (Complex D or E in Figure 7-1.II), using the quenching experimental assay recently developed for the flavin-dependent thymidylate synthase.[221] Complementary to the proposed experiments, future computational efforts can calculate the dissociation constant of the proposed new intermediate and compare its binding affinity with the *in vivo* active form of current drugs targeting TSase, such as 5-fluoro-dUMP. Computations can also design structural analogues of the new intermediate and even TS analogues as potential

inhibitors of ecTSase, which may develop into a novel class of antibiotics targeting DNA biosynthesis.

We also studied the effects of Mg^{2+} on the catalytic mechanism of TSase, which is the first attempt to resolve the mechanism of interaction between Mg^{2+} and TSase. The experimental results suggest that Mg^{2+} affects the binding affinity of both substrates but with opposite trend, i.e. K_d^{dUMP} increases while $K_d^{\mathrm{CH_2H_4folate}}$ decreases in the presence of Mg^{2+}. Another intriguing observation is that, for both Mg^{2+} and dUMP, the dissociation constant of the ternary ecTSase-dUMP-Mg^{2+} complex was determined to be larger than that of the corresponding binary complex (ecTSase-Mg^{2+} and ecTSase-dUMP, respectively). A plausible explanation is that Mg^{2+} chelates with dUMP in solution, and the formed dUMP-Mg^{2+} complex has lower affinity to ecTSase. Future experiments with isothermal titration calorimetry (ITC) can provide details of how Mg^{2+} affects the affinity of both substrates to ecTSase, e.g. by evaluating the changes in the stoichiometry and the enthalpy and entropy of binding. As discussed in Chapter IV, using Mg^{2+} in combination with poly-Glu antifolates might be a promising strategy in designing species-specific drugs that target DNA biosynthesis. Future pursuit in this direction shall employ structural and kinetic studies of TSase enzymes from different species (e.g. human vs. bacteria) using the folate cofactor with poly-Glu moiety in the absence and presence of Mg^{2+}. Since Mg^{2+} has very similar electron density with O^{2-} and thus is difficult to discriminate from water molecules in crystal structures, Mn^{2+} and Ca^{2+} may be used as analogues to probe the binding site for Mg^{2+} in various TSase enzyme complexes. In addition, QM/MM calculations and MD simulations can also assist in elucidating how Mg^{2+} affects the catalytic mechanism of TSase, as well as designing species-specific inhibitors.

Furthermore, both our experiments and computations suggest TSase exploits concerted protein motions in catalyzing chemical transformations.[65-68] Particularly, our experiments with Y209W ecTSase demonstrated that protein motions at various time

scales can affect different parameters of the hydride transfer step (Chapter III); and the analysis of effects of Mg^{2+} on ecTSase suggested a relay between the protein surface and active site (Chapter IV). These results highlight the importance of long-range interactions in TSase-catalyzed reaction. Our computations also suggested that collective protein motions rearrange the network of H-bonds to accompany structural changes in the ligands during and between chemical transformations (Chapter V). An exciting direction of this project is to extend the current findings and examine the "motions-catalysis" relationship with other mutations distant from the active site, which shall continue to use the interactive approach with experimental and computational methods. A "dynamic network of coupled motions" has been proposed for dihydrofolate reductase (DHFR) based on NMR relaxation experiments, genomic analysis, KIE measurements, and QM/MM calculations.[23,108,130-132] Compared with the extensively studied "model protein" DHFR, most enzymes are more similar to TSase, which have more rigid structures and sophisticated mechanisms. Thus, the "motions-catalysis" relationship inferred from our studies of TSase has more general implication to the question how enzymes work.

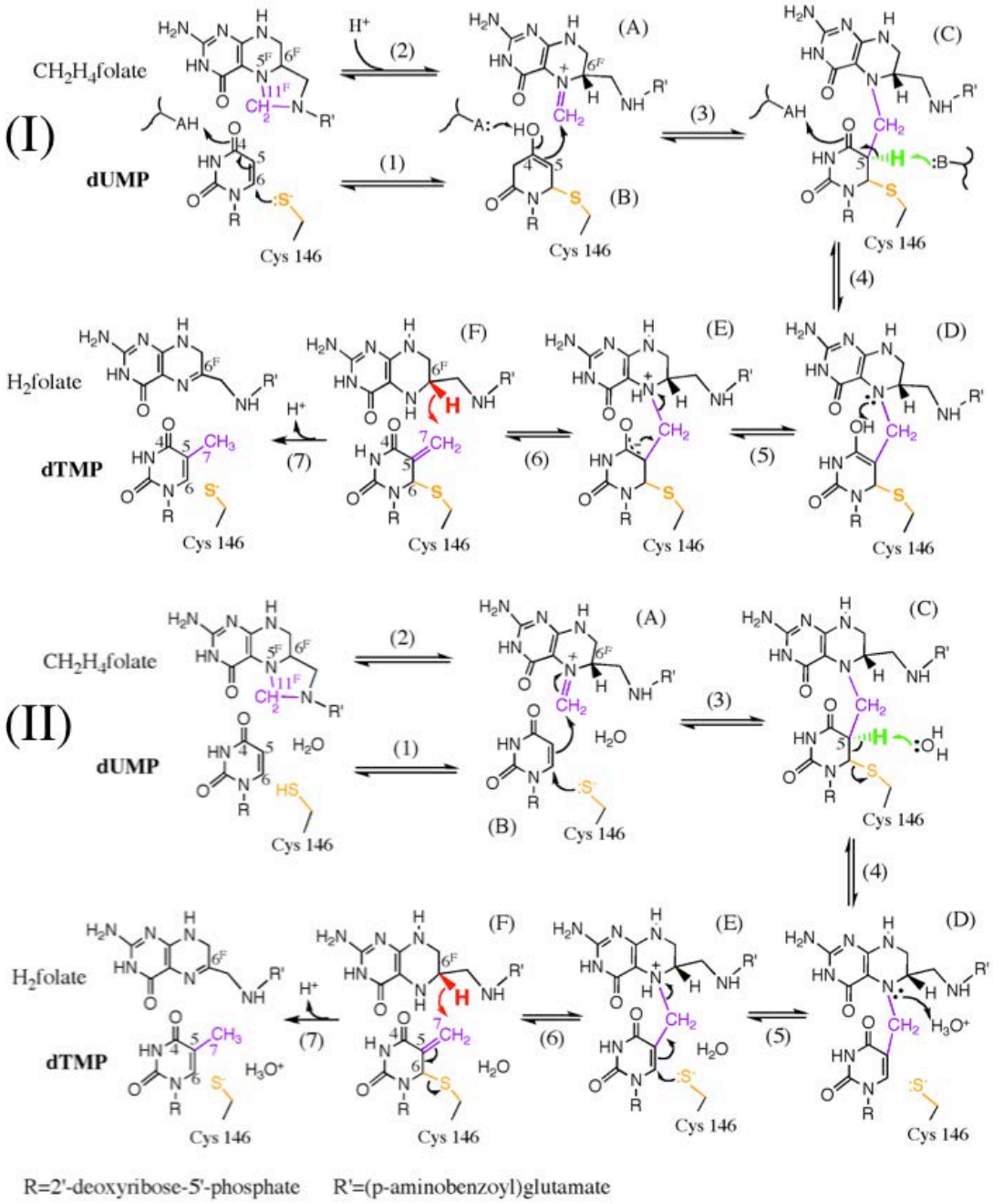

Figure 7-1. Comparison of two proposed catalytic mechanisms of TSase.

The atom labels of CH_2H_4folate are denoted with a subscript F (^{F}) to discriminate from those of the nucleotides.

(I) Early studies proposed a "traditional" mechanism for TSase, mostly based on model reactions in solution and partial reactions in the absence of CH_2H_4folate.[61] Cys146 nucleophilically attacks C6 of dUMP to initiate the reaction, and the "C6-S bond" remains intact throughout the reaction until the last irreversible chemical conversion –

the hydride transfer (step 7). The mechanism was suggested to involve C4-enol/ketone formation in multiple steps (steps 1, 3, 4, 5, and 6).

(II) Our QM/MM calculations have proposed a different mechanism of ecTSase, which exploits the lability of C6-S bond in catalyzing many steps (steps 3, 4, 6, and 7).[67,68,95]

Figure 7-1 ——continued

REFERENCES

(1) Doolittle, W. F. *Sci. Am.* **2000**, *282*, 90-95.

(2) Payen, A.; Persoz, J. F. *Ann. Chim. Phys.* **1833**, *53*, 73-92.

(3) Sumner, J. B. *J. Biol. Chem.* **1926**, *69*, 435-441.

(4) Willstätter, R.; Cornell University. *Problems and Methods in Enzyme Research*; Cornell University: Ithaca, N.Y., 1927.

(5) Kunitz, M. *J. Gen. Physiol.* **1940**, *24*, 15-32.

(6) Kunitz, M.; Northrop, J. H. *J. Gen. Physiol.* **1935**, *18*, 433-458.

(7) Northrop, J. H. *Science* **1929**, *69*, 580.

(8) Ringe, D.; Petsko, G. A. *Science* **2008**, *320*, 1428-1429.

(9) Blow, D. *Structure (London, England : 1993)* **2000**, *8*, R77-R81.

(10) Fischer, E. *Ber. Dtsch. Chem. Ges.* **1894**, *27*, 2985-2993.

(11) Koshland, D. E. *Proc. Natl. Acad. Sci. U.S.A.* **1958**, *44*, 98-104.

(12) Cui, Q.; Karplus, M. *J. Phys. Chem. B* **2002**, *106*, 7927-7947.

(13) Pu, J.; Gao, J.; Truhlar, D. G. *Chem. Rev.* **2006**, *106*, 3140-3169.

(14) Boehr, D. D.; McElheny, D.; Dyson, H. J.; Wright, P. E. *Science* **2006**, *313*, 1638-1642.

(15) Henzler-Wildman, K.; Kern, D. *Nature* **2007**, *450*, 964-972.

(16) Allemann, R. K.; Evans, R. M.; Loveridge, E. J. *Biochem. Soc. Trans.* **2009**, *37*, 349-353.

(17) Schwartz, S. D.; Schramm, V. L. *Nat. Chem. Biol.* **2009**, *5*, 551-558.

(18) Major, D. T.; Heroux, A.; Orville, A. M.; Valley, M. P.; Fitzpatrick, P. F.; Gao, J. *Proc. Natl. Acad. Sci. U.S.A.* **2009**, *106*, 20734-20739.

(19) Nagel, Z. D.; Klinman, J. P. *Chem. Rev.* **2010**, *110*, PR41–PR67.

(20) Truhlar, D. G. *J. Phys. Org. Chem.* **2010**, *23*, 660-676.

(21) Pineda, J. R. E. T.; Antoniou, D.; Schwartz, S. D. *J. Phys. Chem. B* **2010**, *114*, 15985-15990.

(22) Silva, R. G.; Murkin, A. S.; Schramm, V. L. *Proc. Natl. Acad. Sci. U.S.A.* **2011**, *108*, 18661-18665.

(23) Hammes, G. G.; Benkovic, S. J.; Hammes-Schiffer, S. *Biochemistry* **2011**, *50*, 10422-10430.

(24) Hay, S.; Johannissen, L. O.; Hothi, P.; Sutcliffe, M. J.; Scrutton, N. S. *J. Am. Chem. Soc.* **2012**, *134*, 9749-9754.

(25) Hay, S.; Scrutton, N. S. *Nat. Chem.* **2012**, *4*, 161-168.

(26) Glowacki, D. R.; Harvey, J. N.; Mulholland, A. J. *Nat. Chem.* **2012**, *4*, 169-176.

(27) Wang, Z.; Roston, D.; Kohen, A. *Adv. Protein Chem. Struct. Biol.* **2012**, *87*, 155-180.

(28) Cook, P. F. *Enzyme Mechanism from Isotope Effects*; CRC Press: Boca Raton, 1991.

(29) Cook, P. F.; Cleland, W. W. In *Enzyme Kinetics and Mechanism*; Garland Science: London ; New York, 2007, p 253-324.

(30) Kohen, A.; Roston, D.; Stojković, V.; Wang, Z. In *Encyclopedia of Analytical Chemistry*; Meyers, R. A., Ed.; John Wiley & Sons, Ltd: Chichester, UK, 2011; Vol. S1-S3, p 77-99.

(31) Northrop, D. B. In *Isotope Effects on Enzyme-Catalyzed Reactions*; Cleland, W. W., O'Leary, M. H., Northrop, D. B., Eds.; University Park Press: Baltimore, MD., 1977, p 122-152.

(32) Northrop, D. B. *Biochemistry* **1975**, *14*, 2644-2651.

(33) Bigeleisen, J. *J. Chem. Phys.* **1949**, *17*, 675-678.

(34) Bell, R. P. *The Tunnel Effect in Chemistry.*; NY: Chapman & Hall.: London, UK and New York,, 1980.

(35) Agrawal, N.; Hong, B.; Mihai, C.; Kohen, A. *Biochemistry* **2004**, *43*, 1998-2006.

(36) Bandaria, J. N.; Cheatum, C. M.; Kohen, A. *J. Am. Chem. Soc.* **2009**, *131*, 10151-10155.

(37) Kohen, A.; Cannio, R.; Bartolucci, S.; Klinman, J. P. *Nature* **1999**, *399*, 496-499.

(38) Sikorski, R. S.; Wang, L.; Markham, K. A.; Rajagopalan, P. T.; Benkovic, S. J.; Kohen, A. *J. Am. Chem. Soc.* **2004**, *126*, 4778-4779.

(39) Fan, F.; Gadda, G. *J. Am. Chem. Soc.* **2005**, *127*, 17954-17961.

(40) Pudney, C. R.; Johannissen, L. O.; Sutcliffe, M. J.; Hay, S.; Scrutton, N. S. *J. Am. Chem. Soc.* **2010**, *132*, 11329-11335.

(41) Marcus, R. A.; Sutin, N. *Biochim. Biophys. Acta* **1985**, *811*, 265-322.

(42) Franck, J.; Dymond, E. G. *T. Faraday Soc.* **1926**, *21*, 536-542.

(43) Condon, E. *Phys. Rev.* **1926**, *28*, 1182-1201.

(44) Doktorov, E. V.; Malkin, I. A.; Man'ko, V. I. *J. Mol. Spectrosc.* **1977**, *64*, 302-326.

(45) Borgis, D. C.; Lee, S. Y.; Hynes, J. T. *Chem. Phys. Lett.* **1989**, *162*, 19-26.

(46) Kuznetsov, A. M.; Ulstrup, J. *Can. J. Chem.* **1999**, *77*, 1085-1096.

(47) Marcus, R. A. *J. Chem. Phys.* **2006**, *125*, 194504.

(48) Marcus, R. A. *J. Phys. Chem. B* **2007**, *111*, 6643-6654.

(49) Warshel, A.; Florian, J. *Proc. Natl. Acad. Sci. U.S.A.* **1998**, *95*, 5950-5955.

(50) Cannon, W. R.; Benkovic, S. J. *J. Biol. Chem.* **1998**, *273*, 26257-26260.

(51) Rajagopalan, P. T.; Benkovic, S. J. *Chem. Rec.* **2002**, *2*, 24-36.

(52) Hammes-Schiffer, S.; Benkovic, S. J. *Annu. Rev. Biochem.* **2006**, *75*, 519-541.

(53) Warshel, A.; Levitt, M. *J. Mol. Biol.* **1976**, *103*, 227-249.

(54) Maley, F.; Pedersenlane, J.; Changchien, L. M. *Biochemistry* **1995**, *34*, 1469-1474.

(55) Anderson, A. C.; O'Neil, R. H.; DeLano, W. L.; Stroud, R. M. *Biochemistry* **1999**, *38*, 13829-13836.

(56) Saxl, R. L.; Changchien, L. M.; Hardy, L. W.; Maley, F. *Biochemistry* **2001**, *40*, 5275-5282.

(57) Perry, K. M.; Fauman, E. B.; Finer-Moore, J. S.; Montfort, W. R.; Maley, G. F.; Maley, F.; Stroud, R. M. *Proteins: Struct. Func. Genet.* **1990**, *8*, 315-333.

(58) Johnston, P. G.; Lenz, H. J.; Leichman, C. G.; Danenberg, K. D.; Allegra, C. J.; Danenberg, P. V.; Leichman, L. *Cancer Res.* **1995**, *55*, 1407-1412.

(59) Chen, C.-Y.; Chang, Y.-L.; Shih, J.-Y.; Lin, J.-W.; Chen, K.-Y.; Yang, C.-H.; Yu, C.-J.; Yang, P.-C. *Lung Cancer* **2011**, *74*, 132-138.

(60) Bruice, T. W.; Santi, D. V. In *Enzyme Mechanism from Isotope Effects*; Cook, P. F., Ed.; CRC Press: Boca Raton, 1991, p 457-479.

(61) Carreras, C. W.; Santi, D. V. *Annu. Rev. Biochem.* **1995**, *64*, 721-762.

(62) Stroud, R. M.; Finer-Moore, J. S. *Biochemistry* **2003**, *42*, 239-247.

(63) Finer-Moore, J. S.; Santi, D. V.; Stroud, R. M. *Biochemistry* **2003**, *42*, 248-256.

(64) Wang, Z.; Kohen, A. *J. Am. Chem. Soc.* **2010**, *132*, 9820-9825.

(65) Wang, Z.; Abeysinghe, T.; Finer-Moore, J. S.; Stroud, R. M.; Kohen, A. *J. Am. Chem. Soc.* **2012**, *134,* 17722-17730.

(66) Wang, Z.; Abeysinghe, T.; Luzum, C.; Finer-Moore, J. S.; Stroud, R. M.; Kohen, A. Manuscript in preparation, 2012.

(67) Wang, Z.; Silvia, F.; Moliner, V.; Kohen, A. manuscript in preparation, 2012.

(68) Wang, Z.; Silvia, F.; Moliner, V.; Kohen, A. manuscript in preparation, 2012.

(69) Myllykallio, H.; Lipowski, G.; Leduc, D.; Filee, J.; Forterre, P.; Liebl, U. *Science* **2002**, *297*, 105-107.

(70) Murzin, A. G. *Science* **2002**, *297*, 61-62.

(71) Mathews, II; Deacon, A. M.; Canaves, J. M.; McMullan, D.; Lesley, S. A.; Agarwalla, S.; Kuhn, P. *Structure* **2003**, *11*, 677-690.

(72) Leduc, D.; Graziani, S.; Meslet-Cladiere, L.; Sodolescu, A.; Liebl, U.; Myllykallio, H. *Biochem. Soc. Trans.* **2004**, *32*, 231-235.

(73) Wang, Z.; Chernyshev, A.; Koehn, E. M.; Manuel, T. D.; Lesley, S. A.; Kohen, A. *FEBS J.* **2009**, *276*, 2801-2810.

(74) Borgis, D.; Hynes, J. T. *J. Chem. Phys.* **1991**, *94*, 3619-3628.

(75) Roston, D.; Cheatum, C. M.; Kohen, A. *Biochemistry* **2012**, *51*, 6860-6870.

(76) Koehn, E. M.; Fleischmann, T.; Conrad, J. A.; Palfey, B. A.; Lesley, S. A.; Mathews, I. I.; Kohen, A. *Nature* **2009**, *458*, 919-923.

(77) Henzler-Wildman, K. A.; Thai, V.; Lei, M.; Ott, M.; Wolf-Watz, M.; Fenn, T.; Pozharski, E.; Wilson, M. A.; Petsko, G. A.; Karplus, M.; Hubner, C. G.; Kern, D. *Nature* **2007**, *450*, 838-844.

(78) Henzler-Wildman, K. A.; Lei, M.; Thai, V.; Kerns, S. J.; Karplus, M.; Kern, D. *Nature* **2007**, *450*, 913-916.

(79) Fraser, J. S.; Clarkson, M. W.; Degnan, S. C.; Erion, R.; Kern, D.; Alber, T. *Nature* **2009**, *462*, 669-673.

(80) Benkovic, S. J.; Hammes-Schiffer, S. *Science* **2003**, *301*, 1196-1202.

(81) Boehr, D. D.; Dyson, H. J.; Wright, P. E. *Biochemistry* **2008**, *47*, 9227-9233.

(82) Kohen, A. In *Hydrogen-Transfer Reactions*; Hynes, J. T., Klinman, J. P., Limbach, H.-H., Schowen, R. L., Eds.; Wiley_VCH: Weinheim, 2007; Vol. 4, p 1311-1340.

(83) Nagel, Z. D.; Klinman, J. P. *Nat. Chem. Biol.* **2009**, *5*, 543-550.

(84) Schramm, V. L. *Arch. Biochem. Biophys.* **2005**, *433*, 13-26.

(85) Sutcliffe, M. J.; Masgrau, L.; Roujeinikova, A.; Johannissen, L. O.; Hothi, P.; Basran, J.; Ranaghan, K. E.; Mulholland, A. J.; Leys, D.; Scrutton, N. S. *Philos. Trans. R. Soc. Lond. B Biol. Sci.* **2006**, *361*, 1375-1386.

(86) Kiefer, P. M.; Hynes, J. T. In *Isotope Effects in Chemistry and Biology*; Kohen, A., Limbach, H. H., Eds.; Taylor & Francis, CRC Press: Boca Raton, FL, 2006; Vol. Ch. 21, p 549-578.

(87) Knapp, M. J.; Meyer, M.; Klinman, J. P. In *Hydrogen-Transfer Reactions*; Hynes, J. T., Klinman, J. P., Limbach, H.-H., Schowen, R. L., Eds.; Wiley-VCH Verlag GmbH & Co. KGaA: 2007, p 1241-1284.

(88) Schwartz, S. D. In *Isotope Effects in Chemistry and Biology*; Kohen, A., Limbach, H. H., Eds.; Taylor & Francis, CRC Press: Boca Raton, FL, 2006; Vol. Ch. 18, p 475-498.

(89) Truhlar, D. G. In *Isotope Effects in Chemistry and Biology*; Kohen, A., Limbach, H. H., Eds.; Taylor & Francis, CRC Press: Boca Raton, FL, 2006; Vol. Ch. 22, p 579-620.

(90) Warshel, A.; Olsson, M. H. M.; Villá-Freixa, J. In *Isotope Effects in Chemistry and Biology*; Kohen, A., Limbach, H. H., Eds.; Taylor & Francis, CRC Press: Boca Raton, FL, 2006; Vol. Ch. 23, p 621-644.

(91) Roston, D.; Kohen, A. *Proc. Natl. Acad. Sci. U.S.A.* **2010**, *107*, 9572-9577.

(92) Bandaria, J. N.; Dutta, S.; Hill, S. E.; Kohen, A.; Cheatum, C. M. *J. Am. Chem. Soc.* **2008**, *130*, 22-23.

(93) Hong, B.; Haddad, M.; Maley, F.; Jensen, J. H.; Kohen, A. *J. Am. Chem. Soc.* **2006**, *128*, 5636-5637.

(94) Hong, B.; Maley, F.; Kohen, A. *Biochemistry* **2007**, *46*, 14188-14197.

(95) Kanaan, N.; Martí, S.; Moliner, V.; Kohen, A. *Biochemistry* **2007**, *46*, 3704-3713.

(96) Kanaan, N.; Martí, S.; Moliner, V.; Kohen, A. *J. Phys. Chem. A* **2009**, *113*, 2176-2182.

(97) Newby, Z.; Lee, T. T.; Morse, R. J.; Liu, Y.; Liu, L.; Venkatraman, P.; Santi, D. V.; Finer-Moore, J. S.; Stroud, R. M. *Biochemistry* **2006**, *45*, 7415-7428.

(98) Spencer, H. T.; Villafranca, J. E.; Appleman, J. R. *Biochemistry* **1997**, *36*, 4212-4222.

(99) Basran, J.; Harris, R. J.; Sutcliffe, M. J.; Scrutton, N. S. *J. Biol. Chem.* **2003**, *278*, 43973-43982.

(100) Heyes, D. J.; Sakuma, M.; de Visser, S. P.; Scrutton, N. S. *J. Biol. Chem.* **2009**, *284*, 3762-3767.

(101) Santi, D. V.; Stroud, R. M. *Biochemistry* **2002**, *42*, 248-256.

(102) Northrop, D. B. In *Enzyme Mechanism from Isotope Effects*; Cook, P. F., Ed.; CRC Press: Boca Raton, FL., 1991, p 181-202.

(103) Melander, L. C. S.; Saunders, W. H. *Reaction Rates of Isotopic Molecules*; R.E. Krieger Pub. Co.: Malabar, Fla., 1987.

(104) Edwards, S. J.; Soudackov, A. V.; Hammes-Schiffer, S. *J. Phys. Chem. A* **2009**, *113*, 2117-2126.

(105) Liu, H.; Warshel, A. *J. Phys. Chem. B* **2007**, *111*, 7852-7861.

(106) Meyer, M. P.; Klinman, J. P. *Chem. Phys.* **2005**, *319*, 283-296.

(107) Pu, J.; Ma, S.; Gao, J.; Truhlar, D. G. *J Phys Chem B* **2005**, *109*, 8551-8556.

(108) Wang, L.; Goodey, N. M.; Benkovic, S. J.; Kohen, A. *Proc. Natl. Acad. Sci. U.S.A.* **2006**, *103*, 15753-15758.

(109) Pudney, C. R.; Hay, S.; Levy, C.; Pang, J.; Sutcliffe, M. J.; Leys, D.; Scrutton, N. S. *J. Am. Chem. Soc.* **2009**, *131*, 17072-17073.

(110) Changchien, L.-M.; Garibian, A.; Frasca, V.; Lobo, A.; Maley, G. F.; Maley, F. *Prot. Expres. Pur.* **2000**, *19*, 265-270.

(111) Hayatsu, H.; Wataya, Y.; Kai, K.; Iida, S. *Biochemistry* **1970**, *9*, 2858-2865.

(112) Wataya, Y.; Hayatsu, H. *J. Am. Chem. Soc.* **1972**, *94*, 8927-8928.

(113) Wataya, Y.; Hayatsu, H. *Biochemistry* **1972**, *11*, 3583-3588.

(114) Gao, J.; Ma, S.; Major, D. T.; Nam, K.; Pu, J.; Truhlar, D. G. *Chem. Rev.* **2006**, *106*, 3188-3209.

(115) Kohen, A. In *Isotope Effects in Chemistry and Biology*; Kohen, A. L., H.H. Eds., Ed.; Taylor & Francis -CRC Press, Boca Raton, FL: 2006; Vol. Ch. 28, p 743-764.

(116) Quaye, O.; Gadda, G. *Arch. Biochem. Biophys.* **2009**, *489*, 10-14.

(117) Loveridge, E. J.; Allemann, R. K. *Biochemistry* **2010**, *49*, 5390-5396.

(118) Sen, A.; Kohen, A. *J. Phys. Org. Chem.* **2010**, *23*, 613-619.

(119) Warshel, A. *J. Biol. Chem.* **1998**, *273*, 27035-27038.

(120) Bandaria, J. N.; Dutta, S.; Nydegger, M. W.; Rock, W.; Kohen, A.; Cheatum, C. M. *Proc. Natl. Acad. Sci. U.S.A.* **2010**, *107*, 17974-17979.

(121) Stojkovic, V.; Perissinotti, L. L.; Willmer, D.; Benkovic, S. J.; Kohen, A. *J. Am. Chem. Soc.* **2012**, *134*, 1738-1745.

(122) Kanaan, N.; Roca, M.; I., T.; S, M.; Moliner, V. *J. Phys. Chem. B* **2010**, *114*, 13593-13600.

(123) Kanaan, N.; Roca, M.; Tunon, I.; Marti, S.; Moliner, V. *Phys. Chem. Chem. Phys.* **2010**, *12*, 11657-11664.

(124) Kanaan, N.; Ferrer, S.; Marti, S.; Garcia-Viloca, M.; Kohen, A.; Moliner, V. *J. Am. Chem. Soc.* **2011**, *133*, 6692-6702.

(125) Barrett, J. E.; Lucero, C. M.; Schultz, P. G. *J. Am. Chem. Soc.* **1999**, *121*, 7965-7966.

(126) Variath, P.; Liu, Y.; Lee, T. T.; Stroud, R. M.; Santi, D. V. *Biochemistry* **2000**, *39*, 2429-2435.

(127) Fritz, T. A.; Liu, L.; Finer-Moore, J. S.; Stroud, R. M. *Biochemistry* **2002**, *41*, 7021-7029.

(128) Cline, D. J.; Redding, S. E.; Brohawn, S. G.; Psathas, J. N.; Schneider, J. P.; Thorpe, C. *Biochemistry* **2004**, *43*, 15195-15203.

(129) Cook, P. F.; Cleland, W. W. In *Enzyme Kinetics and Mechanism*; Garland Science: London ; New York, 2007, p 121-204.

(130) Agarwal, P. K.; Billeter, S. R.; Rajagopalan, P. T.; Benkovic, S. J.; Hammes-Schiffer, S. *Proc. Natl. Acad. Sci. U.S.A.* **2002**, *99*, 2794-2799.

(131) Wong, K. F.; Selzer, T.; Benkovic, S. J.; Hammes-Schiffer, S. *Proc. Natl. Acad. Sci. U.S.A.* **2005**, *102*, 6807-6812.

(132) Nashine, V. C.; Hammes-Schiffer, S.; Benkovic, S. J. *Curr. Opin. Chem. Biol.* **2010**, *14*, 644-651.

(133) Saen-Oon, S.; Ghanem, M.; Schramm, V. L.; Schwartz, S. D. *Biophys. J.* **2008**, *94*, 4078-4088.

(134) Ghanem, M.; Li, L.; Wing, C.; Schramm, V. L. *Biochemistry* **2008**, *47*, 2559-2564.

(135) Meyer, M. P.; Tomchick, D. R.; Klinman, J. P. *Proc. Natl. Acad. Sci. U.S.A.* **2008**, *105*, 1146-1151.

(136) Agrawal, N.; Kohen, A. *Anal. Biochem.* **2003**, *322*, 179-184.

(137) Blakley, R. L. *Nature* **1960**, *188*, 231-232.

(138) Agrawal, N.; Mihai, C.; Kohen, A. *Anal. Biochem.* **2004**, *328*, 44-50.

(139) Pettersen, E. F.; Goddard, T. D.; Huang, C. C.; Couch, G. S.; Greenblatt, D. M.; Meng, E. C.; Ferrin, T. E. *J. Comput. Chem.* **2004**, *25*, 1605-1612.

(140) Rosenfield, R. E.; Trueblood, K. N.; Dunitz, J. D. *Acta Crystallogr. A* **1978**, *34*, 828-829.

(141) Stern, M. J.; Weston, J. R. E. *J. Chem. Phys.* **1974**, *60*, 2815-2821.

(142) Stern, M. J.; Weston, J. R. E. *J. Chem. Phys.* **1974**, *60*, 2808-2814.

(143) Stern, M. J.; Weston, J. R. E. *J. Chem. Phys.* **1974**, *60*, 2803-2807.

(144) Sen, A.; Yahashiri, A.; Kohen, A. *Biochemistry* **2011**, *50*, 6462-6468.

(145) Dokmanic, I.; Sikic, M.; Tomic, S. *Acta Crystallogr. D* **2008**, *64*, 257-263.

(146) Harding, M. M.; Nowicki, M. W.; Walkinshaw, M. D. *Crystallogr. Rev.* **2010**, *16*, 247-302.

(147) Saris, N. E.; Mervaala, E.; Karppanen, H.; Khawaja, J. A.; Lewenstam, A. *Clin. Chim. Acta* **2000**, *294*, 1-26.

(148) Romani, A. M.; Scarpa, A. *Front Biosci.* **2000**, *5*, D720-734.

(149) Cowan, J. A. *Biometals* **2002**, *15*, 225-235.

(150) Wolf, F. I.; Fasanella, S.; Tedesco, B.; Torsello, A.; Sgambato, A.; Faraglia, B.; Palozza, P.; Boninsegna, A.; Cittadini, A. *Front Biosci.* **2004**, *9*, 2056-2062.

(151) Moncany, M. L.; Kellenberger, E. *Experientia* **1981**, *37*, 846-847.

(152) Chang, C. F.; Shuman, H.; Somlyo, A. P. *J Bacteriol.* **1986**, *167*, 935-939.

(153) Costi, M. P. *Med. Res. Re.v* **1998**, *18*, 21-42.

(154) Costi, M. P.; Tondi, D.; Rinaldi, M.; Barlocco, D.; Pecorari, P.; Soragni, F.; Venturelli, A.; Stroud, R. M. *Biochim. Biophys. Acta* **2002**, *1587*, 206-214.

(155) Kanaan, N.; Roca, M.; Tuñón, I.; Martí, S.; Moliner, V. *J. Phys. Chem. B* **2010**, *114*, 13593-13600.

(156) Maley, G. F.; Maley, F.; Baugh, C. M. *J Biol. Chem.* **1979**, *254*, 7485-7487.

(157) Rode, W.; Jastreboff, M. M. *Mol. Cell. Biochem* **1984**, *60*, 73-76.

(158) Birdsall, D. L.; Finer-Moore, J.; Stroud, R. M. *J. Mol. Biol.* **1996**, *255*, 522-535.

(160) Klinman, J. P.; Matthews, R. G. *J. Am. Chem. Soc.* **1985**, *107*, 1058-1060.

(161) Doan, L. T.; Martucci, W. E.; Vargo, M. A.; Atreya, C. E.; Anderson, K. S. *Biochemistry* **2007**, *46*, 8379-8391.

(162) Martucci, W. E.; Vargo, M. A.; Anderson, K. S. *Biochemistry* **2008**, *47*, 8902-8911.

(163) Kamb, A.; Finer-Moore, J.; Calvert, A. H.; Stroud, R. M. *Biochemistry* **1992**, *31*, 9883-9890.

(164) The PyMOL Molecular Graphics System, Version 1.5.0.4 Schrödinger, LLC.

(165) LiCata, V. J.; Allewell, N. M. *Biophys. Chem.* **1997**, *64*, 225-234.

(166) Swain, C. G.; Stivers, E. C.; Reuwer, J. F.; Schaad, L. J. *J. Am. Chem. Soc.* **1958**, *80*, 5885-5893.

(167) Nagel, Z. D.; Klinman, J. P. *Chem. Rev.* **2006**, *106*, 3095-3118.

(168) Rittle, J.; Green, M. T. *Science* **2010**, *330*, 933-937.

(169) Schramm, V. L. *Chem. Rev.* **2006**, *106*, 3029-3030.

(170) Costi, M. P. *Med. Res. Rev.* **1998**, *18*, 21-42.

(171) Costi, M. P.; Tondi, D.; Rinaldi, M.; Barlocco, D.; Pecorari, P.; Soragni, F.; Venturelli, A.; Stroud, R. M. *Biochim. Biophys. Acta* **2002**, *1587*, 206-214.

(172) Kanaan, N.; Ferrer, S.; Martí, S.; Garcia-Viloca, M.; Kohen, A.; Moliner, V. *J. Am. Chem. Soc.* **2011**, *133*, 6692-6702.

(173) Wataya, Y.; Hayatsu, H.; Kawazoe, Y. *J. Am. Chem. Soc.* **1972**, *94*, 8927-8928.

(174) Santi, D. V.; Brewer, C. F. *Biochemistry* **1973**, *12*, 2416-2424.

(175) Pogolotti, A. L., Jr.; Santi, D. V. *Biochemistry* **1974**, *13*, 456-466.

(176) Garrett, C.; Wataya, Y.; Santi, D. V. *Biochemistry* **1979**, *18*, 2798-2804.

(177) Pogolotti, A. L., Jr.; Weill, C.; Santi, D. V. *Biochemistry* **1979**, *18*, 2794-2798.

(178) Hardy, L. W.; Graves, K. L.; Nalivaika, E. *Biochemistry* **1995**, *34*, 8422-8432.

(179) Gerlt, J. A.; Gassman, P. G. *Biochemistry* **1993**, *32*, 11943-11952.

(180) Pogolotti, A. L.; Santi, D. V. *Biochemistry* **1974**, *13*, 456-466.

(181) Santi, D. V.; Brewer, C. F. *Biochemistry* **1973**, *12*, 2416-2424.

(182) Hyatt, D. C.; Maley, F.; Monfort, W. R. *Biochemistry* **1997**, *36*, 4585-4594.

(183) Fauman, E. B.; Rutenber, E. E.; Maley, G. F.; Maley, F.; Stroud, R. M. *Biochemistry* **1994**, *33*, 1502-1511.

(184) Sage, C. R.; Rutenber, E. E.; Stout, T. J.; Stroud, R. M. *Biochemistry* **1996**, *35*, 16270-16281.

(185) Huang, W.; Santi, D. V. *Biochemistry* **1997**, *36*, 1869-1873.

(186) Liu, Y.; Barrett, J. E.; Schultz, P. G.; Santi, D. V. *Biochemistry* **1999**, *38*, 848-852.

(187) Saxl, R. L.; Reston, J.; Nie, Z.; Kalman, T. I.; Maley, F. *Biochemistry* **2003**, *42*, 4544-4551.

(188) Field, M. J. *A Practical Introduction to the Simulation of Molecular Systems*; Cambridge University Press: Cambridge, 1999.

(189) Field, M. J.; Albe, M.; Bret, C.; Proust-De Martin, F.; Thomas, A. *J. Comput. Chem.* **2000**, *21*, 1088-1100.

(190) Olsson, M. H. M.; Søndergaard, C. R.; Rostkowski, M.; Jensen, J. H. *J. Chem. Theory and Comput.* **2011**, *7*, 525-537.

(191) Singh, U. C.; Kollman, P. A. *J. Comput. Chem.* **1986**, *7*, 718-730.

(192) Dewar, M. J. S.; Zoebisch, E. G.; Healy, E. F.; Stewart, J. J. P. *J. Am. Chem. Soc.* **1985**, *107*, 3902-3909.

(193) Becke, A. D. *J. Chem. Phys.* **1993**, *98*, 5648-5652.

(194) Miehlich, B.; Savin, A.; Stoll, H.; Preuss, H. *Chem. Phys. Lett.* **1989**, *157*, 200-206.

(195) Kaminiski, G. A.; Friesner, R. A.; Tirado-Rives, J.; Jorgensen, W. L. *J. Phys. Chem. B* **2001**, *105*, 6474-6487.

(196) Jorgensen, W. L.; Chandrasekhar, J.; Madura, J. D.; Impey, R. W.; Klein, M. L. *J. Chem. Phys.* **1983**, *79*, 926-935.

(197) Verlet, L. *Phys. Rev.* **1967**, *159*, 98-103.

(198) Brooks, B. R.; Bruccoleri, R. E.; Olafson, B. D.; States, D. J.; Swaminathan, S.; Karplus, M. *J. Comput. Chem.* **1983**, *4*, 187-217.

(199) Martí, S.; Moliner, V.; Tunon, I. *J. Chem. Theory and Comput.* **2005**, *1*, 1008-1016.

(200) Kumar, S.; Bouzida, D.; Swendsen, R. H.; Kollman, P. A.; Rosenberg, J. M. *J. Comput. Chem.* **1992**, *13*, 1011-1021.

(201) Torrie, G. M.; Valleau, J. P. *J. Comput. Phys.* **1977**, *23*, 187-199.

(202) Kuhn, P.; Lesley, S. A.; Mathews, II; Canaves, J. M.; Brinen, L. S.; Dai, X.; Deacon, A. M.; Elsliger, M. A.; Eshaghi, S.; Floyd, R.; Godzik, A.; Grittini, C.; Grzechnik, S. K.; Guda, C.; Hodgson, K. O.; Jaroszewski, L.; Karlak, C.; Klock, H. E.; Koesema, E.; Kovarik, J. M.; Kreusch, A. T.; McMullan, D.; McPhillips, T. M.; Miller, M. A.; Miller, M.; Morse, A.; Moy, K.; Ouyang, J.; Robb, A.; Rodrigues, K.; Selby, T. L.; Spraggon, G.; Stevens, R. C.; Taylor, S. S.; van den Bedem, H.; Velasquez, J.; Vincent, J.; Wang, X.; West, B.; Wolf, G.; Wooley, J.; Wilson, I. A. *Proteins: Struct., Funct., Genet.* **2002**, *49*, 142-145.

(203) Agrawal, N.; Lesley, S. A.; Kuhn, P.; Kohen, A. *Biochemistry* **2004**, *43*, 10295-10301.

(204) Graziani, S.; Bernauer, J.; Skouloubris, S.; Graille, M.; Zhou, C. Z.; Marchand, C.; Decottignies, P.; van Tilbeurgh, H.; Myllykallio, H.; Liebl, U. *J. Biol. Chem.* **2006**, *281*, 24048-24057.

(205) Griffin, J.; Roshick, C.; Iliffe-Lee, E.; McClarty, G. *J. Biol. Chem.* **2005**, *280*, 5456-5467.

(206) Myllykallio, H.; Leduc, D.; Filee, J.; Liebl, U. *Trends Microbiol.* **2003**, *11*, 220-223.

(207) Mason, A.; Agrawal, N.; Washington, M. T.; Lesley, S. A.; Kohen, A. *Chem. Commun.* **2006**, 1781-1783.

(208) Chernyshev, A.; Fleischmann, T.; Koehn, E. M.; Lesley, S. A.; Kohen, A. *Chem. Commun.* **2007**, 2861-2863.

(209) Mattevi, A. *Trends Biochem. Sci.* **2006**, *31*, 276-283.

(210) Segel, I. H. *Enzyme Kinetics: Behavior and Analysis of Rapid Equilibrium and Steady State Enzyme Systems*; Wiley: New York, 1975.

(211) Cook, P. F.; Cleland, W. W. *Enzyme Kinetics and Mechanism*; Taylor & Francis Group: New York, 2007.

(212) Blankenhorn, G. *Eur. J. Biochem.* **1975**, *50*, 351-356.

(213) Massey, V.; Ghisla, S. *Ann. N. Y. Acad. Sci.* **1974**, *227*, 446-465.

(214) Filisetti, L.; Valton, J.; Fontecave, M.; Niviere, V. *FEBS Lett.* **2005**, *579*, 2817-2820.

(215) Hunter, J. H.; Gujjar, R.; Pang, C. K.; Rathod, P. K. *PLoS ONE* **2008**, *3*, e2237.

(216) Ulmer, J. E.; Boum, Y.; Thouvenel, C. D.; Myllykallio, H.; Sibley, C. H. *J. Bacteriol.* **2008**, *190*, 2056-2064.

(217) Zhou, M.; Diwu, Z.; Panchuk-Voloshina, N.; Haugland, R. P. *Anal. Biochem.* **1997**, *253*, 162-168.

(218) Gattis, S. G.; Palfey, B. A. *J. Am. Chem. Soc.* **2005**, *127*, 832-833.

(219) Motulsky, H.; Christopoulos, A. *Fitting Models to Biological Data Using Linear and Nonlinear Regression: A Practical Guide to Curve Fitting*; Oxford University Press: Oxford ; New York, 2004.

(220) Wang, Z.; Toraason, M.; Luzum, C.; Kohen, A. manuscript in preparation, 2012.

(221) Mishanina, T. V.; Koehn, E. M.; Conrad, J. A.; Palfey, B. A.; Lesley, S. A.; Kohen, A. *J. Am. Chem. Soc.* **2012**, *134*, 4442-4448.